Introduction to Magnetism (2) : Magnetism today or How performs the micromagnetic theory now?

André Thiaville

Laboratoire de Physique des Solides
Université Paris-Sud & CNRS, Orsay

CENTRE NATIONAL DE LA RECHERCHE SCIENTIFIQUE

LPS ORSAY

UNIVERSITÉ PARIS-SUD XI

1- Introduction

2 - Micromagnetic theory and applications
- statics
- domain walls
- dynamics

3 - Micromagnetics of nano-elements
- macrospin limit
- quasi-uniform structures
- dynamics

4 - Beyond micromagnetics
- molecular magnetism
- clusters of a few atoms
- spin-polarized transport

Nanometric size structures are already used

HITACHI
Inspire the Next

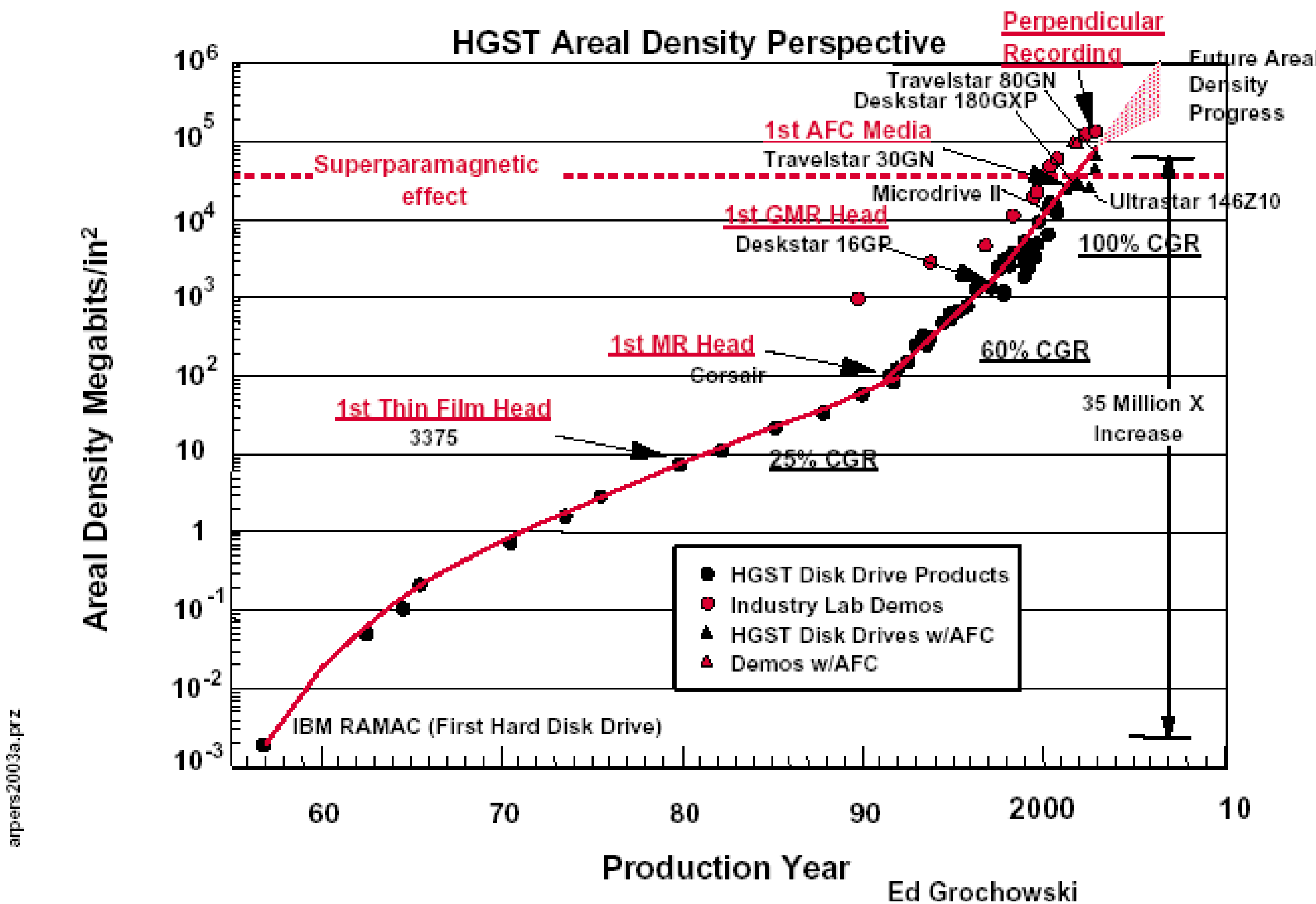

HITACHI
Inspire the Next

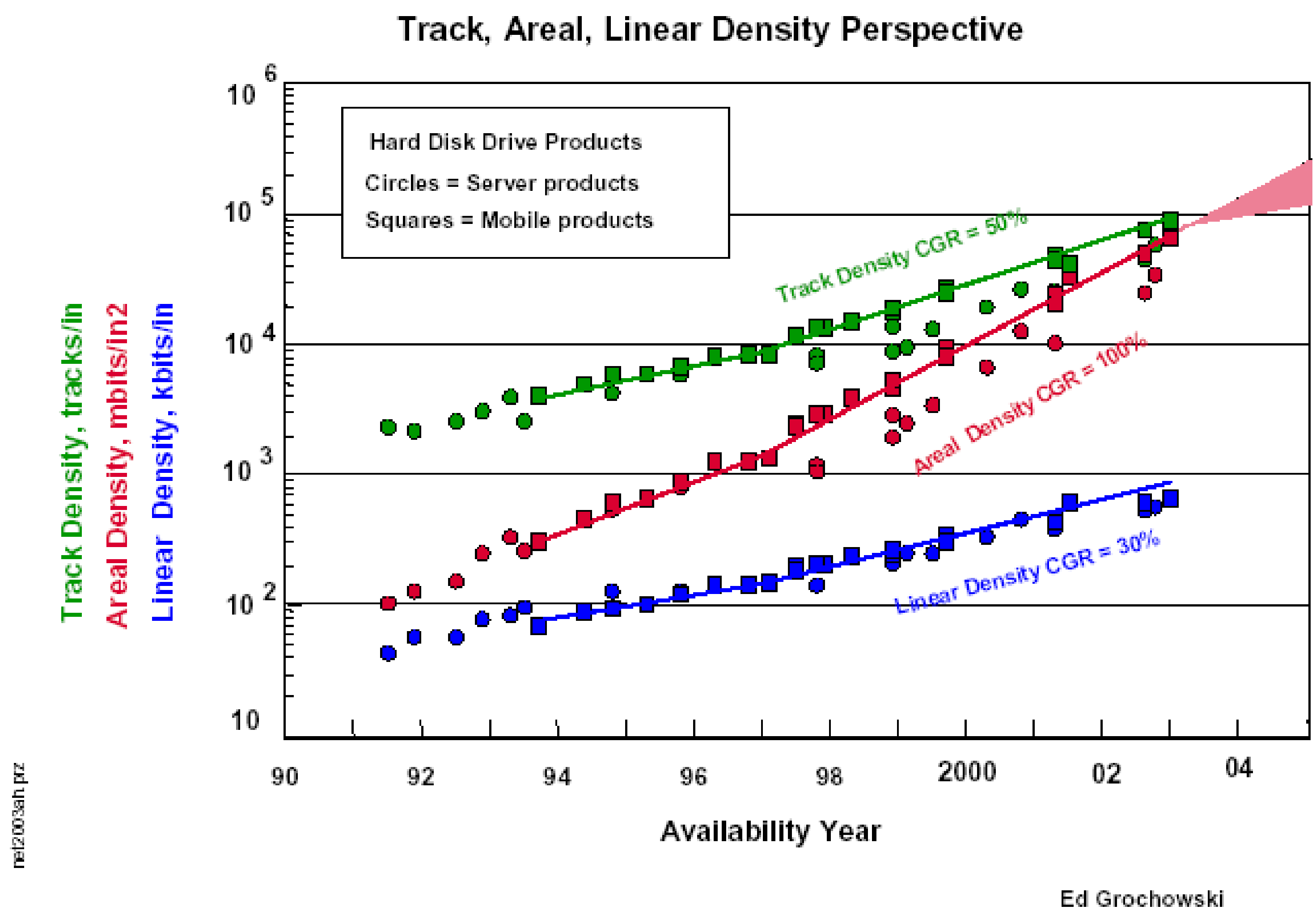

for
10^3 kbit/in
1 bit = 25 nm

San Jose Research Center
Hitachi Global Storage Technologies

Spacing-Areal Density Perspective

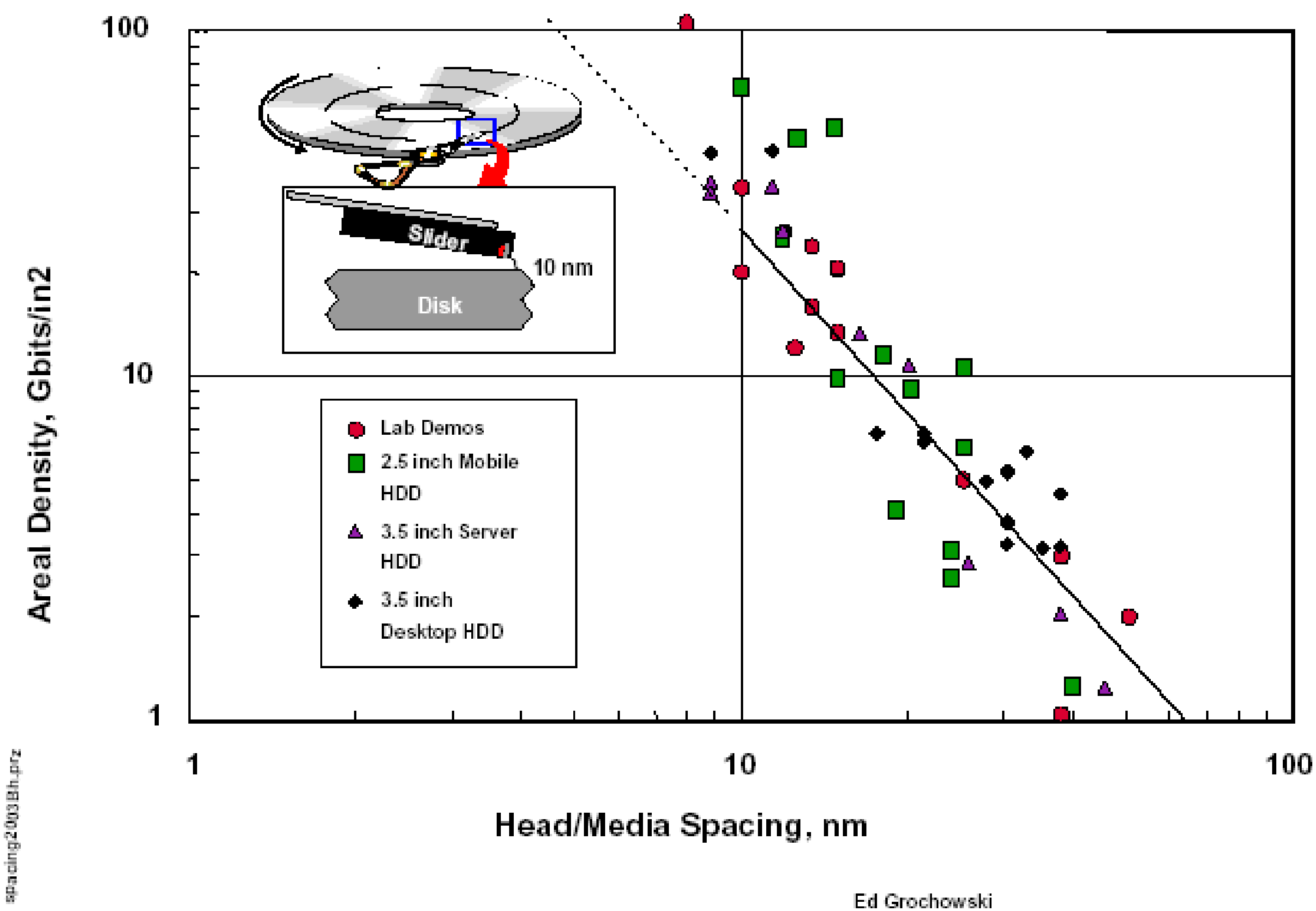

Ed Grochowski

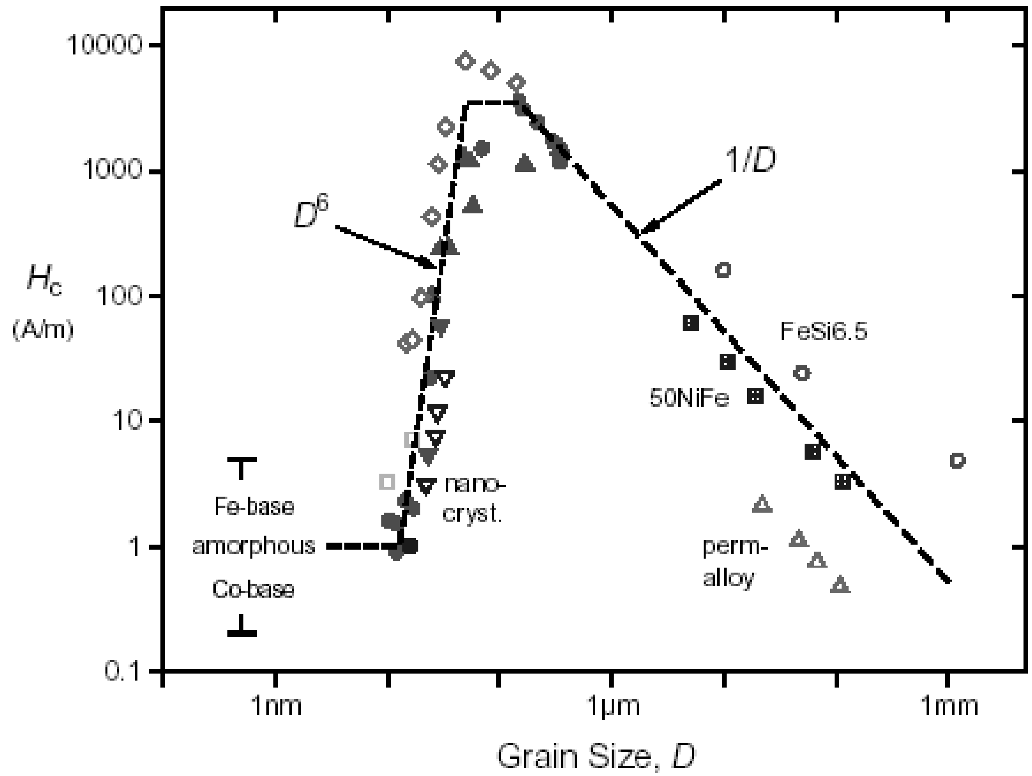

Figure 1. Coercivity, H_c, vs. grain size, D, for various soft magnetic metallic alloys (after [8,9]): Fe-$Nb_3Si_{13.5}B_9$ (solid up triangles), Fe-$Cu_1Nb_{1\text{-}3}Si_{\sim 13}B_{\sim 9}$ (solid circles), Fe-$Cu_1V_{3\text{-}6}Si_{12.5}B_8$ (solid down triangles), Fe-$Cu_1V_xSi_{19\text{-}x}B_8$ (open down triangles), Fe-$Cu_{0\text{-}1}Zr_{\sim 7}B_{2\text{-}6}$ (open squares), $Fe_{60}Co_{30}Zr_{10}$ (open diamonds), NiFe-alloys (+ center squares and open up triangles) and FeSi6.5wt% (open circles).

G. Herzer, Amorphous and nanocrystalline Soft magnets, in Magnetic hysteresis in novel materials, G.C. Hadjipanayis Ed., Nato ASI E338 (Kluwer, Dordrecht, 1997)

"Standard" Micromagnetics

The "micromagnetic" description of magnetism

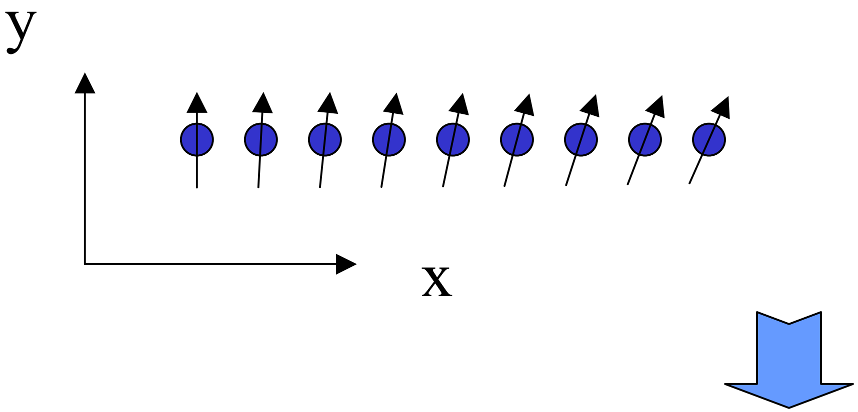

atomic spins

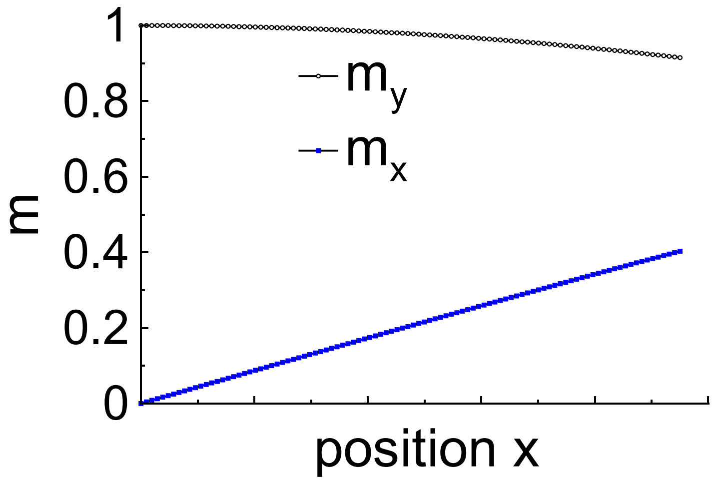

continuous distribution

Assumes that structures to describe are large compared to atomic sizes

Magnetic Interactions

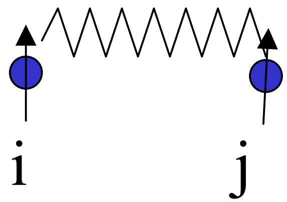

$$E = -J\,\overrightarrow{S_i}\cdot\overrightarrow{S_j}$$

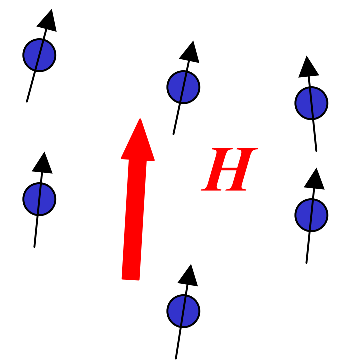

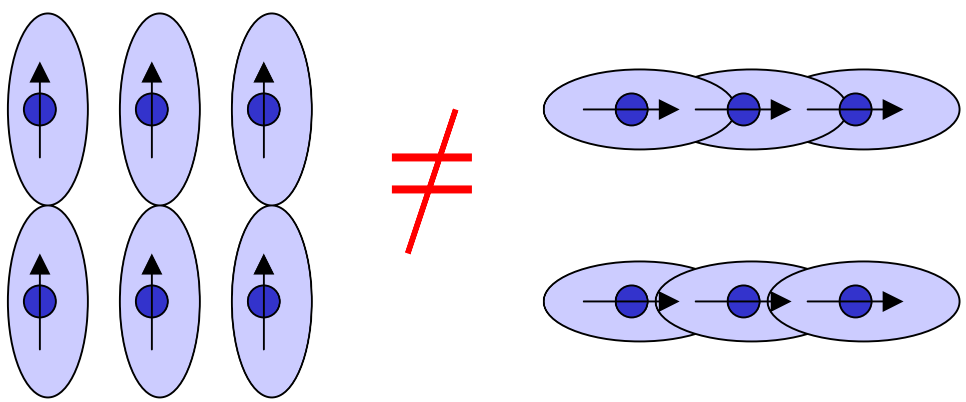

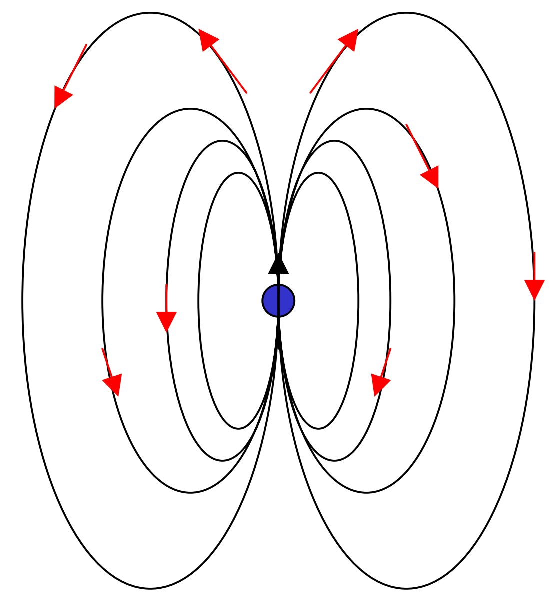

Micromagnetic equations

$\overrightarrow{M} = M_s(T)\overrightarrow{m}$ $\left|\overrightarrow{m}\right| = 1$ no thermal fluctuations

$$E = A(\overrightarrow{\nabla}\overrightarrow{m})^2 + KG(\overrightarrow{m}) - \mu_0 M_s \overrightarrow{m}\cdot\overrightarrow{H} - \frac{1}{2}\mu_0 M_s \overrightarrow{m}\cdot\overrightarrow{H_D}$$

exchange anisotropy applied field demagnetizing field

Statics : minimise ∫E ⟹ Brown equations $\boxed{\overrightarrow{H}_{eff} \, x \, \vec{m} = \vec{0}}$

+ boundary conditions $\boxed{\frac{\partial \vec{m}}{\partial \vec{n}} = \vec{0}}$

effective field

$$\overrightarrow{H}_{eff} = \overrightarrow{H}_{applied} + \overrightarrow{H}_{demag} + \overrightarrow{H}_{aniso} + \overrightarrow{H}_{exchange}$$

$$\boxed{\overrightarrow{H}_{eff} = -\frac{1}{\mu_0 M_s}\frac{\delta E}{\delta \overrightarrow{m}}}$$

$$\frac{2A}{\mu_0 M_s}\Delta\overrightarrow{m}$$

Magnetostatics of matter

$$\vec{B} = \mu_0\left(\vec{H} + \vec{M}\right) \quad \text{with} \quad div\,\vec{B} = 0 \quad \text{and} \quad \overrightarrow{rot}\,\vec{H} = \vec{j}$$

$$\begin{cases} div\,\vec{H}_D = -div\,\vec{M} \\ \overrightarrow{rot}\,\overrightarrow{H}_D = \vec{0} \end{cases} \qquad \begin{cases} div\,\overrightarrow{H}_{ext} = 0 \\ \overrightarrow{rot}\,\vec{H}_{ext} = \vec{j}_{ext} \end{cases}$$

+ boundary conditions

$$(\vec{H}_D^{ext} - \vec{H}_D^{\text{int}}) \cdot \vec{n} = \vec{M} \cdot \vec{n}$$

$$(\vec{H}_D^{ext} - \vec{H}_D^{\text{int}}) \cdot \vec{t} = 0$$

demagnetizing field   *applied field*

Magnetostatic energy

$$E_D = -\frac{1}{2}\mu_0 \int_V \vec{M} \cdot \vec{H}_D = \frac{1}{2}\mu_0 \int_{R^3} \left(\vec{H}_D\right)^2 \geq 0$$

proof : introduce the scalar potential $\vec{H}_D = -\vec{\nabla}\phi$

$$\Delta\phi = div\vec{M} \qquad \phi = -\frac{1}{4\pi}\int_V \frac{div\vec{M}}{|\vec{r} - \vec{r}\,'|} + \frac{1}{4\pi}\int_{\partial V} \frac{\vec{M} \cdot \vec{n}}{|\vec{r} - \vec{r}\,'|}$$

and transform by integration by parts both expressions into

$$\frac{1}{2}\mu_0 \int_{\partial V} (\vec{M} \cdot \vec{n})\phi - \frac{1}{2}\mu_0 \int_V div\vec{M}\,\phi$$

Characteristic lengths

$$\boxed{\Delta = \sqrt{\frac{A}{K}}}$$

Bloch wall width parameter

$A = 10^{-11}$ J/m, $K = 10^{2} - 10^{5}$ J/m^{3}

$\Delta =$ 1 - 100 nm

$$\boxed{\Lambda = \sqrt{\frac{2A}{\mu_0 M_s^2}}}$$

exchange length

$M_s = 10^{6}$ A/m

$\Lambda =$ some nm

$$\boxed{Q = \frac{2K}{\mu_0 M_s^2} = \left(\frac{\Lambda}{\Delta}\right)^2}$$

Quality factor

$Q > 1$ hard material

$Q << 1$ soft material

The Bloch wall (1932)

Easy axis

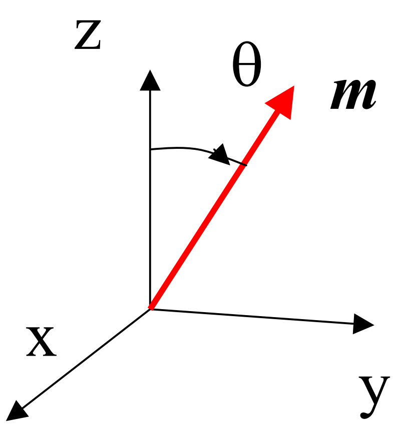

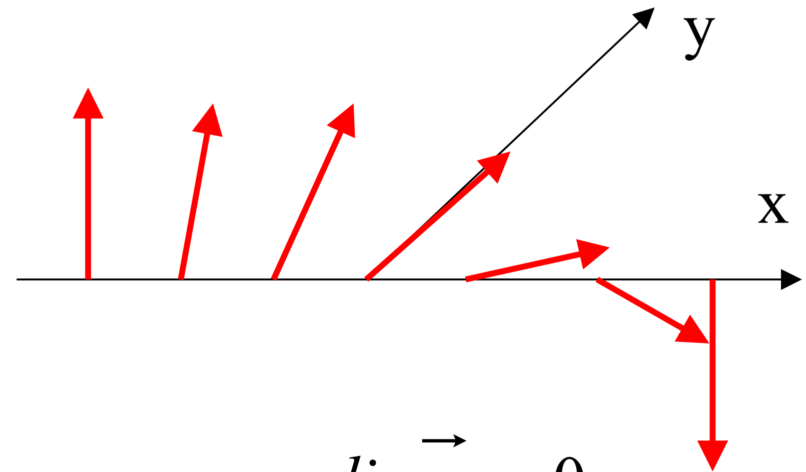

No demag energy $\quad div\,\overrightarrow{m} = 0$

$$\vec{m} = \begin{pmatrix} 0 \\ \sin\theta(x) \\ \cos\theta(x) \end{pmatrix}$$

$$E = A\left(\frac{d\theta}{dx}\right)^2 + K\sin^2\theta \qquad \theta(-\infty) = 0, \quad \theta(+\infty) = \pi$$

Energy minimization equation

$$-2A\frac{d^2\theta}{dx^2} + 2K\sin\theta\cos\theta = 0$$

$$\times \frac{d\theta}{dx} \text{ and } \int dx$$

First integral

$$-A\left(\frac{d\theta}{dx}\right)^2 + K\sin^2\theta = C^{st} = 0$$

$$\frac{d\theta}{dx} = \pm\frac{\sin\theta}{\Delta}$$

$$\boxed{\Delta = \sqrt{\frac{A}{K}}}$$

Bloch wall width parameter

$$\theta = 2\,\mathrm{Atan}\left[\exp\left(\frac{x - x_0}{\Delta}\right)\right] \quad (+\pi)$$

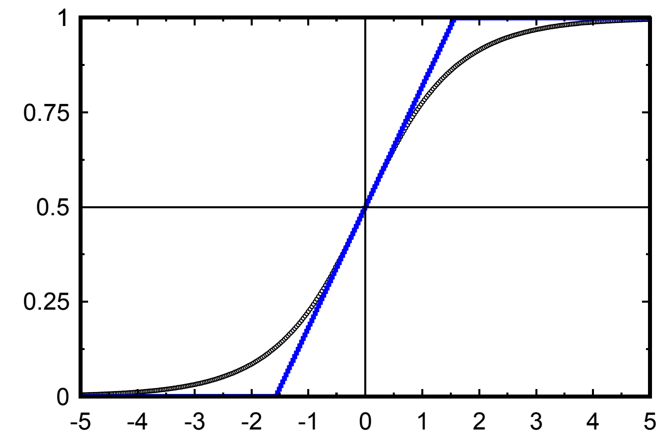

Linear width : $\pi\Delta$

Properties of the Bloch wall

Integrated exchange energy = $\dfrac{2A}{\Delta} = 2\sqrt{AK}$

Integrated anisotropy energy = $2K\Delta = 2\sqrt{AK}$

Integrated hard axis component $\displaystyle\int m_y dx = \int \sin\theta\, dx = \Delta\int d\theta = \pi\,\Delta$

$$\int m_y{}^2 dx = \int \sin^2\theta\, dx = \Delta\int \sin\theta\, d\theta = 2\,\Delta$$

etc.

The vortex

2D magnetization

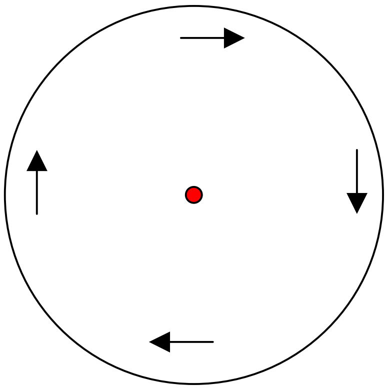

$$\vec{m} = \begin{pmatrix} y/r \\ -x/r \\ 0 \end{pmatrix} \qquad \begin{cases} div\,\vec{m} = 0 \\ \vec{m}\cdot\vec{n} = 0 \end{cases}$$

Divergence of the exchange energy $E_{ech} = A\left(\vec{\nabla}\vec{m}\right)^2 = A/r^2$

3D magnetization

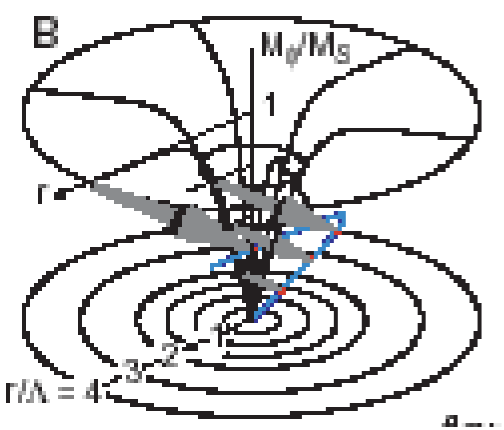

approximation

$$\vec{m} = \begin{pmatrix} \sin\theta(r)\ y/r \\ -\sin\theta(r)\,x/r \\ \cos\theta(r) \end{pmatrix} \qquad \begin{cases} div\,\vec{m} = 0 \\ \vec{m}\cdot\vec{n} \neq 0 \end{cases}$$

$$E_{ech} = A\left[\sin^2\theta/r^2 + \left(\frac{d\theta}{dr}\right)^2\right]$$

$$\vec{m} = \begin{pmatrix} -\sin\theta(r)\, y/r \\ \sin\theta(r)\, x/r \\ \cos\theta(r) \end{pmatrix}$$

$$E_{ech} = A\left[\left(\frac{d\theta}{dr}\right)^2 + \frac{\sin^2\theta}{r^2}\right]$$

$$E_{dem} = \frac{\mu_0 M_s^2}{2}\cos^2\theta$$

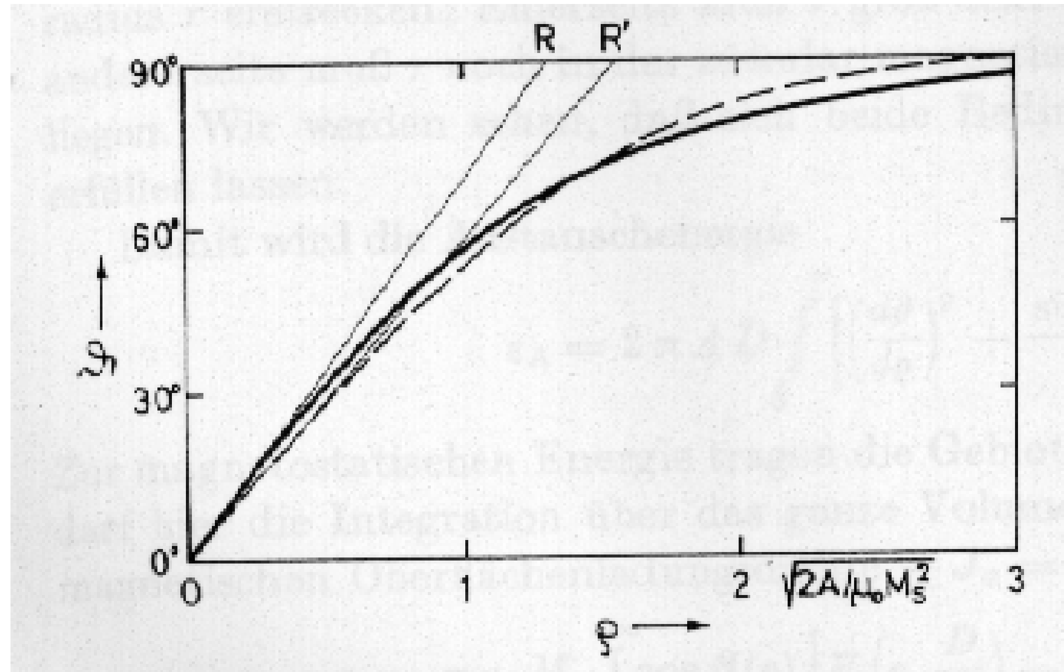

E. Feldtkeller, H. Thomas, Phys. kondens. Materie **4**, 8 (1965)

$$\frac{d^2(2\theta)}{dr^2} + \frac{1}{r}\frac{d(2\theta)}{dr} + \left(\frac{1}{\Lambda^2} - \frac{1}{r^2}\right)\sin 2\theta = 0$$

$$\boxed{\Lambda = \sqrt{\frac{2A}{\mu_0 M_s^2}}}$$

Variational calculation

Normalized widths W / Λ

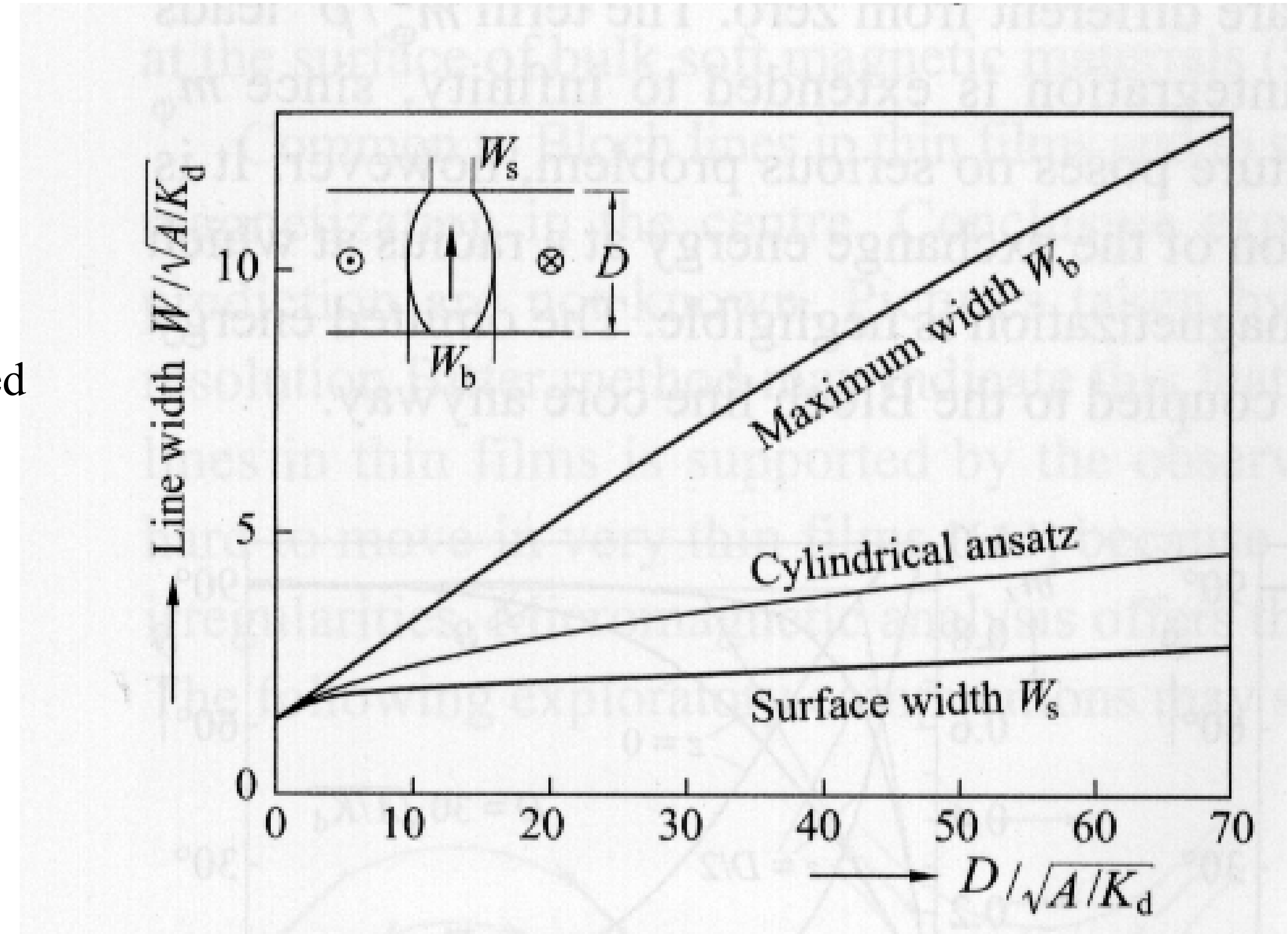

Normalized thickness D / Λ

A.Hubert et R. Schäfer *Magnetic Domains* (Springer, 1998)

Walls in films with perpendicular anisotropy

Epaisseur 30 nm, facteur de qualité Q= 1.77
boîte 60 nm de large

Λ= 4 nm

composante

⊗

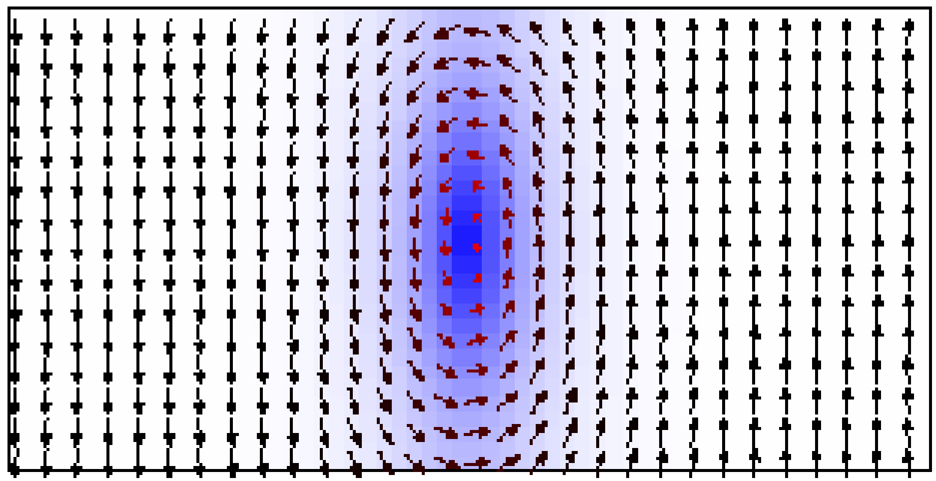

Bloch

composante

→

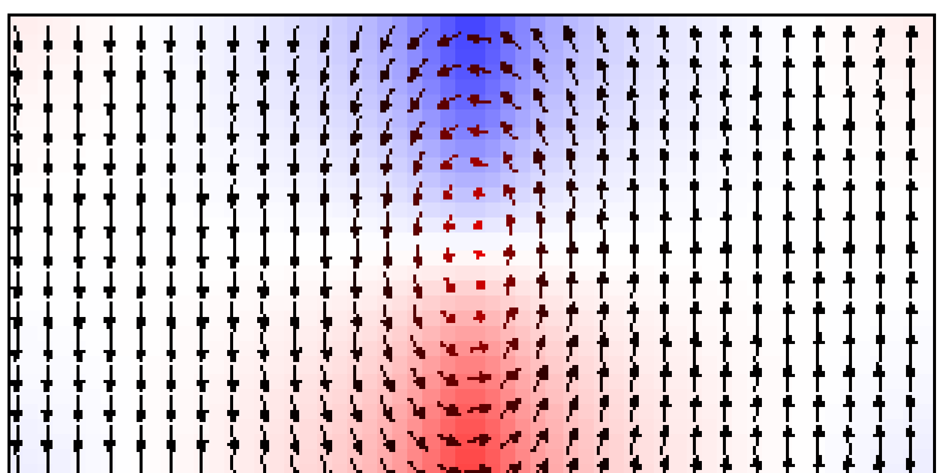

Néel

Néel

The Néel wall (1955)

Thin film without anisotropy, or small in-plane anisotropy

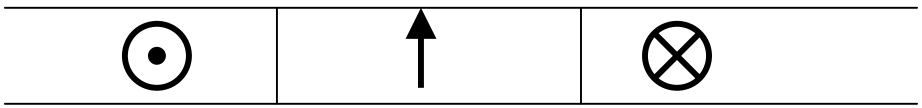

Bloch wall

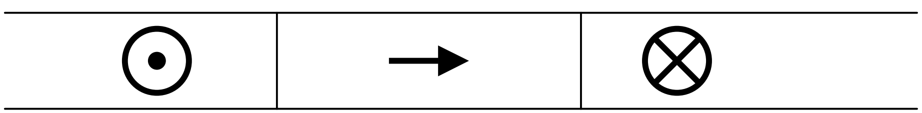

Néel wall

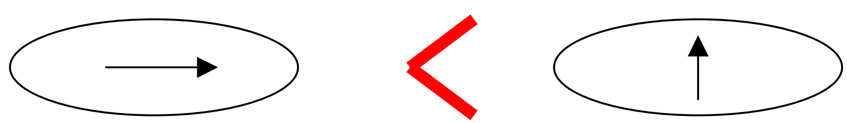

Approximate analytical model

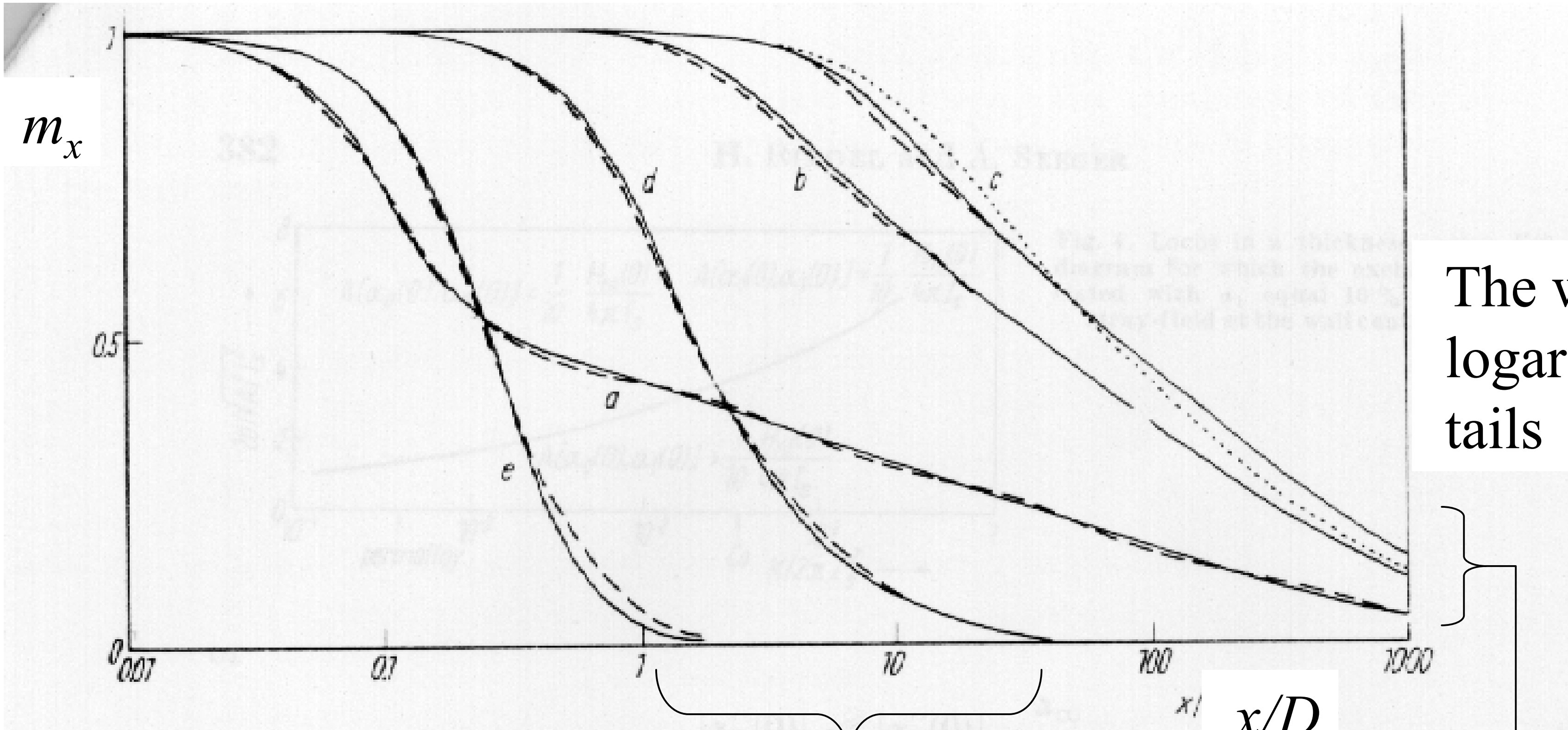

The wall has logarithmic tails

Q= 0.04, 1.88
D= 2.5 Λ

Q= 2-2.5 10^{-4}
D= 20, 2.5 et 1.45 Λ

H. Riedel, A. Seeger, phys. stat. sol. **46** 377 (1971)

Walls in soft thin films

paroi de Néel symétrique

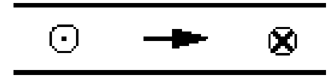

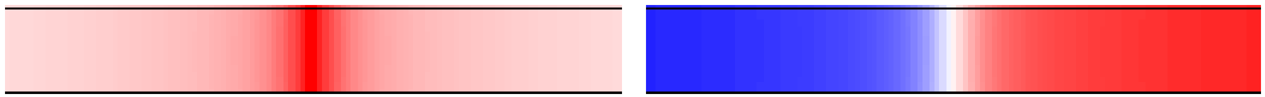

composante → NiFe 30 nm composante ⊙

paroi de Néel asymétrique

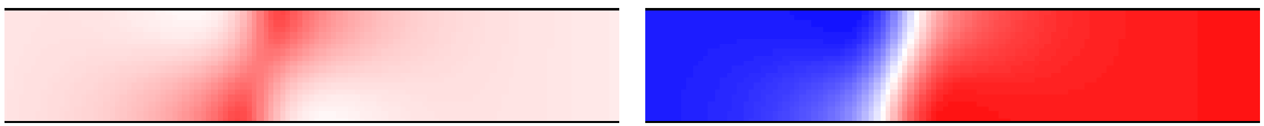

NiFe 40 nm

paroi de Bloch asymétrique

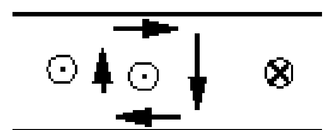

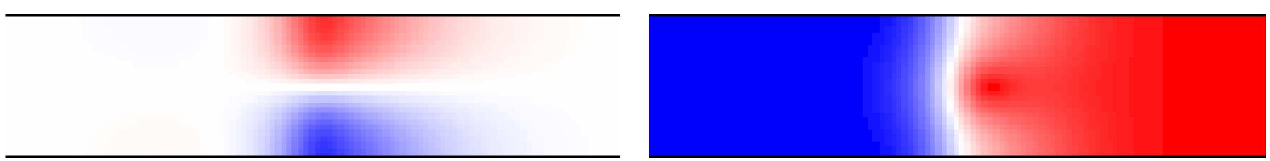

NiFe 50 nm

2D instability of the Néel wall : cross-tie

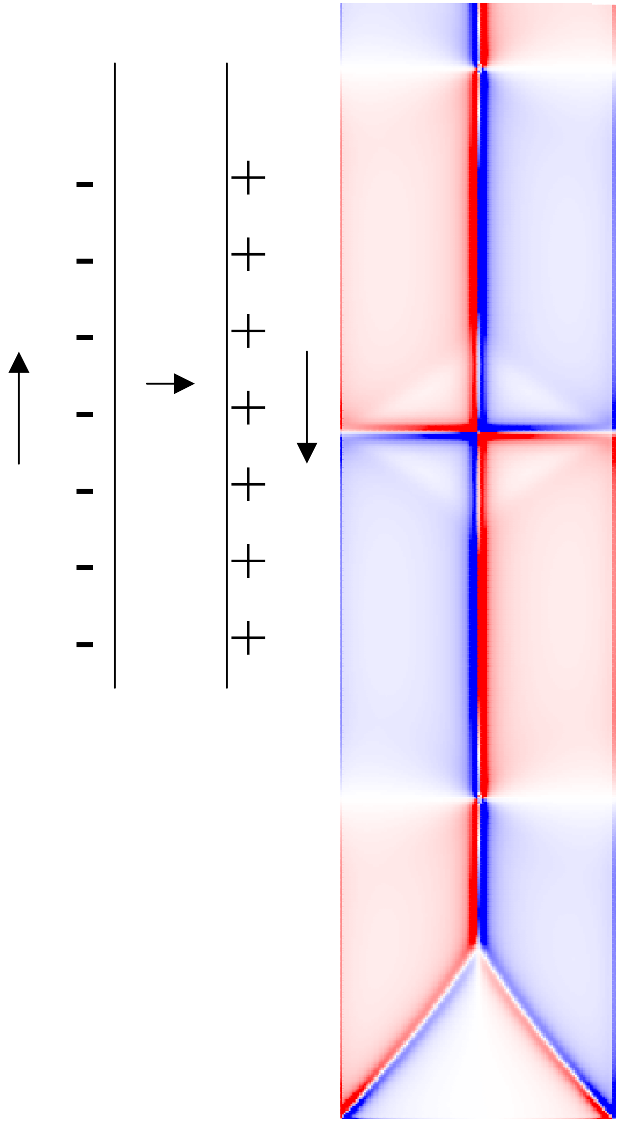

map of the magnetic charges

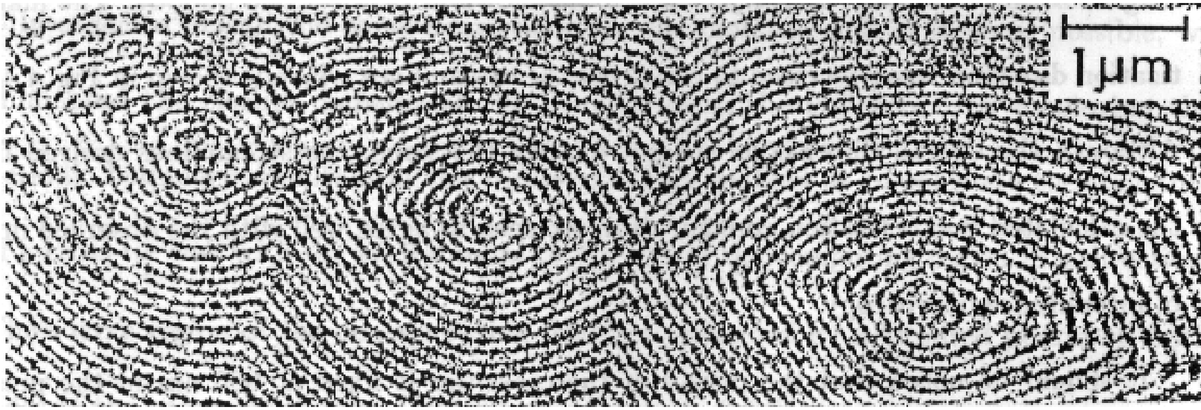

electron holography image

A. Tonomura et al., Phys. Rev. **B25** 6799 (1982)

Magnetization dynamics

$$\vec{L} = -\vec{M} / \gamma$$

γ gyromagnetic ratio (>0)

$$\gamma = \frac{g\mu_B}{\hbar} = g\,\frac{e}{2m}$$

Angular momentum dynamics

$$\frac{d\vec{L}}{dt} = \vec{\Gamma}$$

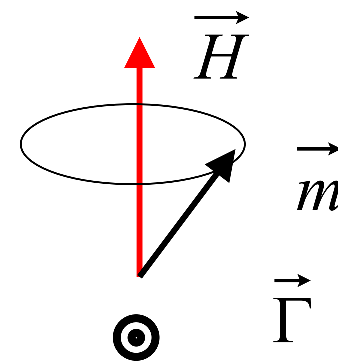

$$\vec{\Gamma} = \mu_0 M_s \vec{m} \times \vec{H}$$

$$\frac{d\vec{m}}{dt} = \gamma_0 \vec{H} \times \vec{m}$$

$$\gamma_0 = \mu_0 \gamma \approx 2.2\ 10^5\ S.I.$$

Can be found directly from quantum mechanics

0.28 GHz/ mT

Dynamics of a magnetization continuum

Effective field

$$\vec{H}_{eff} = \vec{H}_{applied} + \vec{H}_{demag} + \vec{H}_{anisotropy} + \vec{H}_{exchange}$$

$$\vec{H}_{exchange} = \frac{2A}{\mu_0 M_s} \Delta \vec{m}$$

$$\boxed{\vec{H}_{eff} = -\frac{1}{\mu_0 M_s} \frac{\delta E}{\delta \vec{m}}}$$

$$\boxed{\frac{d\vec{m}}{dt} = \gamma_0 \vec{H}_{eff} \times \vec{m} + \alpha \vec{m} \times \frac{d\vec{m}}{dt}}$$

Landau-Lifshitz-Gilbert

$$= \frac{\gamma_0}{1+\alpha^2} \left[\vec{H}_{eff} \times \vec{m} + \alpha \vec{m} \times \left(\vec{H}_{eff} \times \vec{m} \right) \right]$$

α : Gilbert damping parameter

another magnetization dynamics equation

$$\frac{d\vec{m}}{dt} = \gamma_0 \vec{H}_{eff} \times \vec{m} + \alpha \vec{m} \times \frac{d\vec{m}}{dt}$$ Landau-Lifshitz-Gilbert (1955)

$$\frac{d\vec{m}}{dt} = \gamma_L \vec{H}_{eff} \times \vec{m} + \lambda \vec{m} \times \left(\vec{H}_{eff} \times \vec{m} \right)$$ Landau-Lifshitz (1935)

are mathematically equivalent

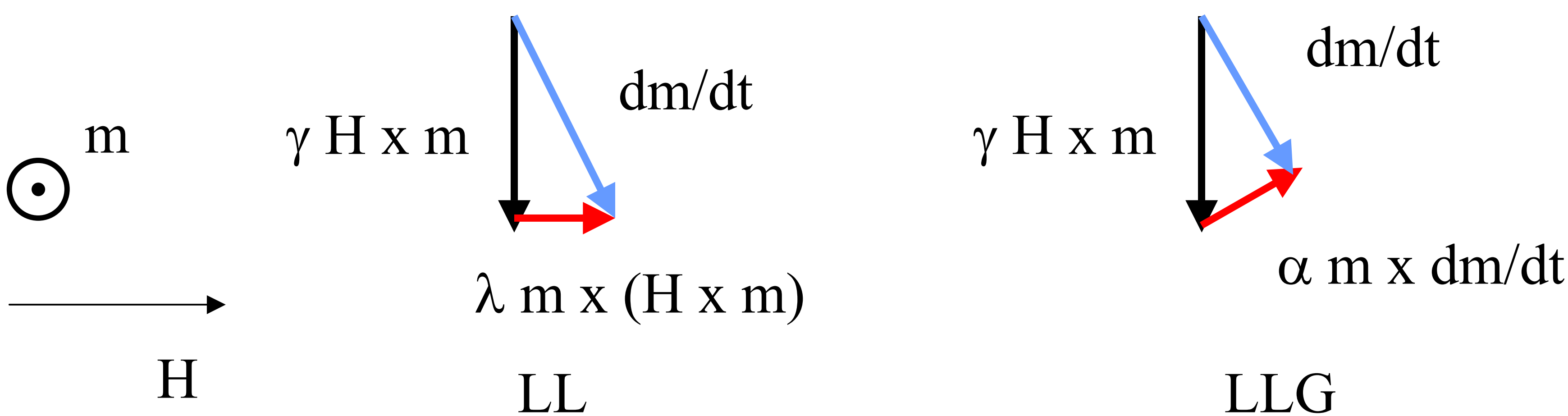

Properties of the magnetization dynamics

1) $$\frac{d(\vec{m}^2)}{dt} = 2\vec{m}.\frac{d\vec{m}}{dt} = 0$$ Conservation of the magnetization modulus

2) $$\frac{dE}{dt} = -\mu_0 M_s \overrightarrow{H}_{eff} . \frac{d\overrightarrow{m}}{dt} = -\alpha\mu_0 M_s \overrightarrow{H}_{eff} . \left(\vec{m} \; x \; \frac{d\overrightarrow{m}}{dt} \right)$$

$$= -\alpha\mu_0 M_s \frac{d\overrightarrow{m}}{dt} . \left(\overrightarrow{H}_{eff} \; x \; \vec{m} \right) = -(\alpha\mu_0 M_s / \gamma) \left(\frac{d\overrightarrow{m}}{dt} \right)^2$$

Decrease of the energy with time : the magnetic system is not isolated

Micromagnetics & Nano-objects

Nanoparticles and small elements

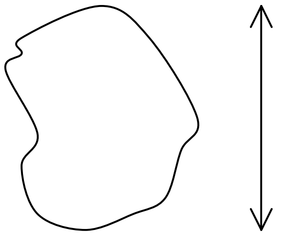

L

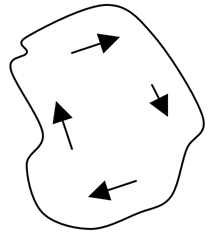

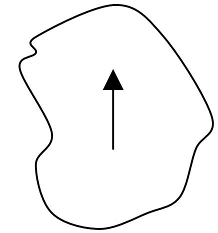

$$E_{ech} \approx A\left(\frac{\pi}{L}\right)^2, E_{dem} \approx 0 \qquad E_{ech} \approx 0, E_{dem} \approx \frac{1}{3}\frac{\mu_0 M_s^2}{2}$$

stable monodomain state for $\frac{1}{3}\frac{\mu_0 M_s^2}{2} < A\left(\frac{\pi}{L}\right)^2 \Leftrightarrow L < \pi\sqrt{3}\Lambda$

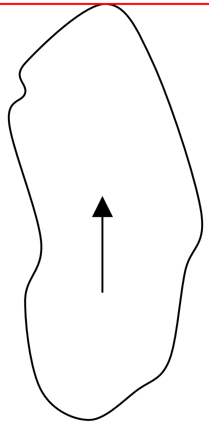

Demagnetising factor N

$$L < \pi \frac{\Lambda}{\sqrt{N}}$$

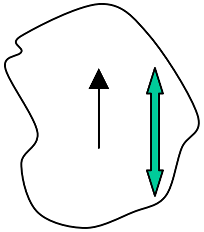

With anisotropy, the transition size increases too

Nanoparticles in the monodomain state

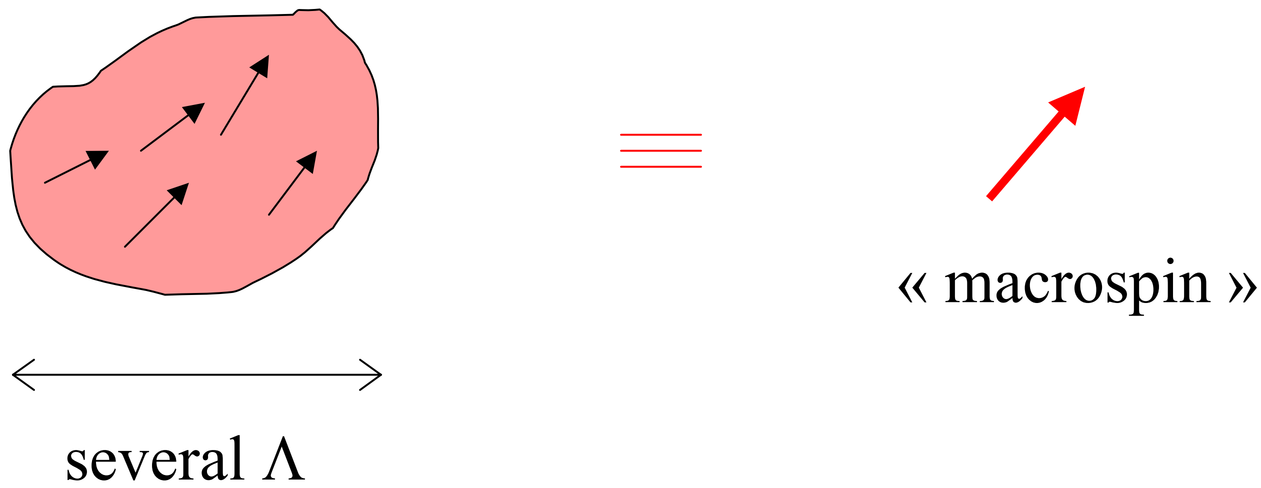

$$E = V\left(K\, G(\vec{m}) - \mu_0 M_s \vec{H}\cdot\vec{m}\right) \qquad |\vec{m}| = 1$$

$$H_K = \frac{2K}{\mu_0 M_s} \qquad \boxed{U = V_{\vec{H}}(\vec{m}) = G(\vec{m}) - 2\vec{h}\cdot\vec{m}}$$

Uniaxial case of degree 2
(Stoner-Wohlfarth 1948, Slonczewski 1956)

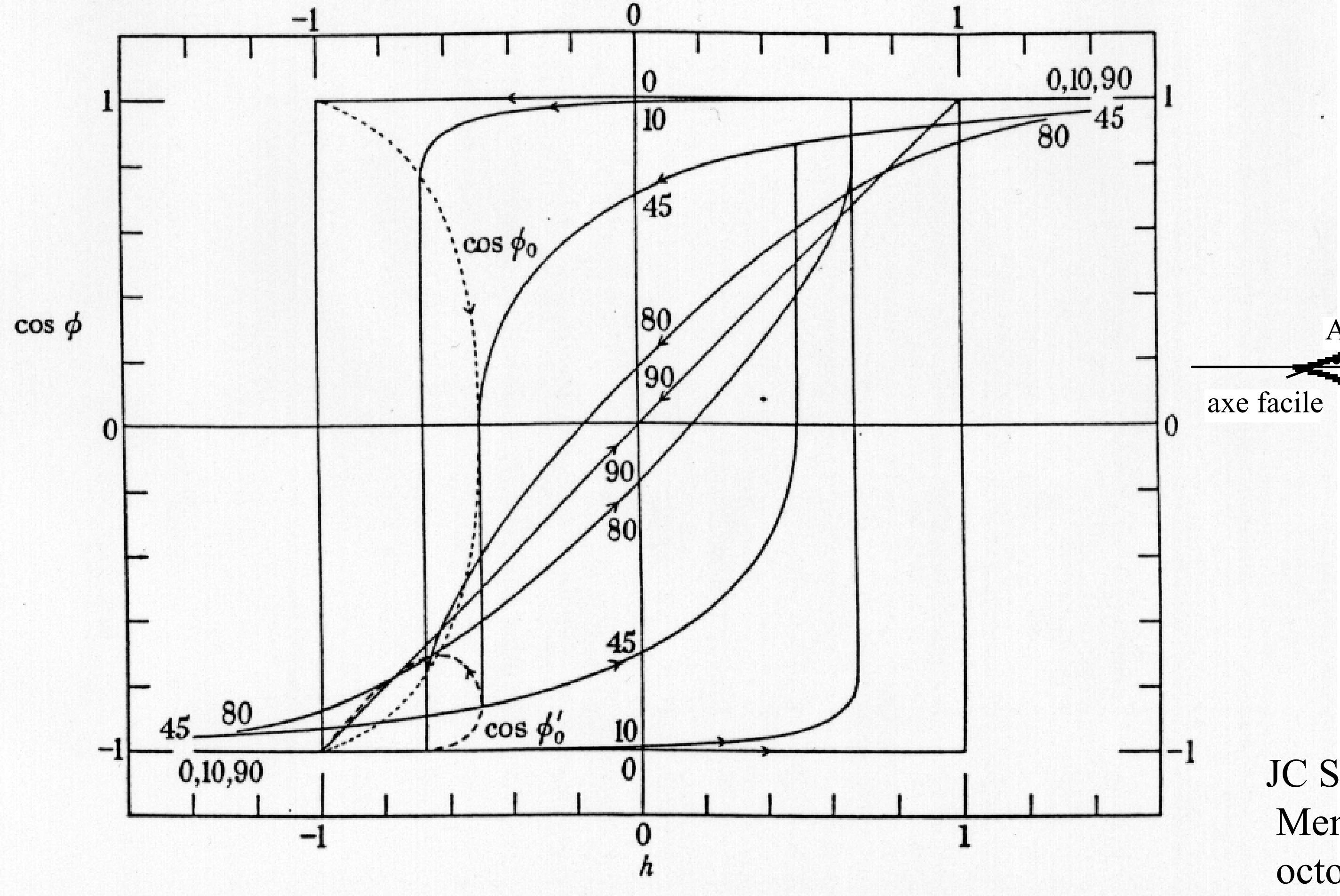

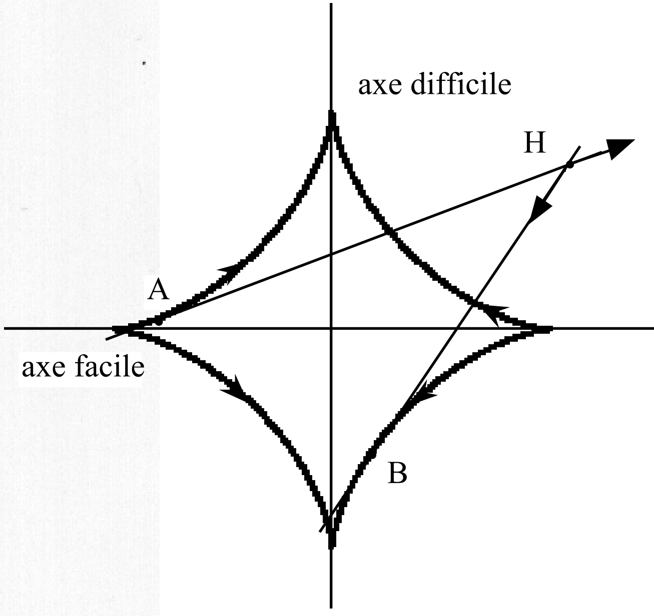

« astroid »

JC Slonczewski, IBM Research Memorandum RM 003.111.224, october 1956 (unpublished)

EC Stoner, EP Wohlfarth Phil. Trans. Roy. Soc. London **A240** 599 (1948), reprinted IEEE Trans. Magn. **27** 3475 (1991)

Geometric solution
(inspired from J.C. Slonczewski, IBM report, 1956)

$$U = V_{\vec{H}}\left(\vec{m}\right) = G\left(\vec{m}\right) - 2\vec{h}\cdot\vec{m}$$

Initial problem (statics) : given *H* , find *m*

Dual problem : given *m*, find *H*

equilibrium : $\vec{u}\cdot\dfrac{dU}{d\vec{m}} = 0$

stability : $\vec{u}\cdot\dfrac{d^2U}{d\vec{m}^2}\vec{u} > 0$

$\forall\vec{u}\perp\vec{m}$

3D Solution in spherical angles

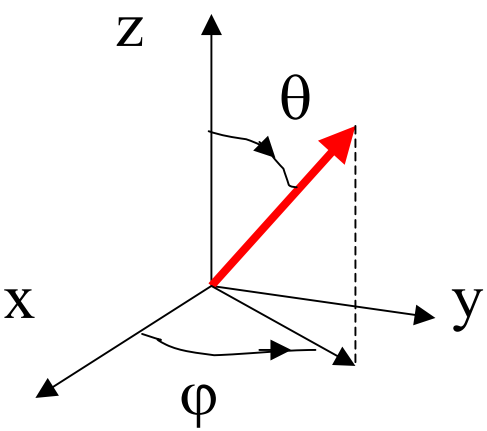

$$G_\theta - 2\vec{h}\cdot\vec{e_\theta} = 0 \qquad G_\varphi - 2\sin\theta\,\vec{h}\cdot\vec{e_\varphi} = 0$$

equilibrium

$$\vec{h} = \frac{1}{2}G_\theta\cdot\vec{e_\theta} + \frac{1}{2\sin\theta}G_\varphi\cdot\vec{e_\varphi} + \lambda\vec{m} = 0$$

$$U_{\theta\theta} = G_{\theta\theta} + 2\lambda \qquad U_{\theta\varphi} = \sin\theta\frac{\partial}{\partial\theta}\left(\frac{G_\varphi}{\sin\theta}\right) \qquad U_{\varphi\varphi} = G_{\varphi\varphi} + \sin\theta\cos\theta\,G_\theta + 2\lambda\sin^2\theta$$

stability

$$U_{\theta\theta} + U_{\varphi\varphi} > 0$$

$$U_{\theta\theta}U_{\varphi\varphi} - (U_{\theta\varphi})^2 > 0$$

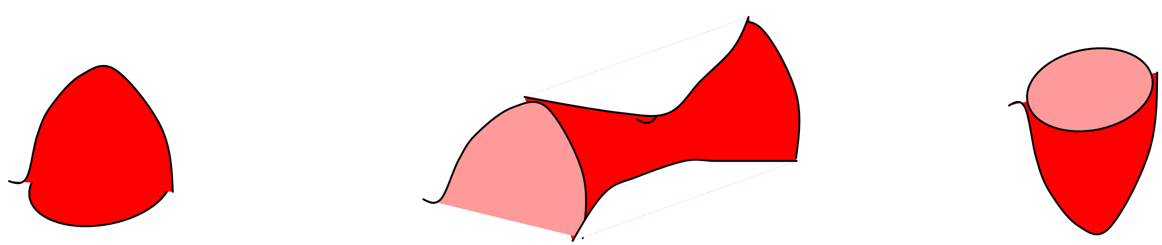

$$G = m_x^2 + 0.5 m_y^2$$

surface S_+ surface S_-

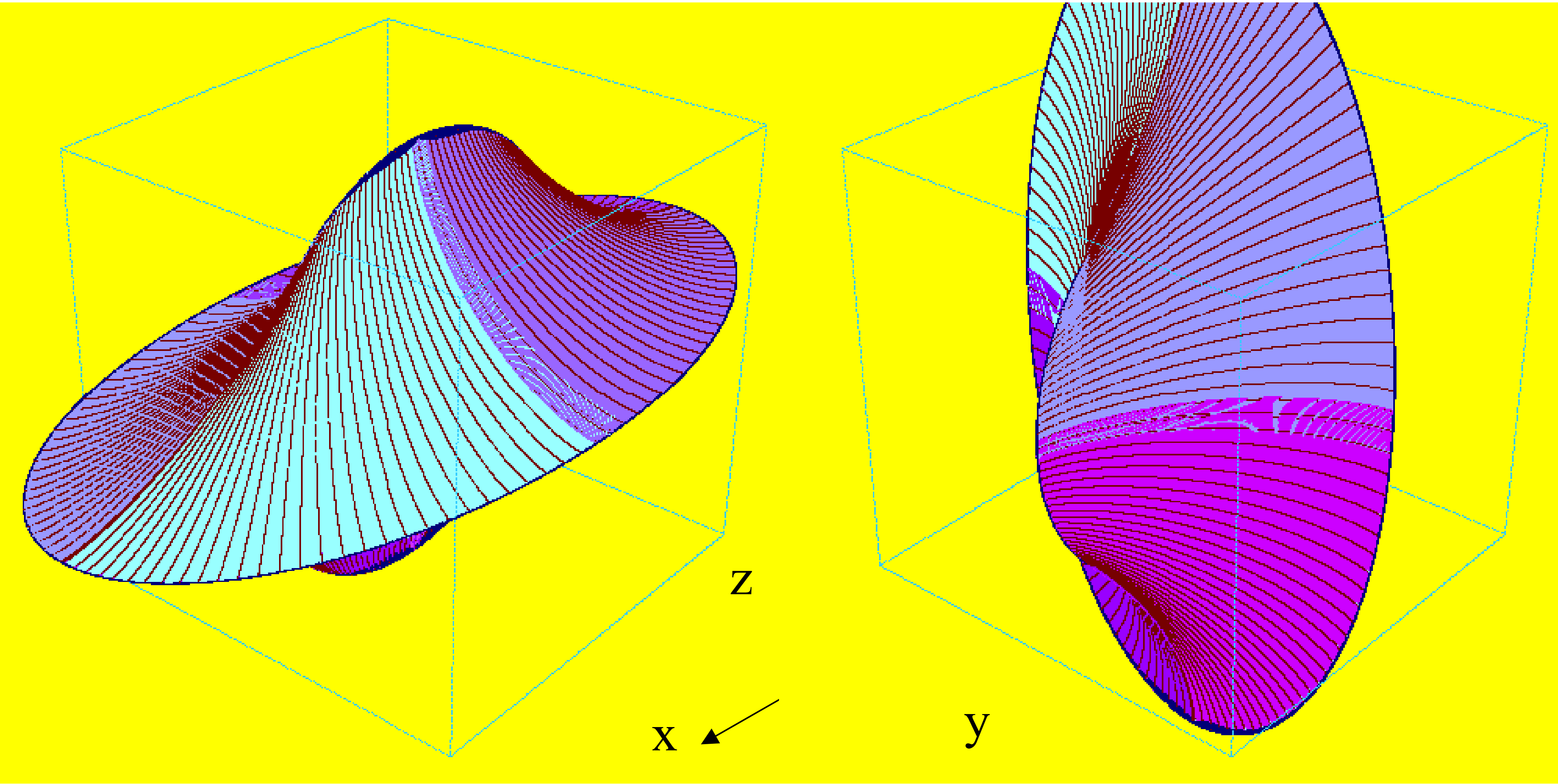

x : hard axis ; z : easy axis ; y : intermediate

$$G = m_x^2 m_y^2 + m_y^2 m_z^2 + m_z^2 m_x^2$$

surface S_+ surface S_-

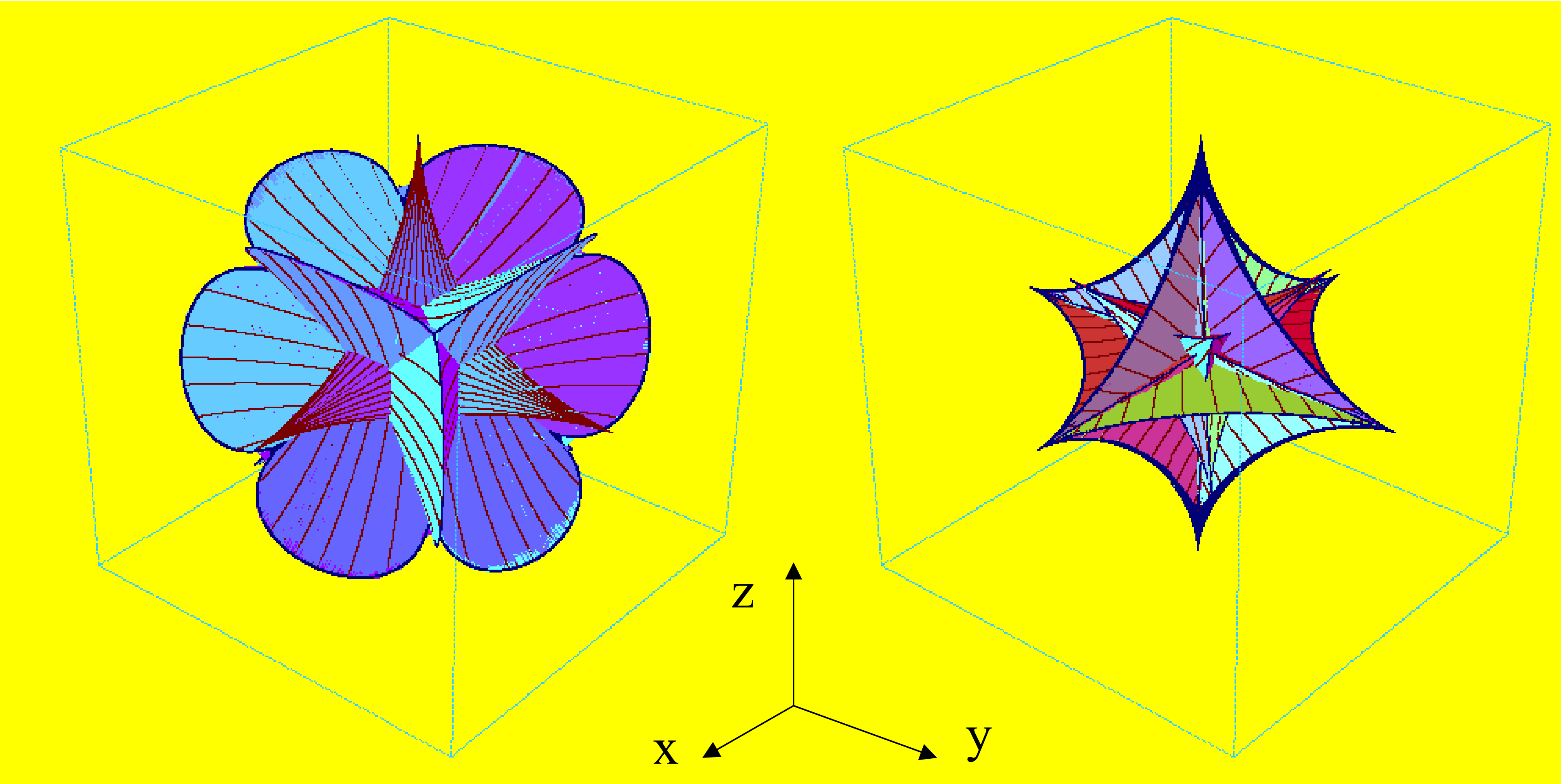

iron sphere nickel sphere

A. Thiaville, Phys. Rev. **B61** 12221 (2000)

Measurements on an isolated nanoparticle

(E. Bonet et coll., Phys. Rev. Lett. 83, 4188 (1999))

Zone axis for 18 cuts

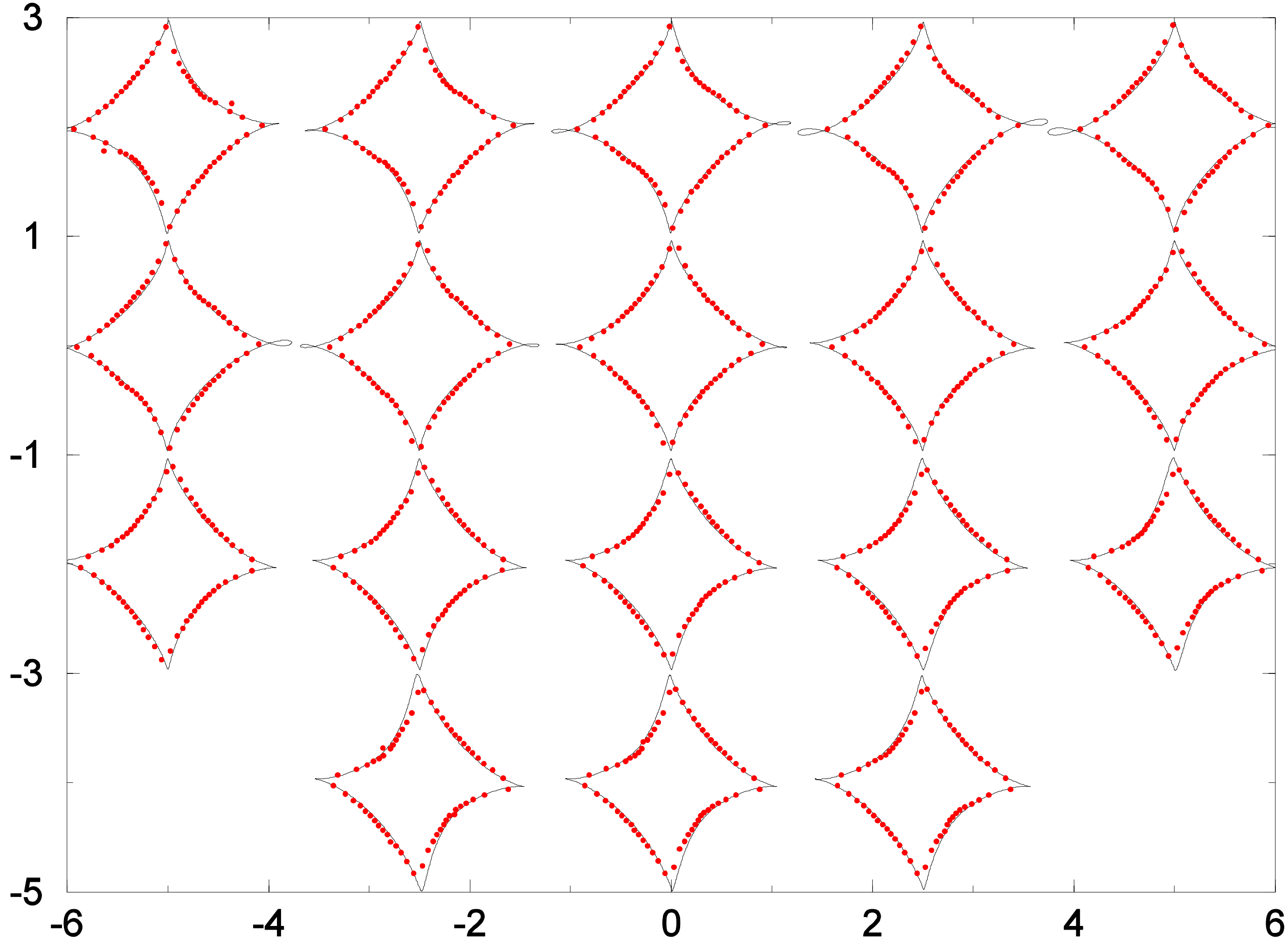

G= degree 2 +(degree 4 et 6, disoriented)

The anisotropy energy of that nanoparticle

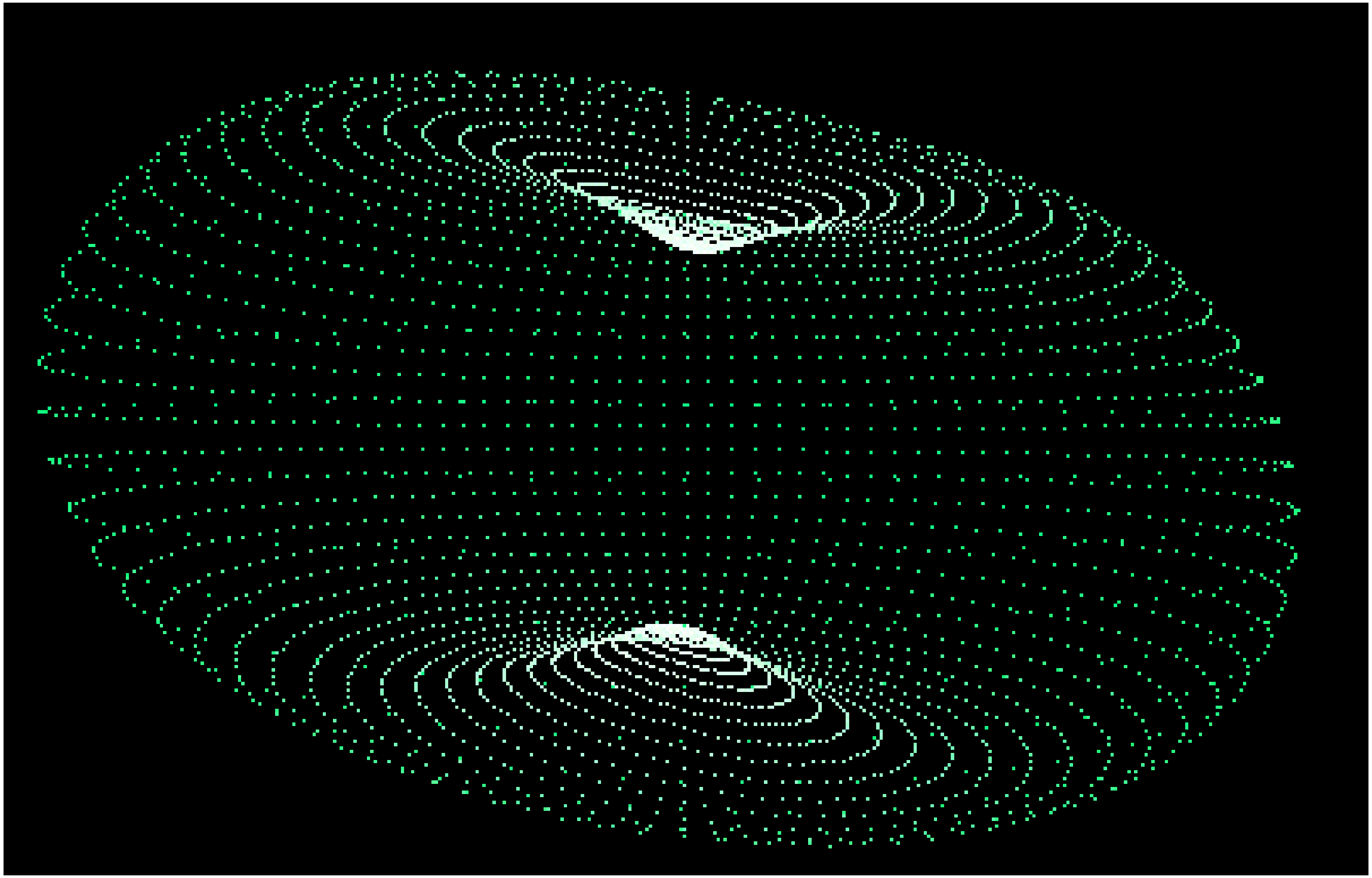

3 nm cobalt cluster

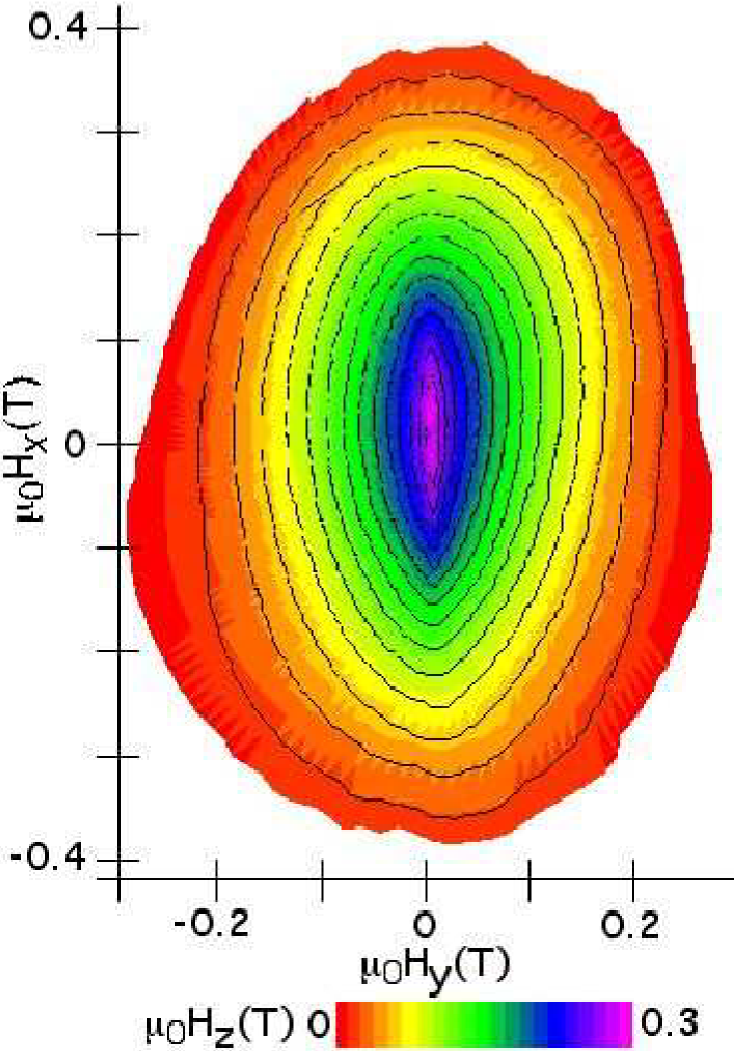

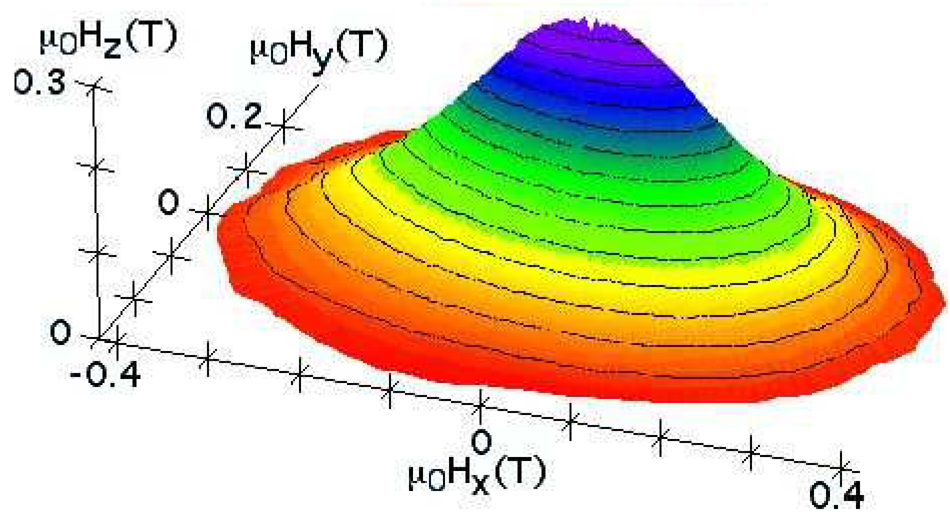

Thèse M. Jamet, Lyon 2001
W. Wernsdorfer
Adv. Chem. Phys.
118 (2001)

Fig. 2.6 Top view and side view of the experimental three dimensional angular dependen
of the switching field of a 3 nm Co cluster at 35 mK. This surface is symmetrical with resp
to the H_x–H_y–plane and only the upper part ($\mu_0 H_z > 0$ T) is shown. Continuous lines
the surface are contour lines on which $\mu_0 H_z$ is constant.

Surface anisotropy in ultrathin films

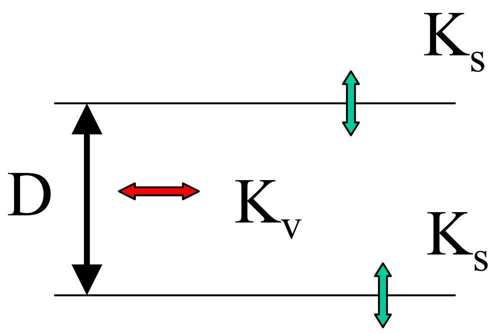

$$K_{eff} = K_v + 2\ K_s/D$$

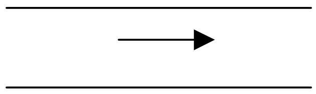

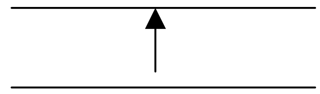

$K_{eff} < \mu_0\ M_s^2/2$ | $K_{eff} > \mu_0\ M_s^2/2$

K_s : 10^{-3} J/m^2

D_c : 1 nm

Transition thickness $$D_c = \frac{2K_s}{\mu_0 M_s^2 / 2 - K_v}$$

Another 3 nm cobalt cluster

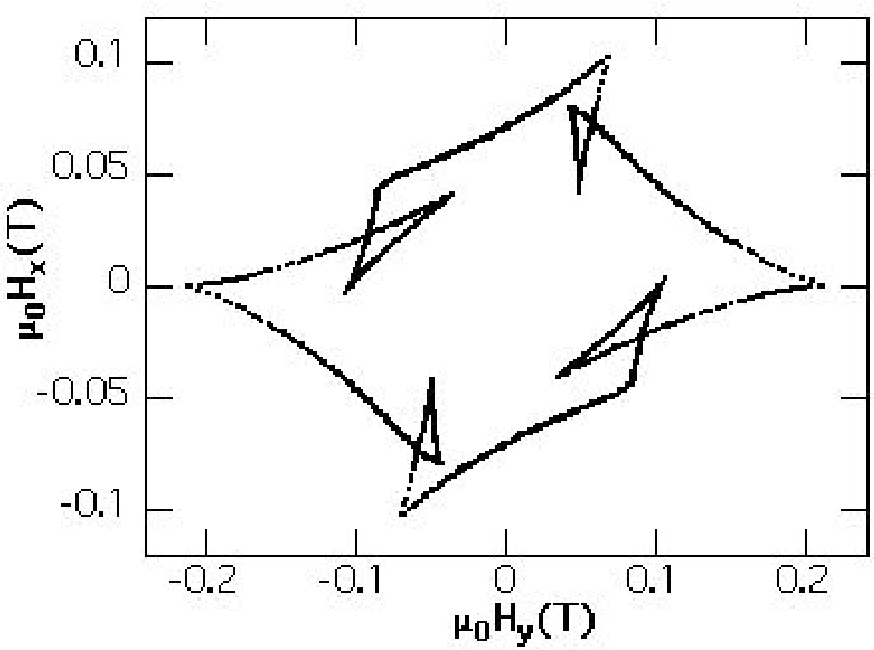

Fig. 2.11 Angular dependence of the switching field of a 3 nm Co cluster showing a strong influence of crystalline anisotropy.

W. Wernsdorfer Adv. Chem. Phys. **118** (2001)

A cube with uniaxial anisotropy

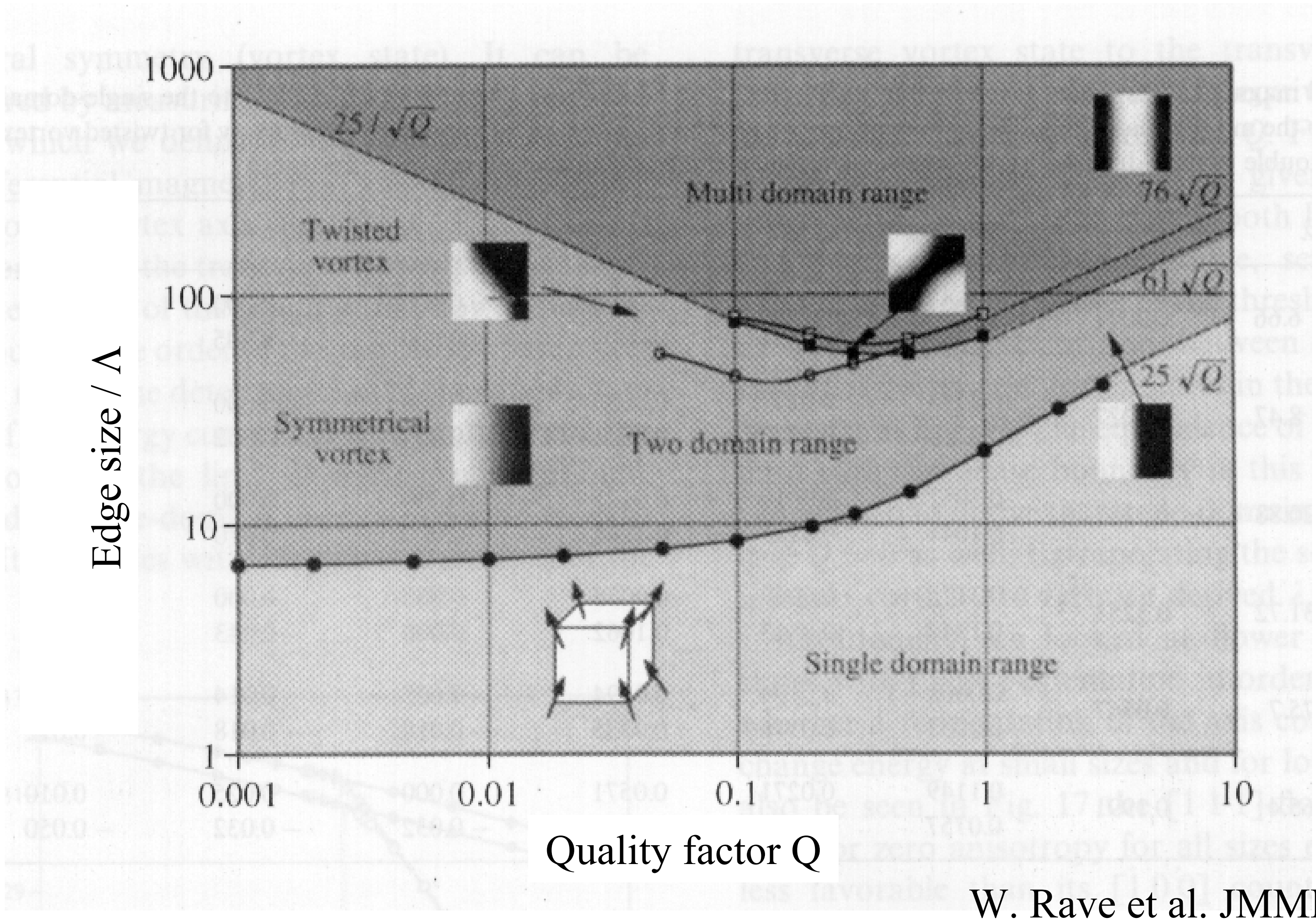

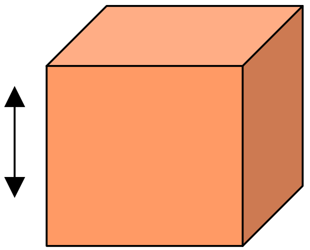

$$Q = \frac{2K}{\mu_0 M_s^2}$$

W. Rave et al. JMMM **190** 332 (1998)

A square platelet

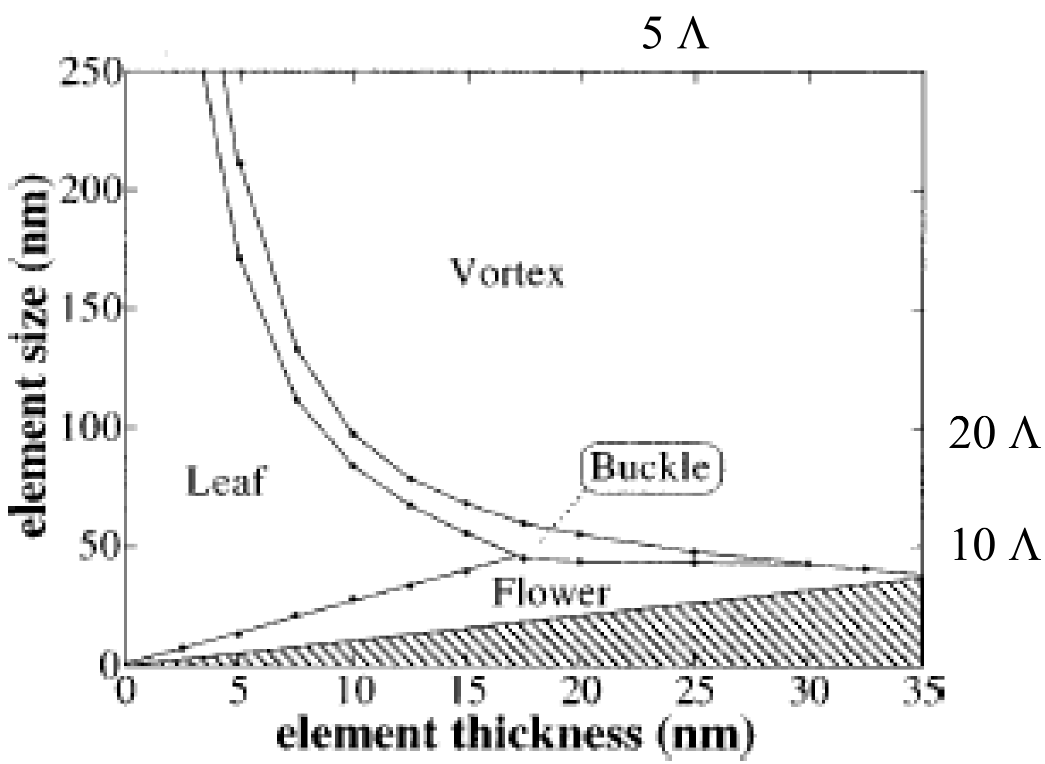

FIG. 3. The magnetic phase diagram of square planar nanostructures. The diagram gives the (global) lowest energy magnetization configuration as a function of the magnetic element size and thickness. The shaded region represents columnar elements which have not been addressed in this work.

permalloy Λ= 5 nm

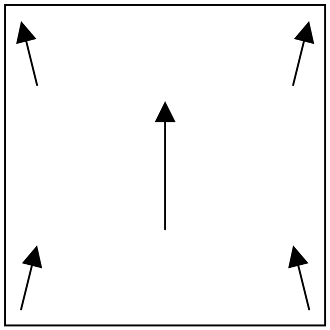

flower

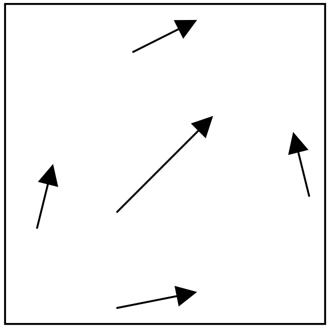

leaf

R.P. Cowburn et al. APL 72 2041 (1998)

Configuration anisotropy

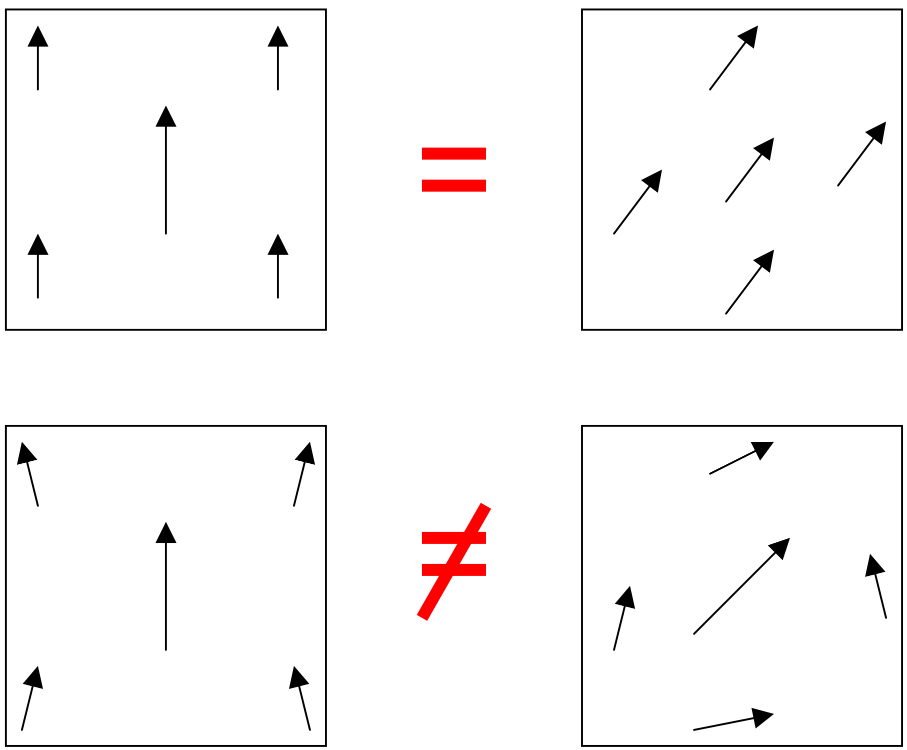

permalloy :
no anisotropy

R.P. Cowburn et al. APL **72** 2041 (1998); Phys. Rev. B (1998)

Phase diagram of domain walls in a soft nanostrip

permalloy $\Lambda = 5$ nm

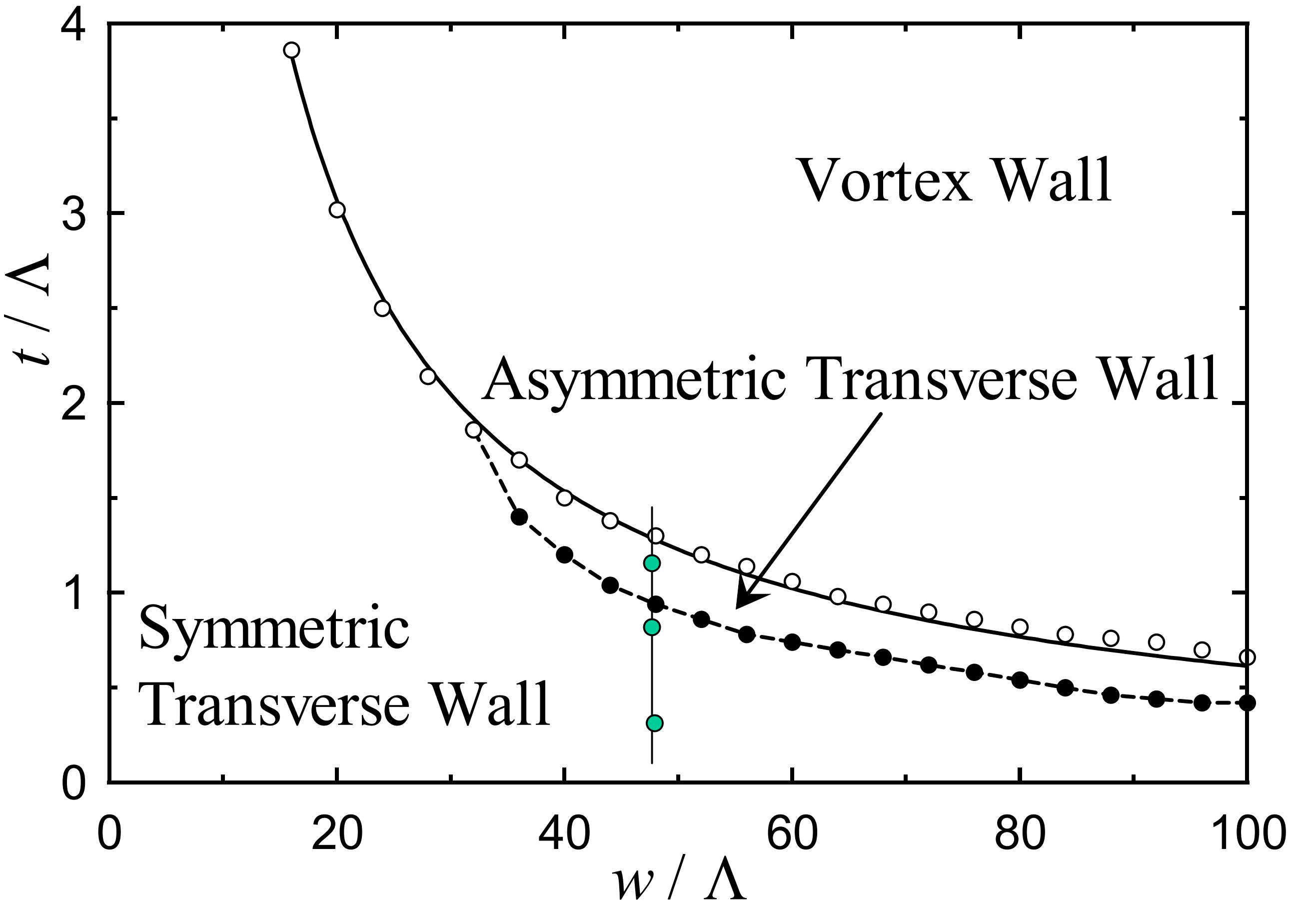

$t = 7.5$ nm : VW

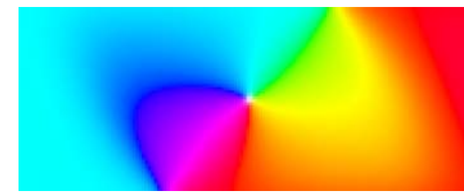

$t = 6.0$ nm : ATW

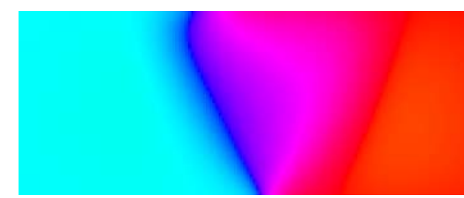

$t = 3.5$ nm : TW

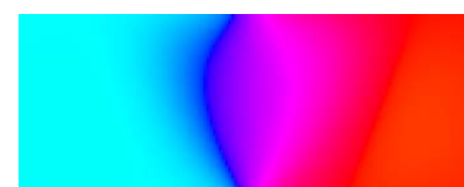

Y. Nakatani et al. JMMM **290-291** 750 (2005)

Macrospin : magnetization reversal strategies

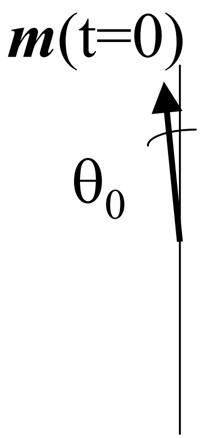

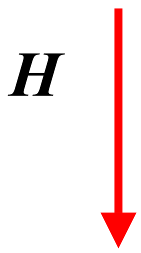

$d\varphi/dt = \gamma_0 H$

$d\theta/dt = \alpha\gamma_0 H\theta$

$\theta = \alpha\theta_0 \quad \gamma_0 H t$

θ_0 : thermal fluctuations

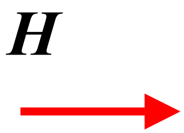

$d\theta/dt = \gamma_0 H$

$\theta = \gamma_0 H t$

Precessional switching

Precessional switching in a platelet

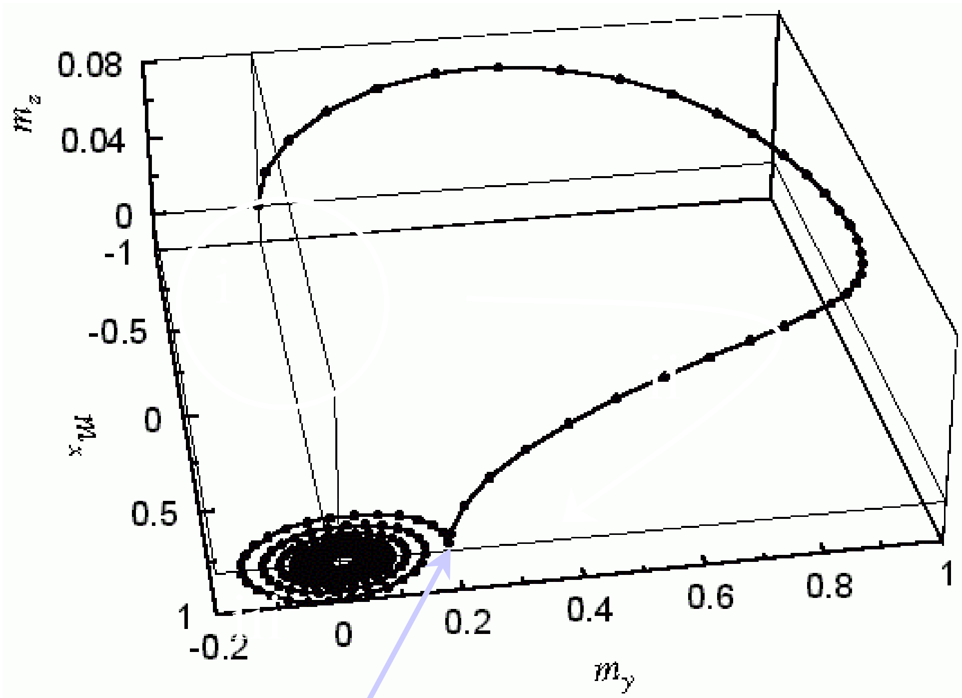

A basically 2 step process

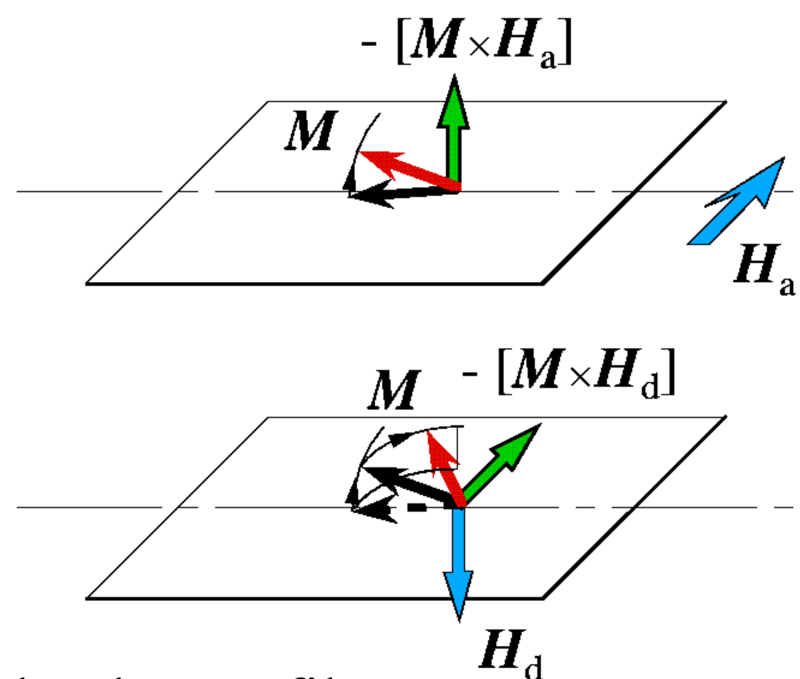

Field cutoff strategy: Magnetisation vector back to the film plane

Field pulse profile

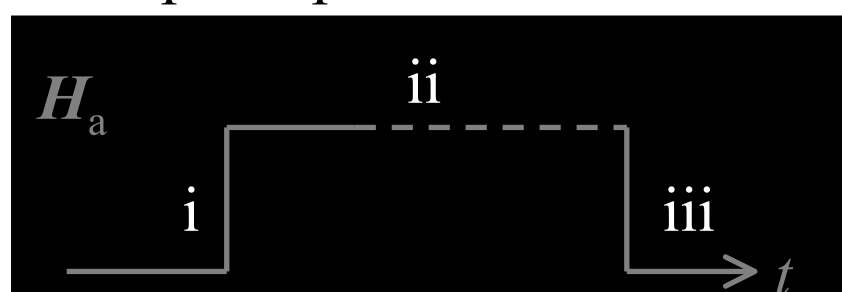

Thèse G. Albuquerque, Orsay, 2002

Macrospin magnetisation trajectories

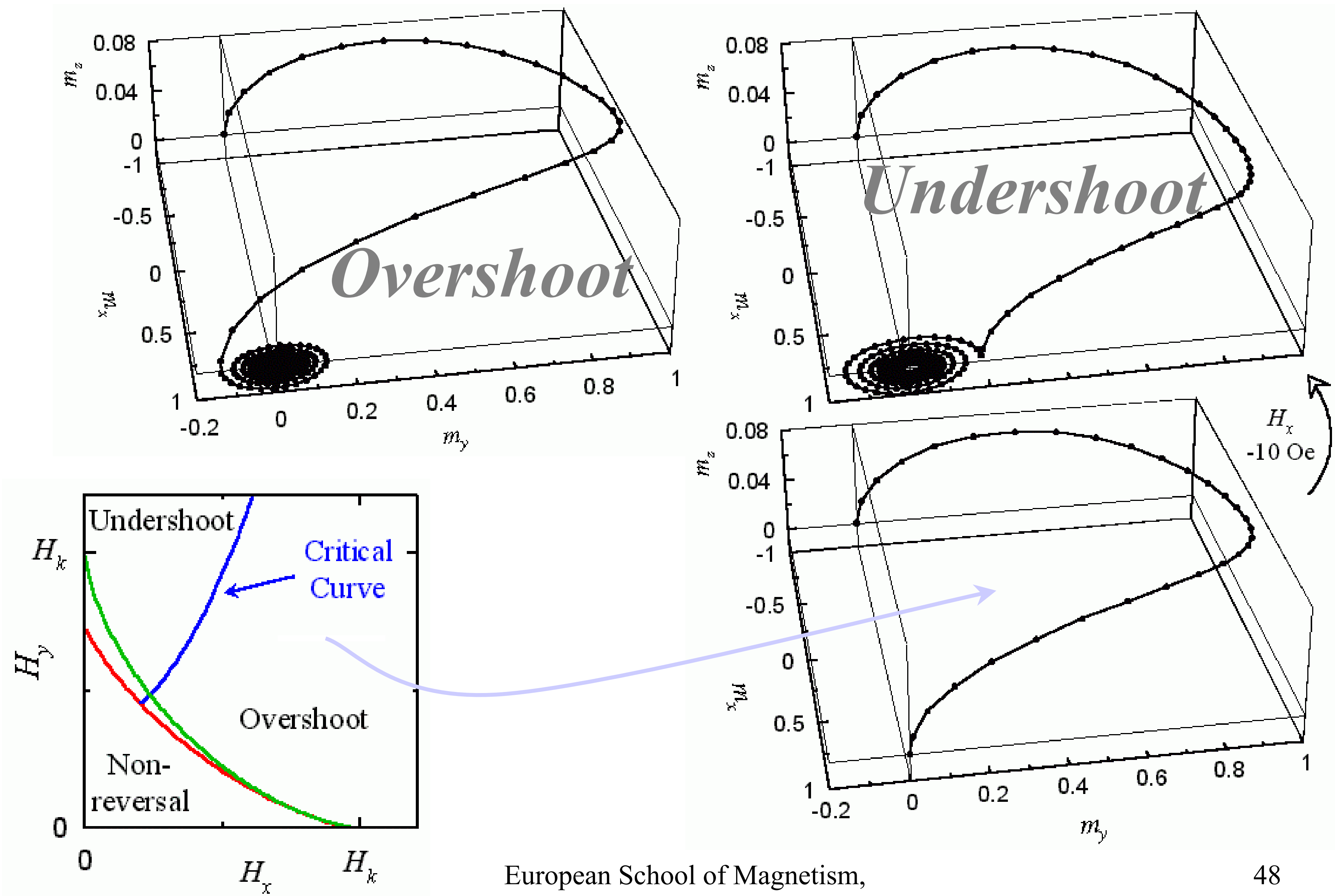

Thèse G. Albuquerque, Orsay, 2002

Macrospin precessional dynamics : switching phase diagram

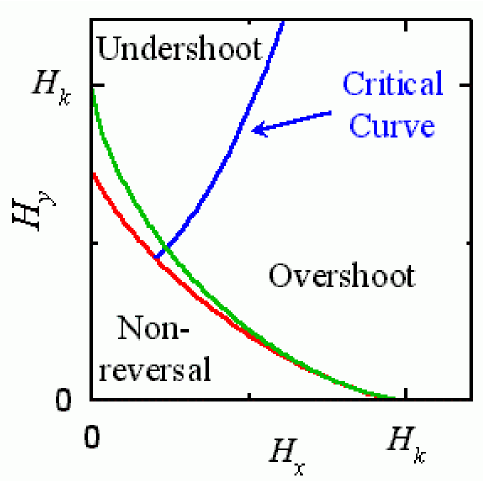

Green: Static switching threshold
Red: Dynamic switching threshold
Blue: Ballistic trajectories

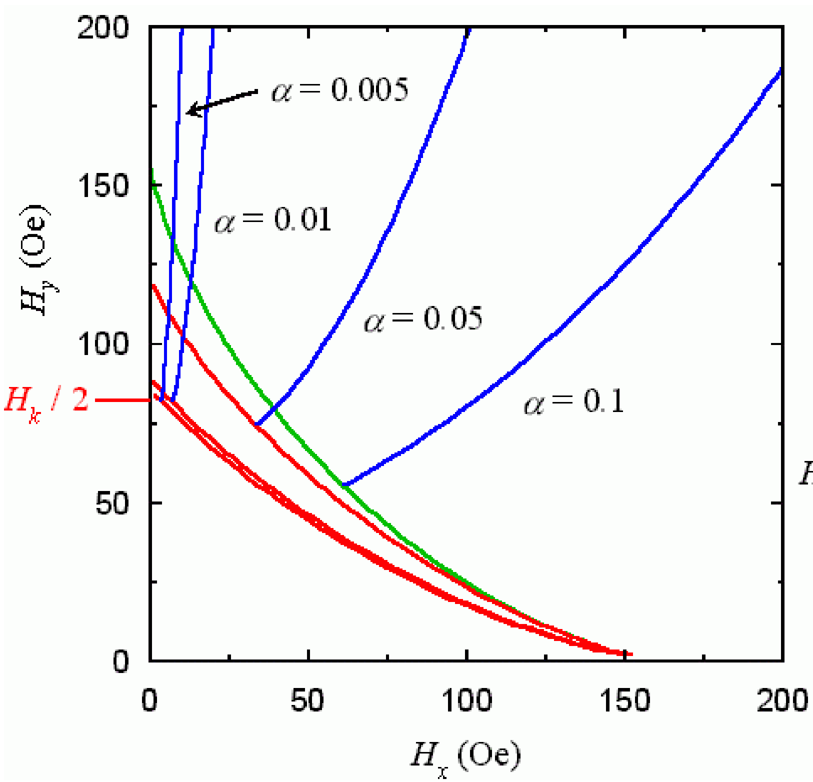

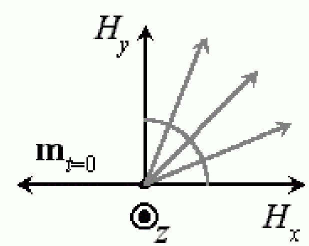

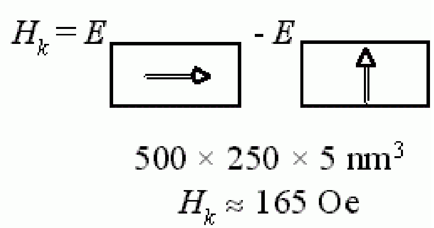

Main Conclusion:
Switching possible below the static threshold

Most favorable case:
Transverse field
$H_y = H_k/2$

Thèse G. Albuquerque, Orsay, 2002

Precessional switching of a MRAM memory cell

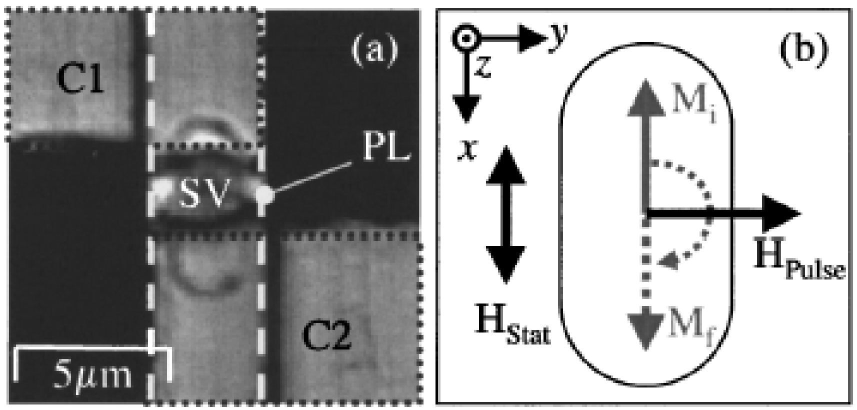

FIG. 1. Magnetic memory cell used in the experiments. (a) Optical micrograph. Spin valve cell (SV) with electrical contacts (C1, C2, surrounded by the dotted lines) and buried pulse line (PL, marked by the white dashed line). (b) Sketch of the magnetic field configuration H_{pulse} (along y) is applied perpendicular to the initial and final magnetization $\boldsymbol{M}_i$, $\boldsymbol{M}_f$.

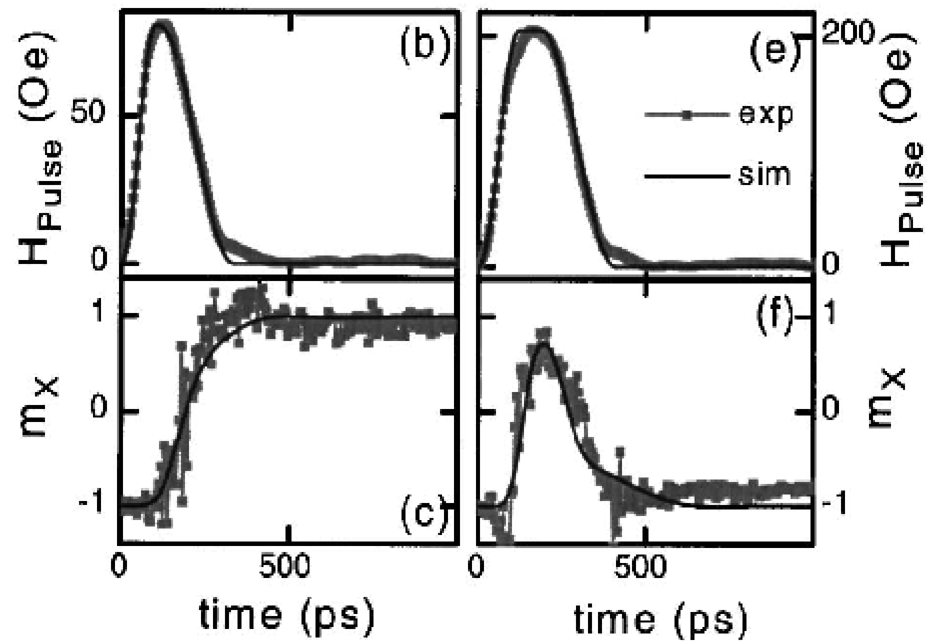

H= 81 Oe
T= 175 ps

H= 205 Oe
T= 240 ps

H.W. Schumacher et al.
Phys. Rev. Lett. **90** 017204 (2003)

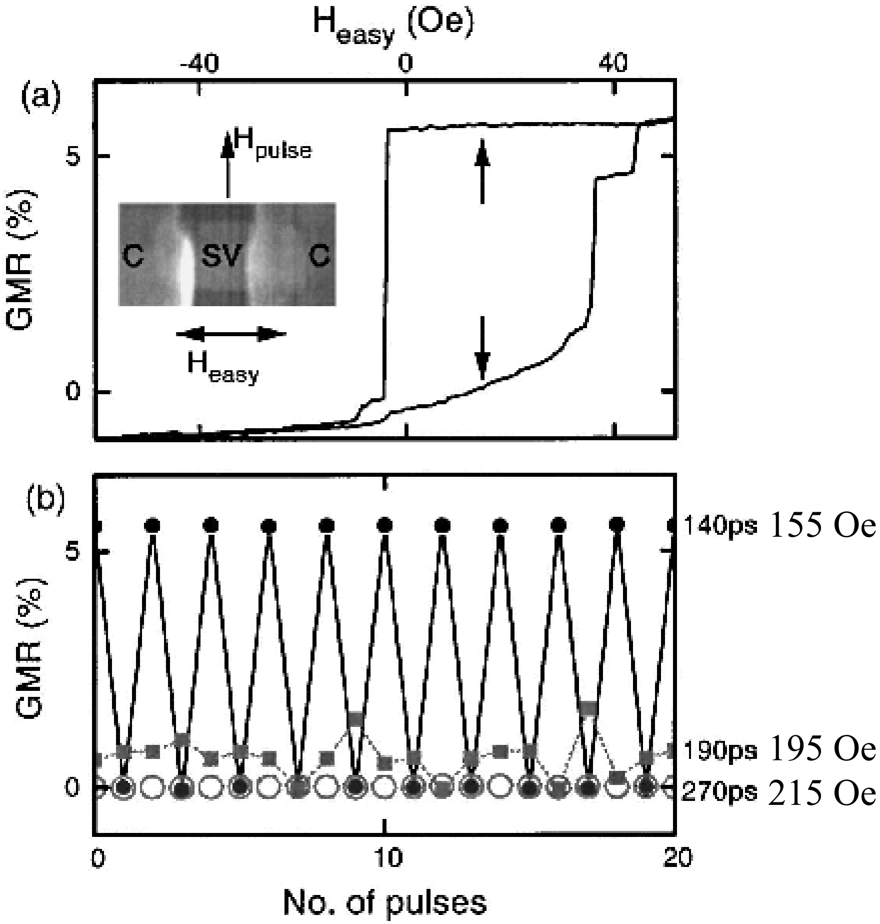

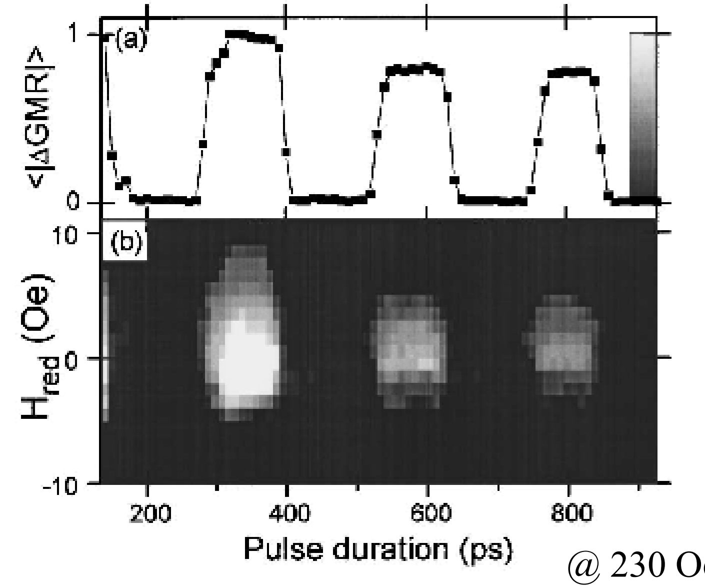

H.W. Schumacher et al.
Phys. Rev. Lett. **90** 017201 (2003)

Precessional reversal of small elements

NiFe 500x 250x 5 nm,   « S » state

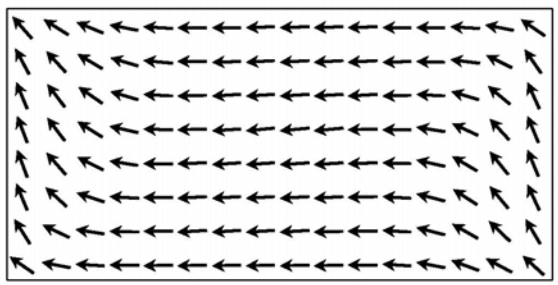

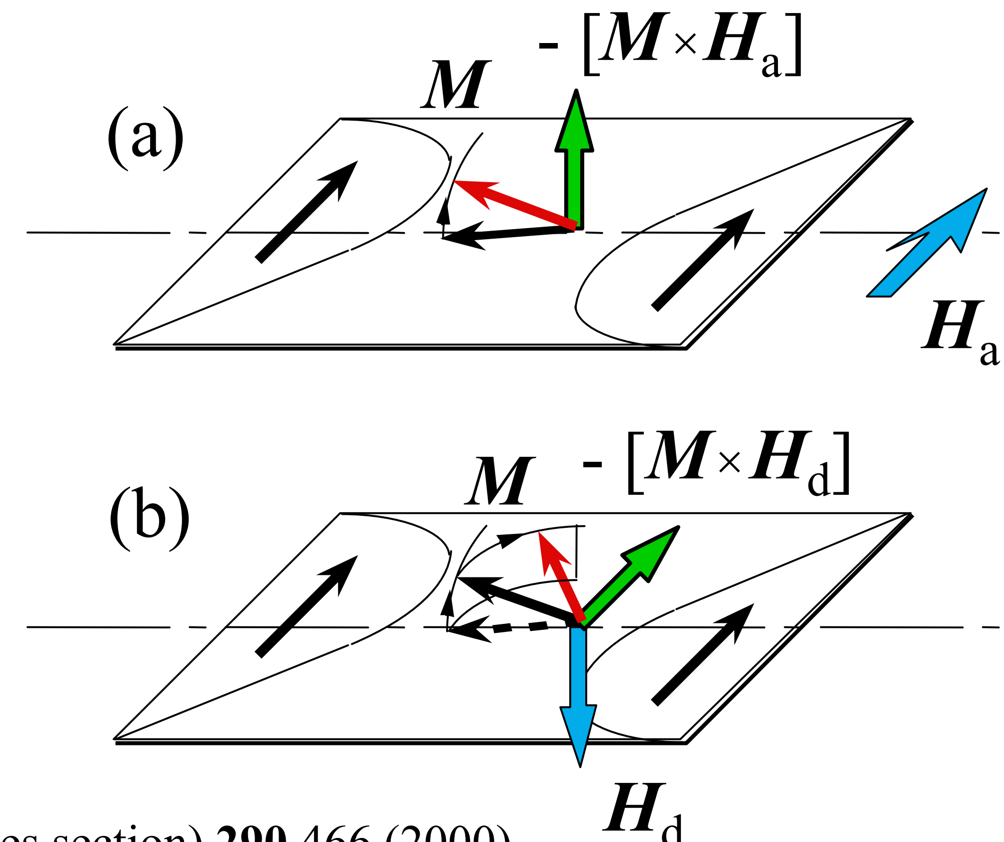

J. Miltat, A. Thiaville Science (perspectives section) **290** 466 (2000)

(1) Initial phase :
quasi-coherent
reversal

250 ps

J. Miltat et al., in
Spin Dynamics in confined structures I,
B. Hillebrands and
K. Ounadjela Eds.
(Springer, 2002)

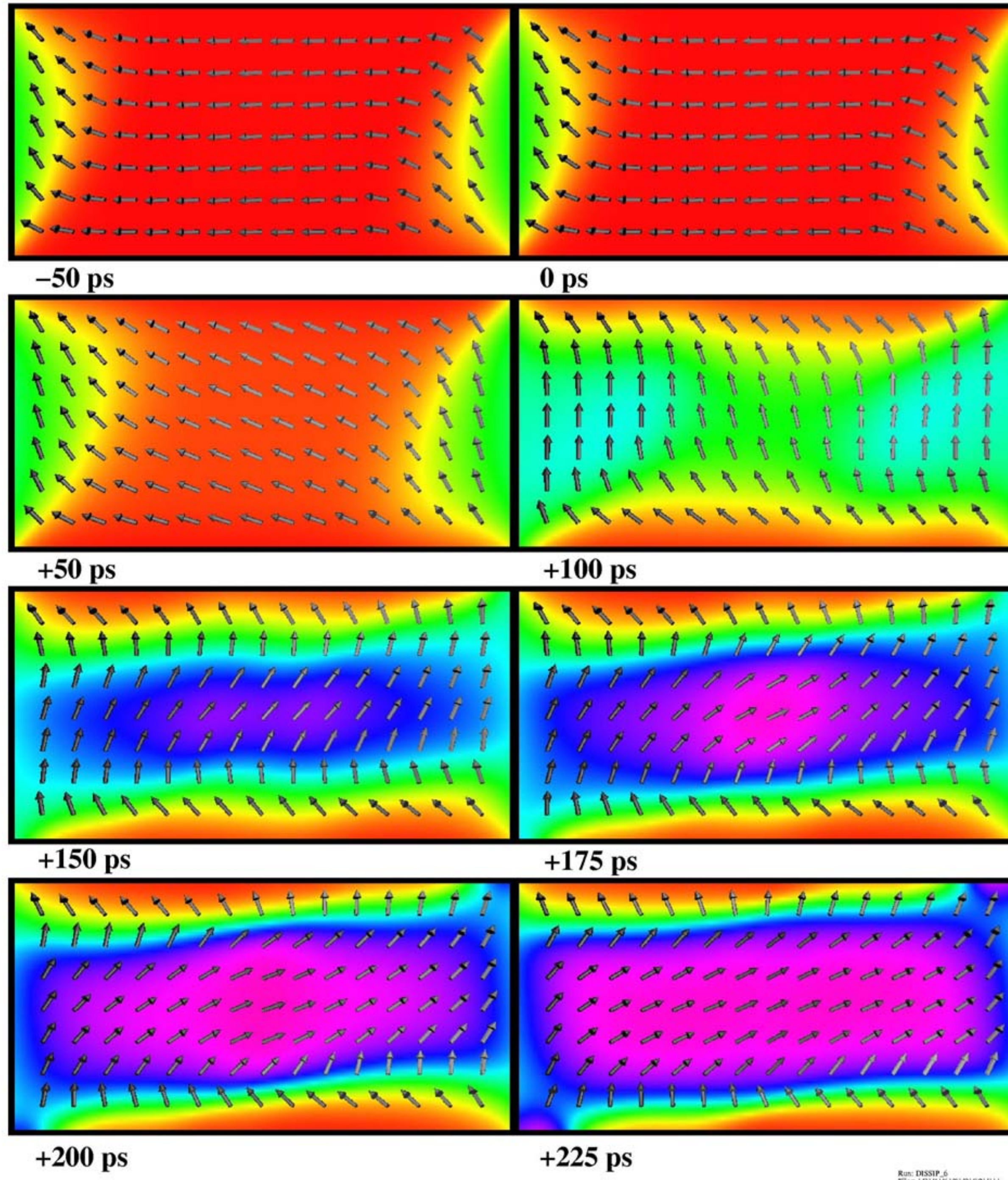

(2) Breaking into magnetization waves with large out of plane components

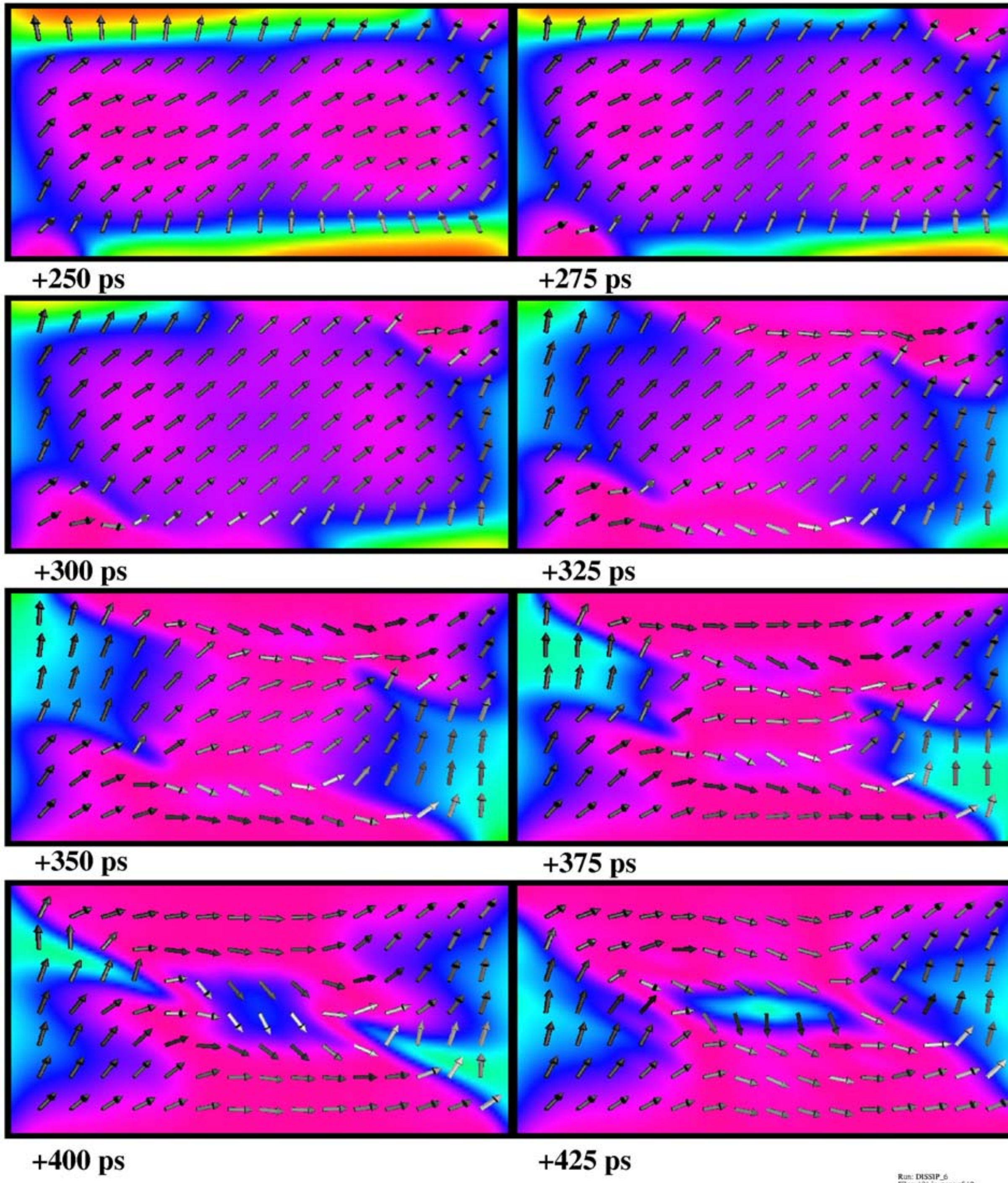

MFM of magnetic dots in a vortex state

First observation: T. Shinjo et al., Science **289** (2000) 930

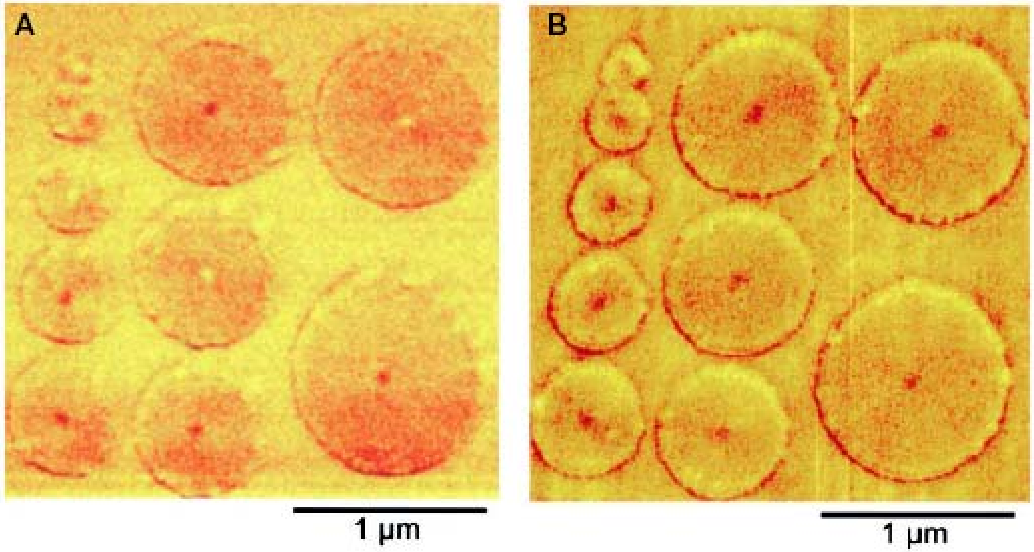

Natural state After saturation under 1 T

Sample : permalloy, 50 nm thick

Vortex core switching : Experimental measurements
T. Okuno *et al.*, J. Magn. Magn. Mater. 240, 1 (2002)

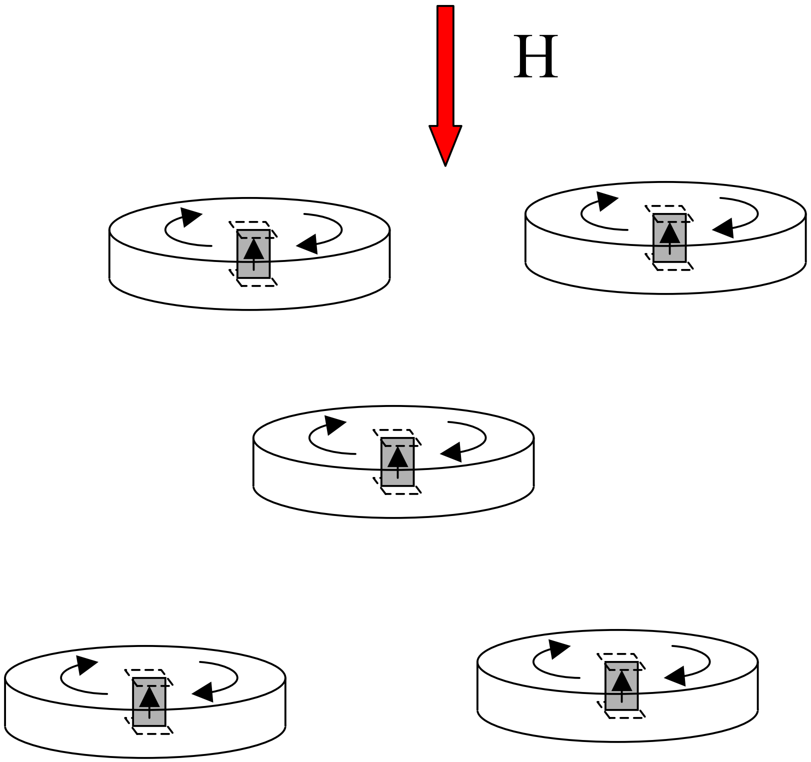

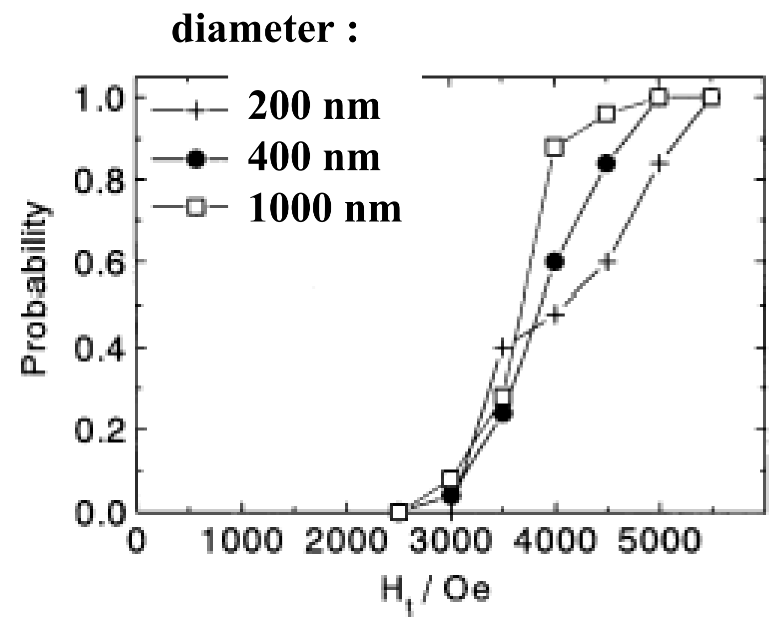

Fig. 5. Switching probability of a turned-up magnetization in circular dots with the diameter of 0.2, 0.4 and 1 μm as a function of magnetic field normal to the sample plane. The average switching field is 4100, 3900 and 3650 Oe in the sample of 0.2, 0.4 and 1 μm in diameter, respectively.

A Bloch point mediates the vortex core switching

B: from 331 to 332 mT
at *t*=0

d=100 nm
thickness=50 nm
mesh: 4x4x5 nm
damping α= 0.5

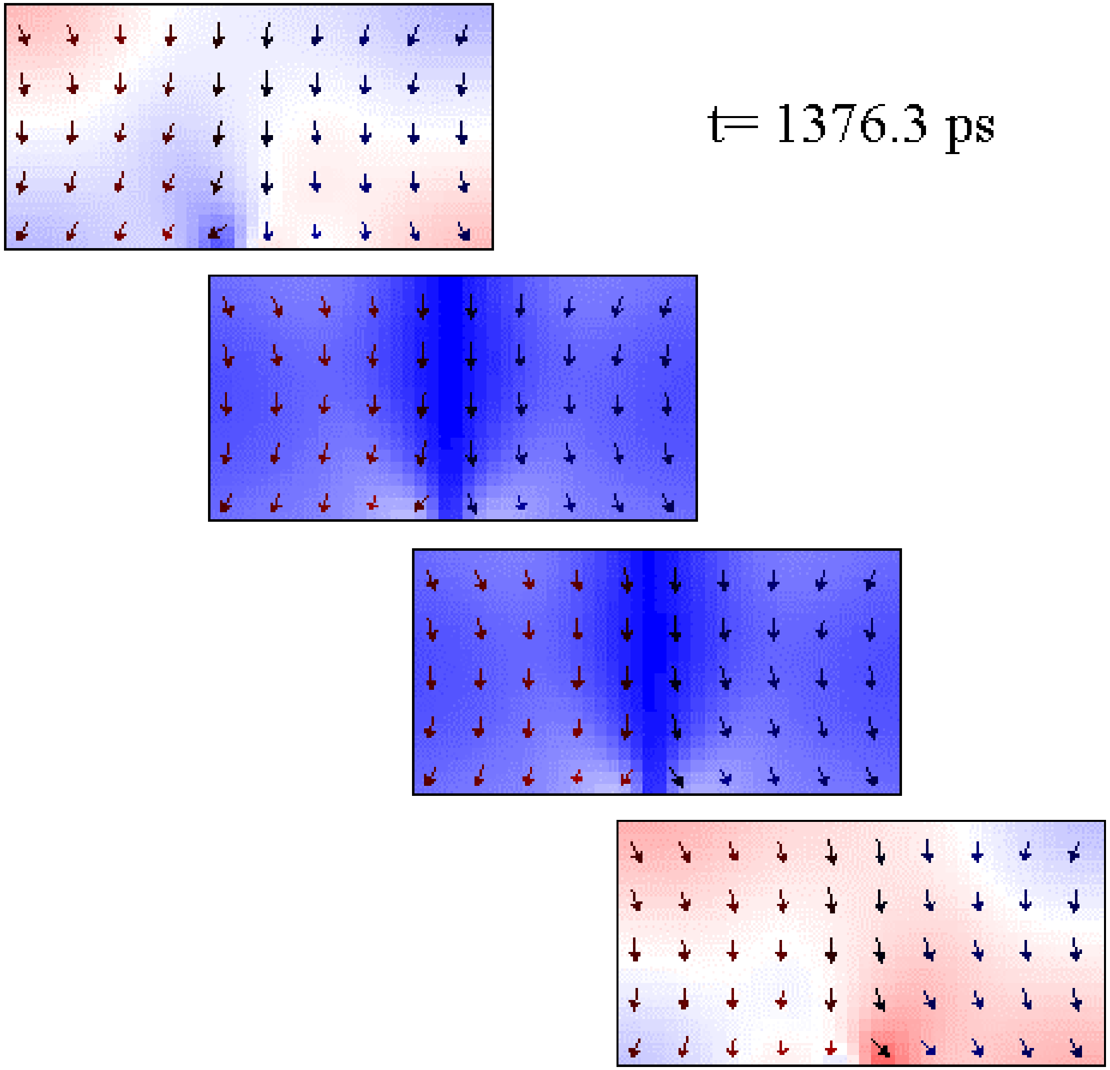

t= 1376.3 ps

Bloch points at zero field

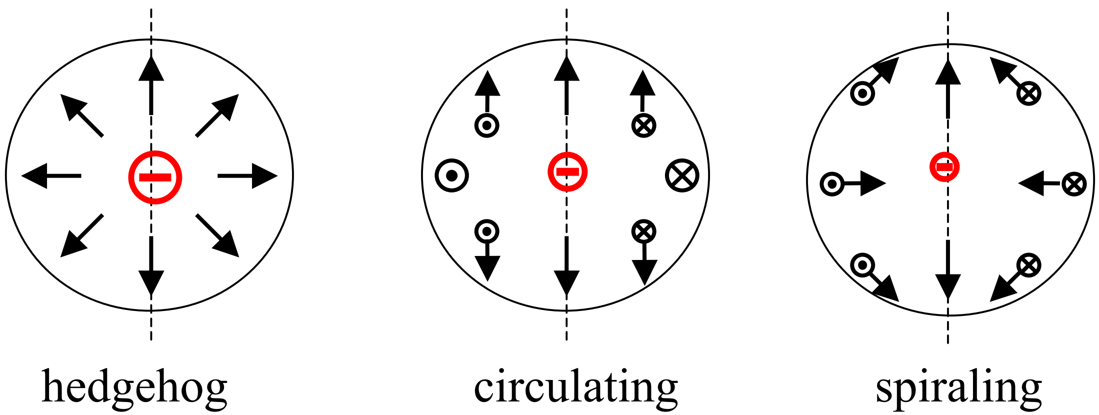

E. Feldtkeller
Z. angew. Phys.**19** 530 (1965)

The exchange energy density diverges at the center (singularity)

It is lowest when $\vec{m}=\frac{\vec{r}}{r}$ up to a uniform rotation

$\varepsilon_A = (2A/r^2)$ $E_A = 8\pi\, A\, R$ R: radius of the BP structure

Bloch points at zero field : calculated structure

Vortex (diameter=200 nm, thickness=50 nm, meshing=2.5 nm; image size: 60nm)

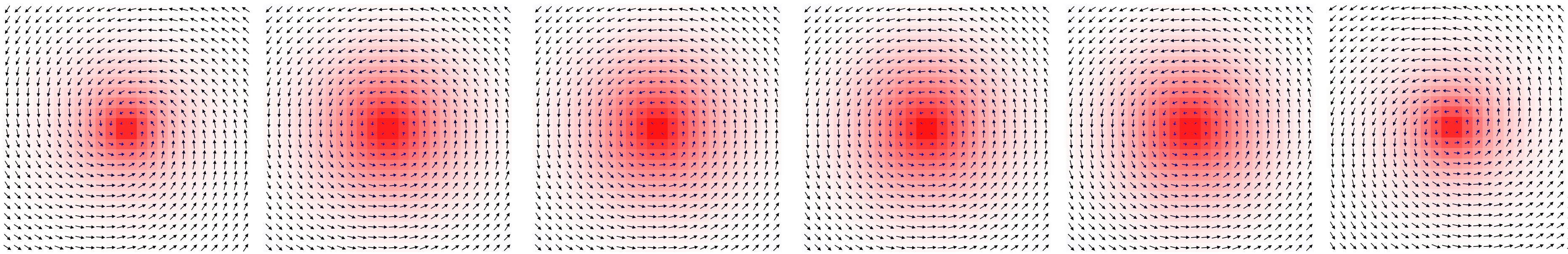

z= 0 nm | z= 22 nm | z= 24 nm | z= 26 nm | z= 28 nm | z= 50 nm

color code

Vortex with a Bloch point in the middle

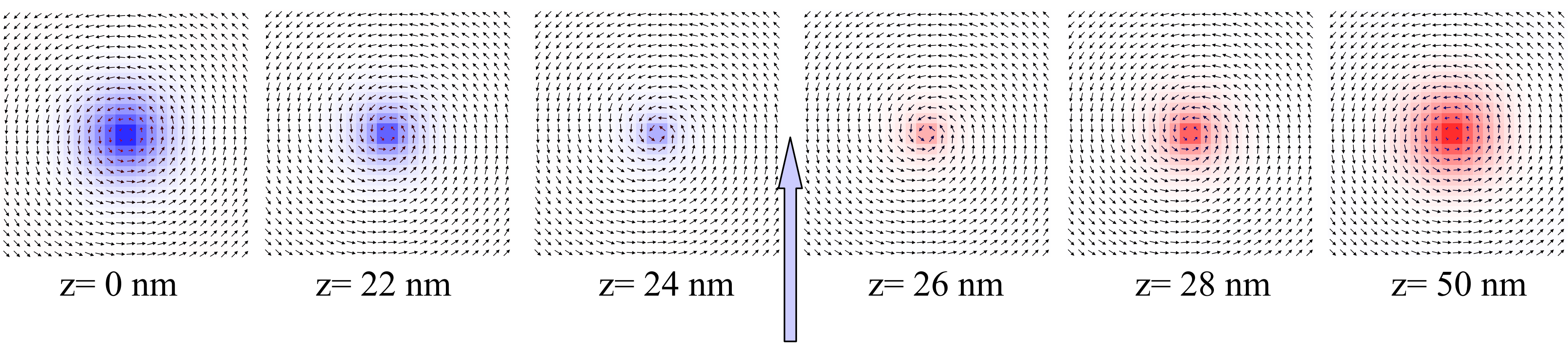

z= 0 nm | z= 22 nm | z= 24 nm | z= 26 nm | z= 28 nm | z= 50 nm

The BP is stabilized at zero H because of mesh friction; as soon as the BP is not perfectly centered it is expelled

A. Thiaville et al. PRB **67** 094410 (2003)

Domain wall dynamics in nanowires

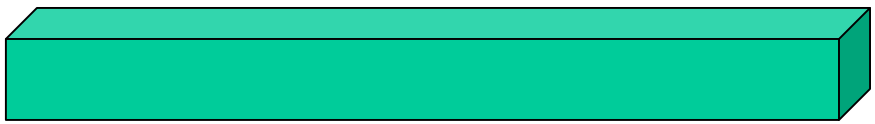

Cobalt 30 x 30 nm

diamètre 32, 64 nm

Permalloy $Ni_{80}Fe_{20}$

200 x 5 nm

Confinement effect on the domain wall width

P. Bruno, Phys. Rev. Lett. **83** 2425 (1999)

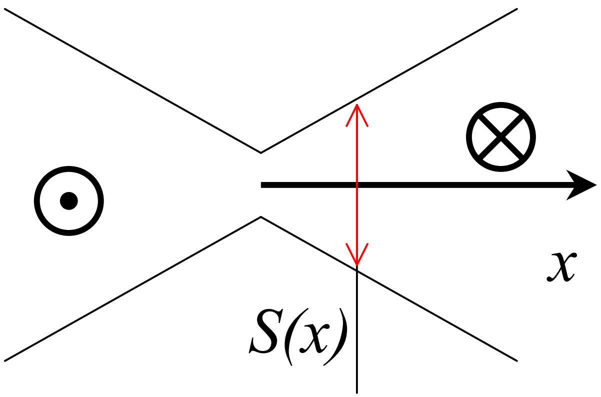

$$E = \int \left[A\left(\frac{d\theta}{dx}\right)^2 + K \sin^2\theta \right] S(x)\,dx$$

$$\cancel{2K \sin\theta \cos\theta S} - \frac{d}{dx}\left(2A\frac{d\theta}{dx}S\right) = 0$$

$$\theta = C\int \frac{dx}{S(x)}$$

$$S = S_0\left(1 + \left(\frac{x}{d}\right)^2\right) \Rightarrow \theta = Arctg\left(\frac{x}{d}\right)$$

$$S = S_0\left(1 + \frac{|x|}{d}\right)^2 \Rightarrow \theta = \frac{\pi}{2}\frac{x}{|x| + d}$$

$\vdots$

wall width $\propto d$

Wall structure in a nanowire

Cobalt, 30x30 nm, maille 3 nm (167x 10x 10 points)

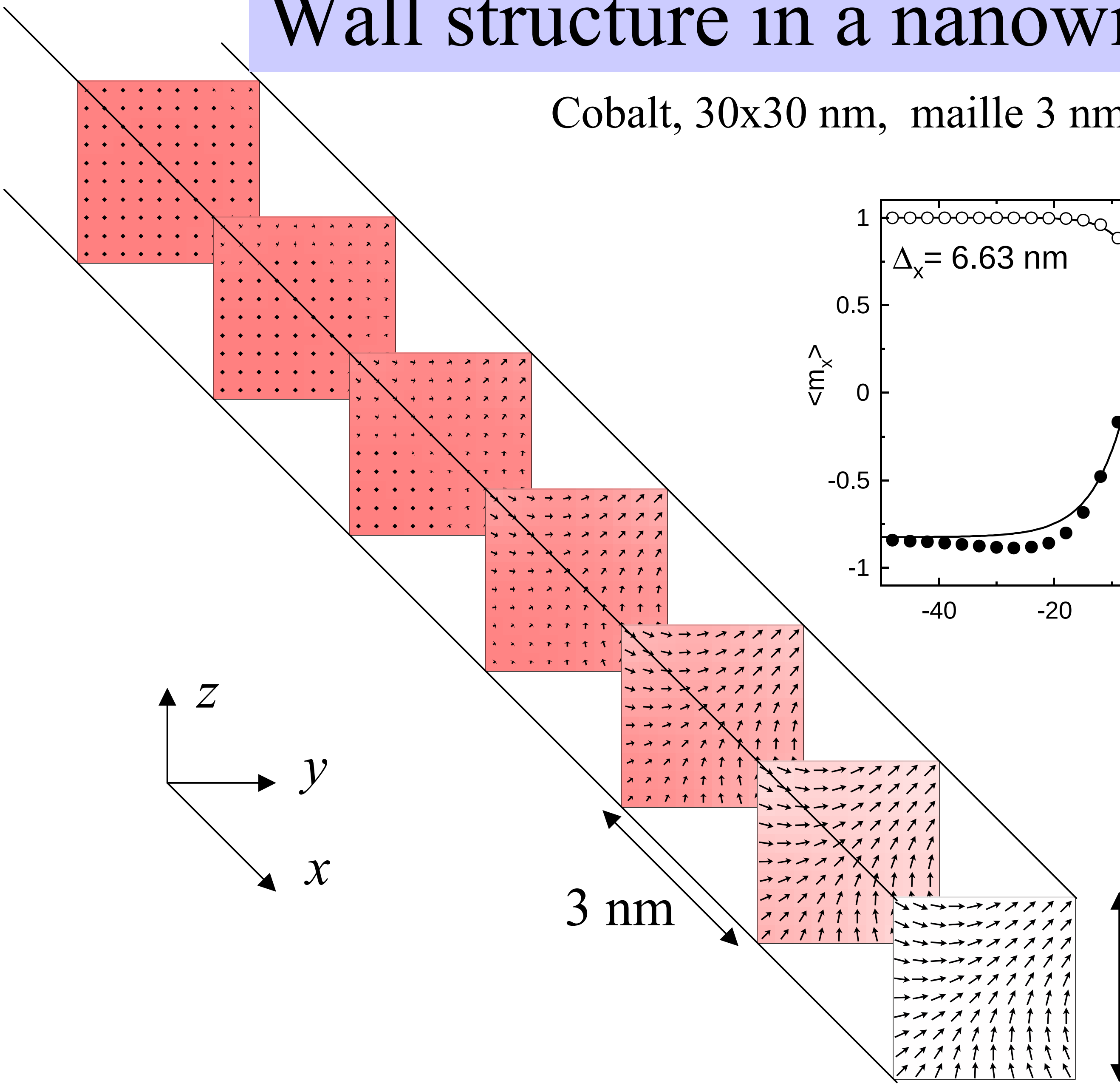

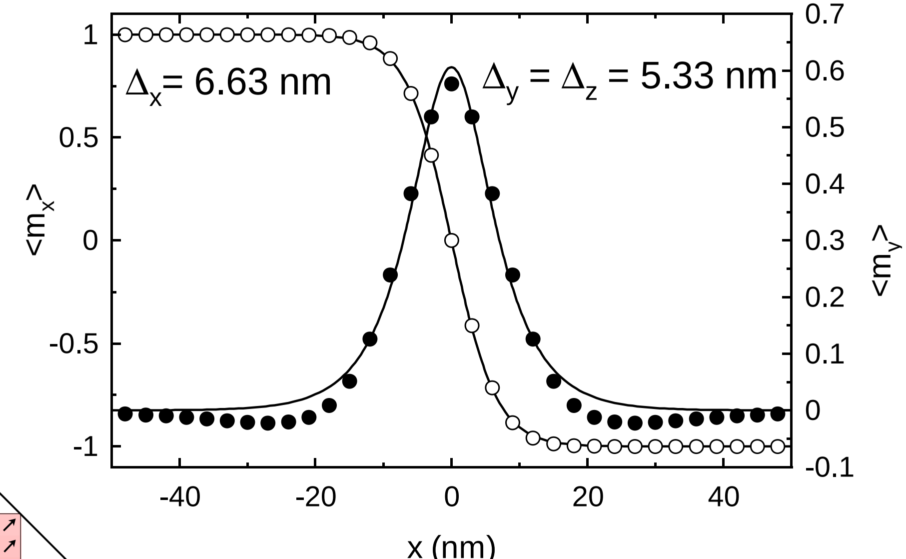

$$m_x \approx -\tanh(x/\Delta)$$
$$m_y \approx 1/\mathrm{ch}(x/\Delta)$$

Wall dynamics under field

Damping constant α= 0.1

H = 50 Oe

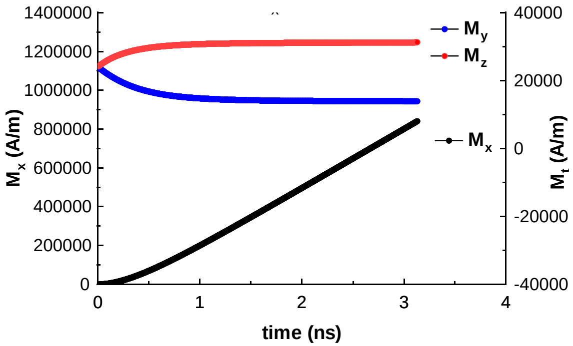

H = 100 Oe

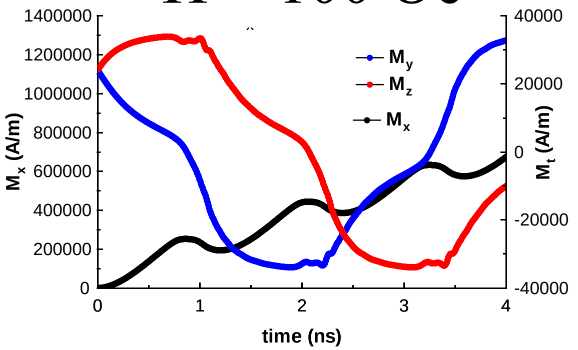

H = 150 Oe

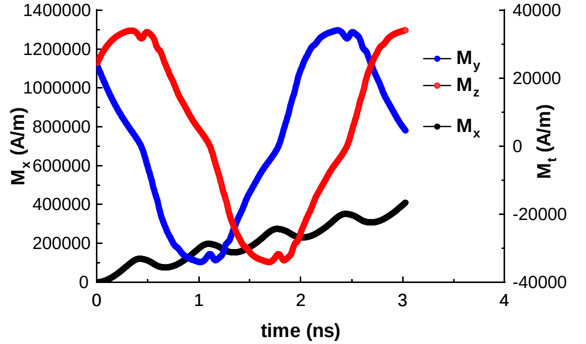

Angle of the transverse magnetization

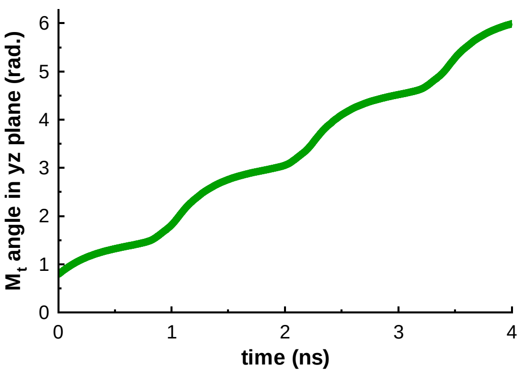

(

Bloch point wall in a cobalt nanowire

Cobalt, 30x30 nm, mesh 3 nm (167x 10x 10 points)

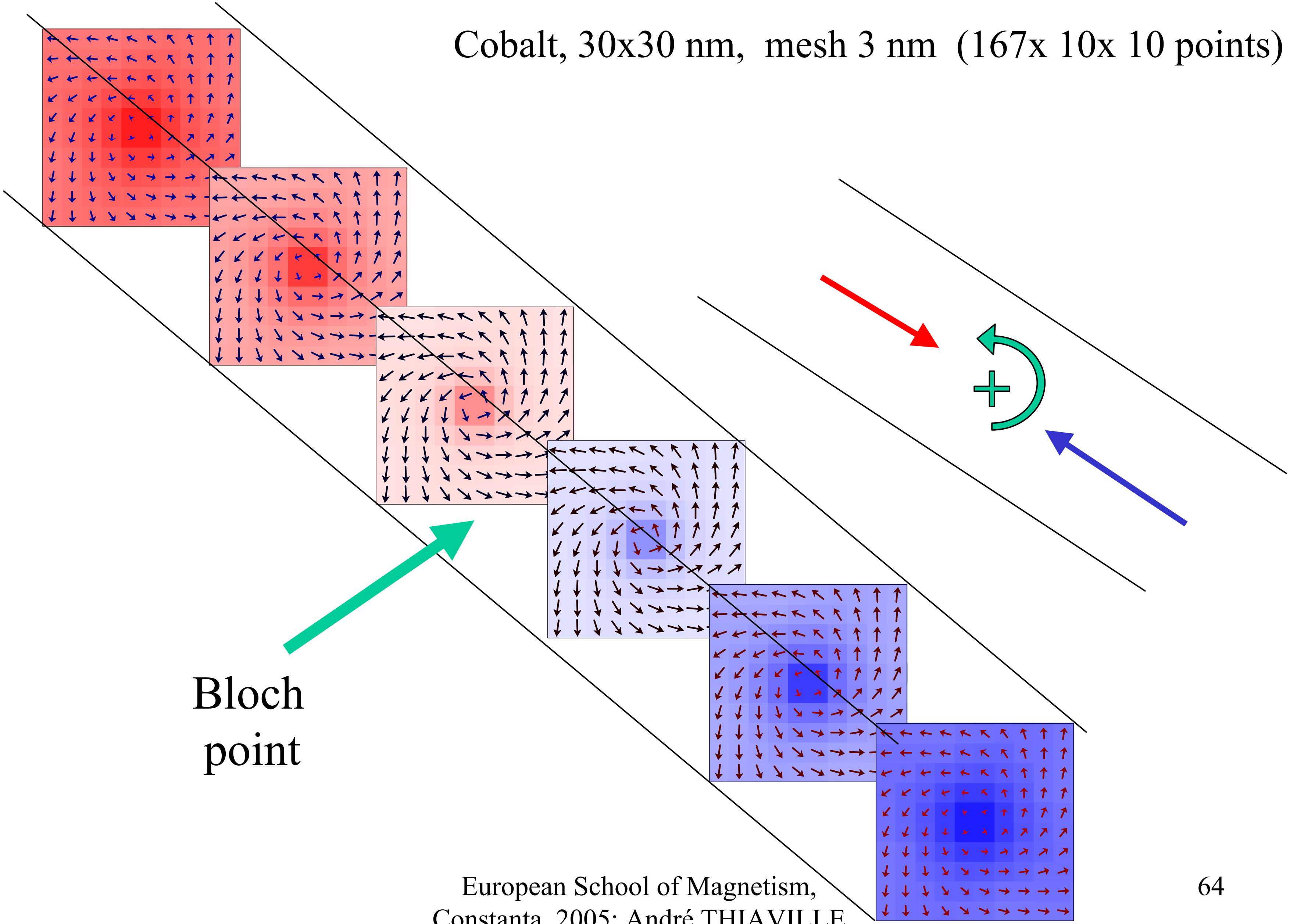

A permalloy nanostrip

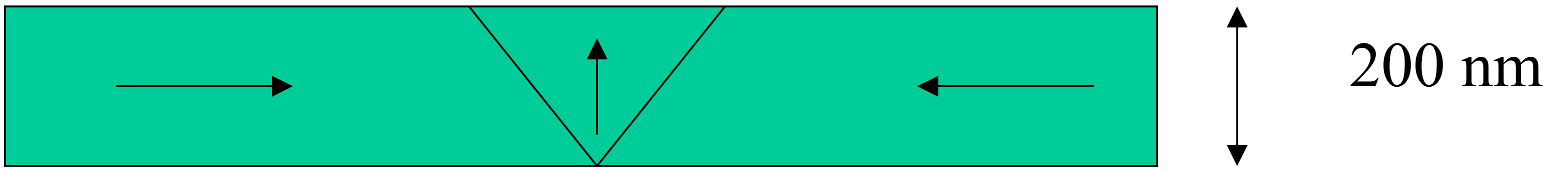

thickness 5nm $\approx \Lambda = (2A/\mu_0 M_s^2)^{1/2}$

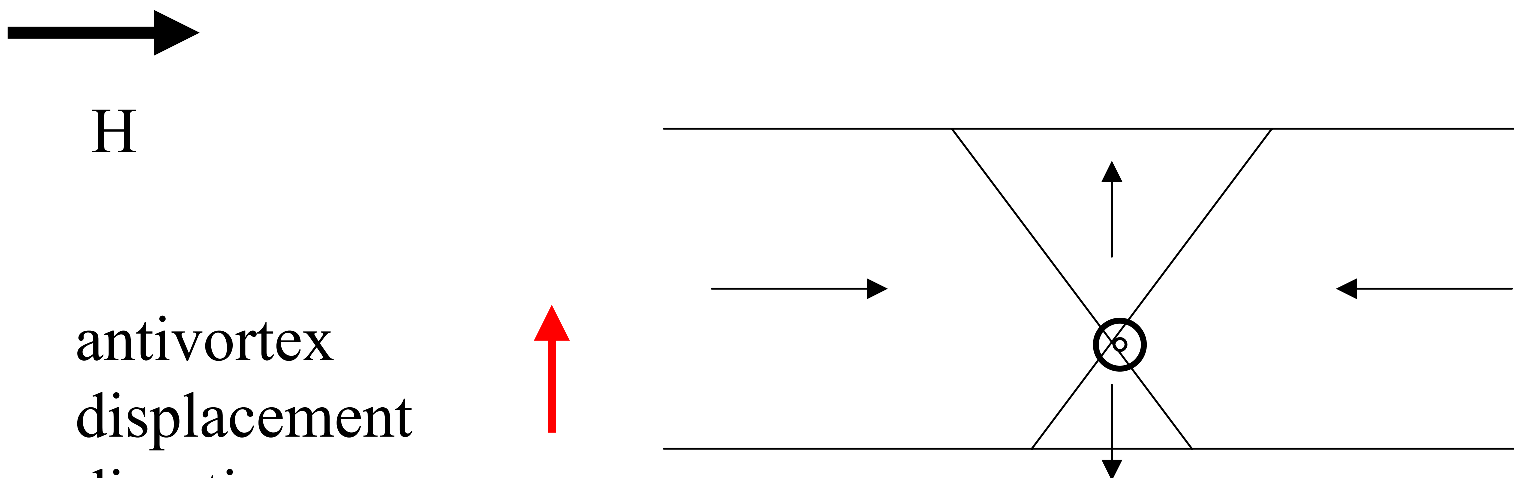

Y. Nakatani et al. Nature Mater. **2**, 521-523 (2003)

Domain wall dynamics in a permalloy nanostrip (200 x 5 nm)

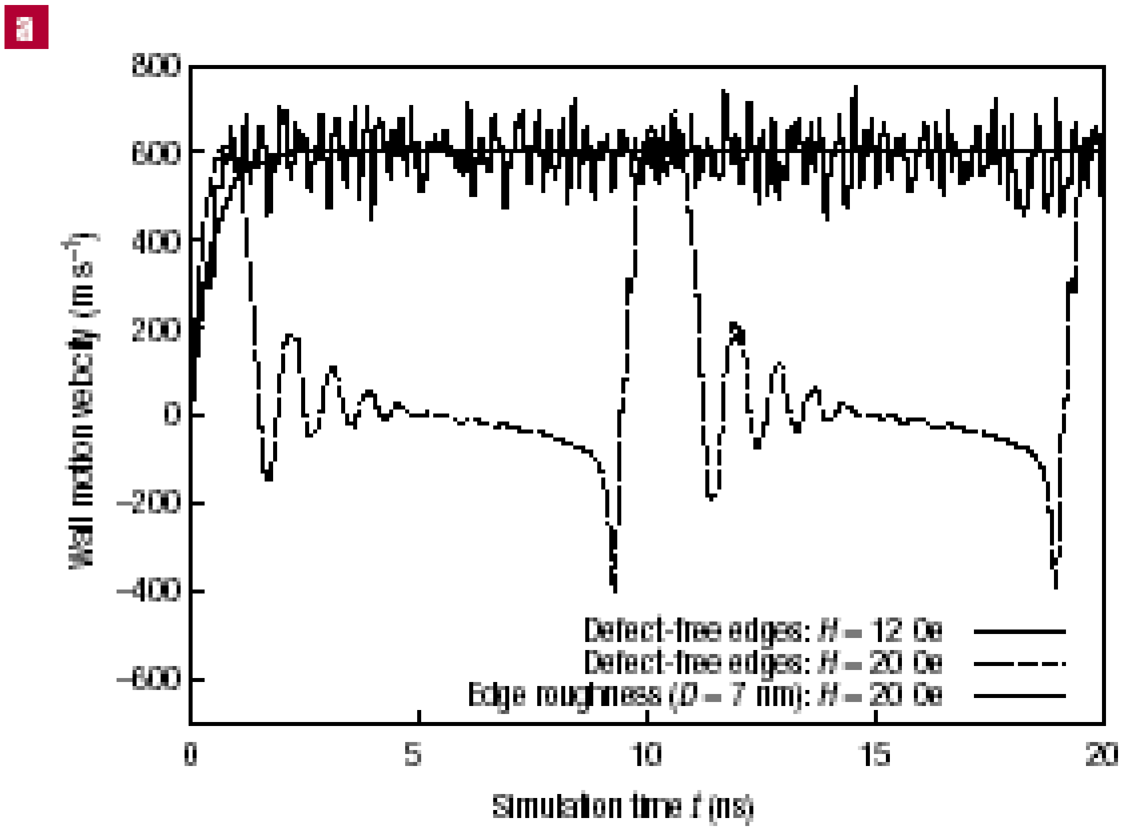

Y. Nakatani et al. Nature Mater. **2**, 521-523 (2003)

Perfect strip

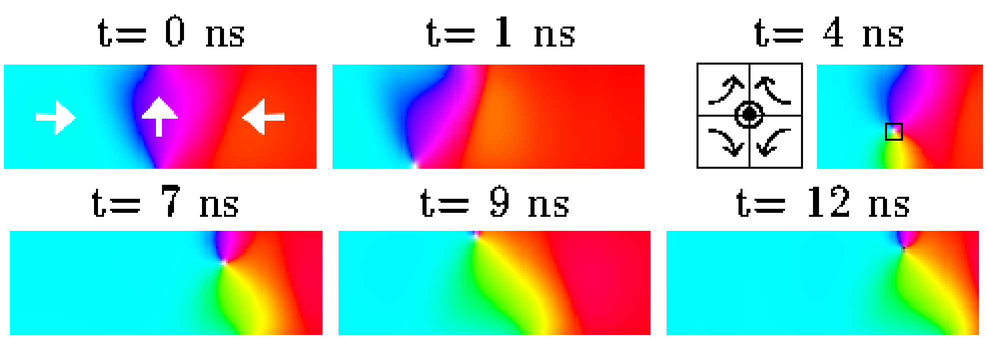

Effect of the roughness of strip edges

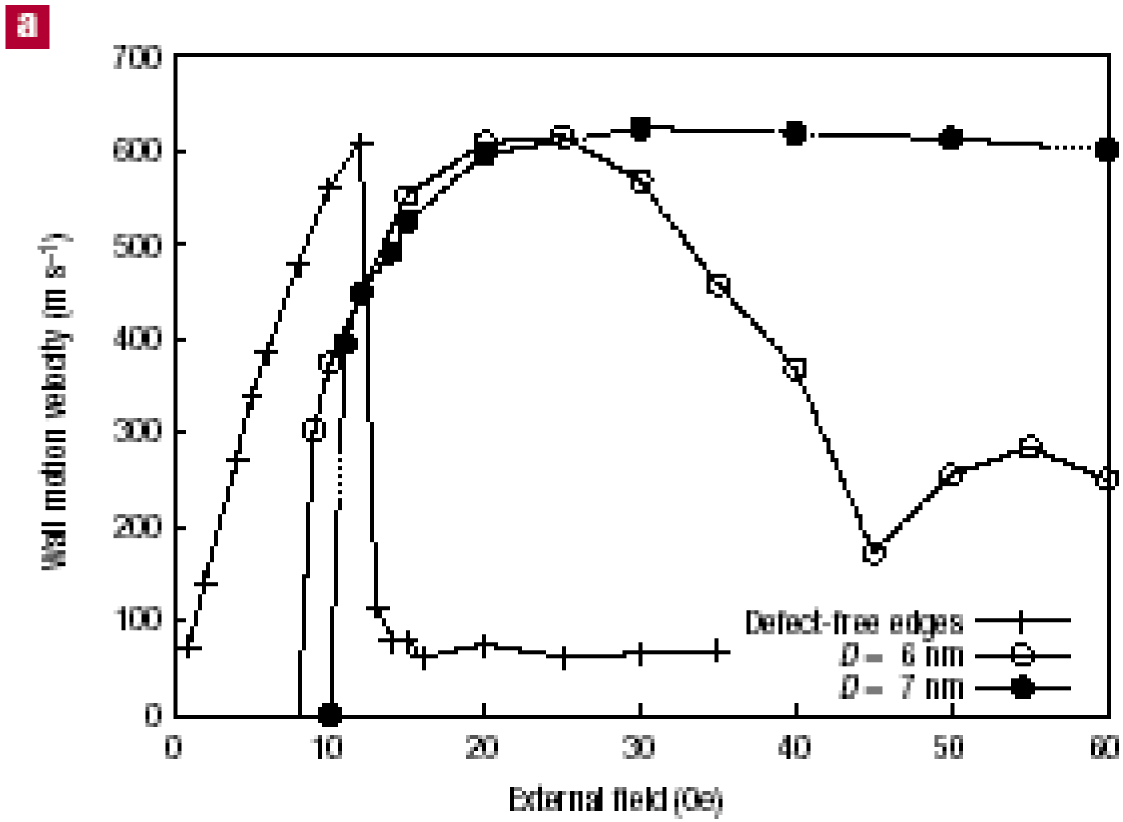

Thermodynamics of a macrospin

$E = K\,V\,\sin^2\theta$ $\quad$ $dS = \sin\theta\; d\theta\; d\varphi\,/4\pi \rightarrow \sin\theta\; d\theta\,/\,2$

Maxwell-Boltzmann statistics :

$p(E) = \exp(-E/k_B T)\,/\,Z$

$\dfrac{K\,V}{k_B T}$ parameter

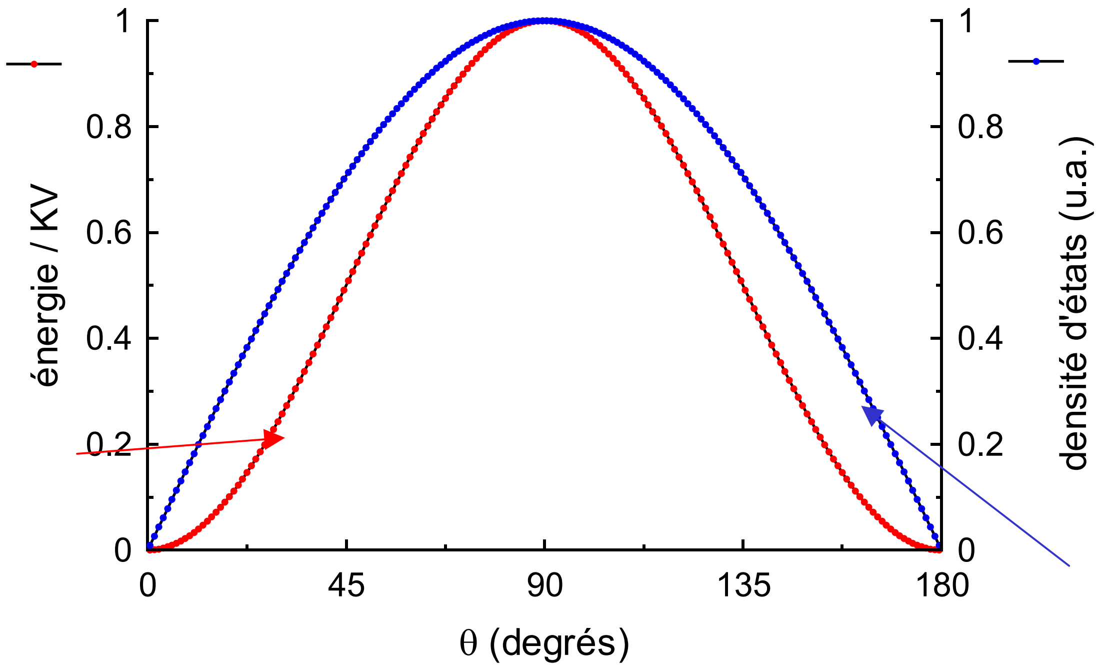

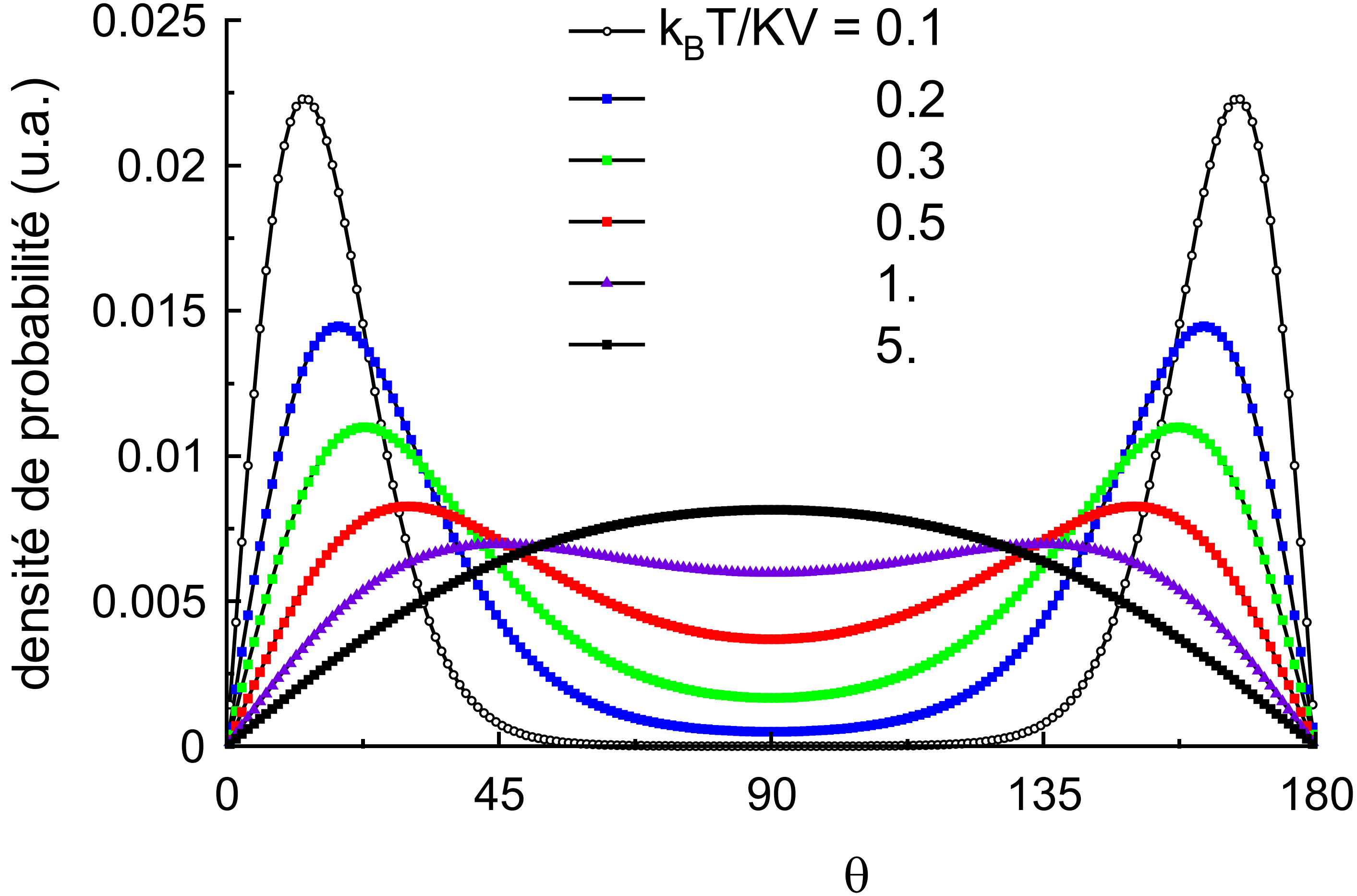

densité de probabilité (u.a.)
0.025
0.02
0.015
0.01
0.005
0
k_BT/KV = 0.1
0.2
0.3
0.5
1.
5.
0
45
90
135
180
θ

Discrete orientation model (Néel-Brown)

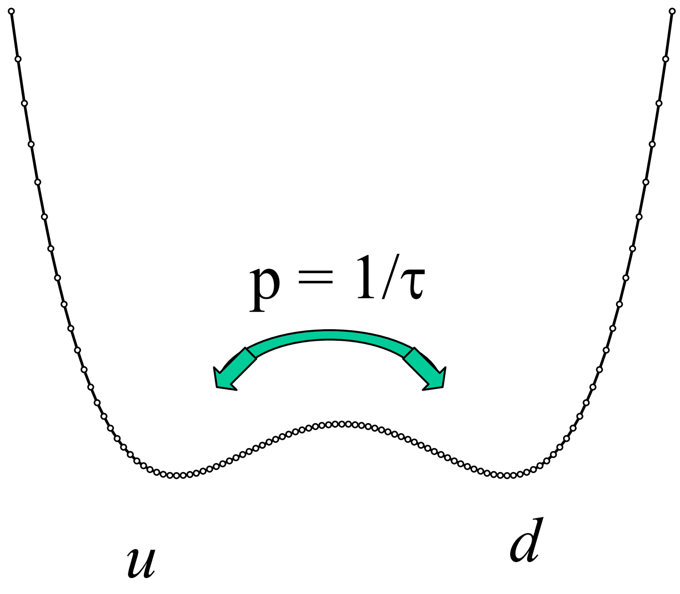

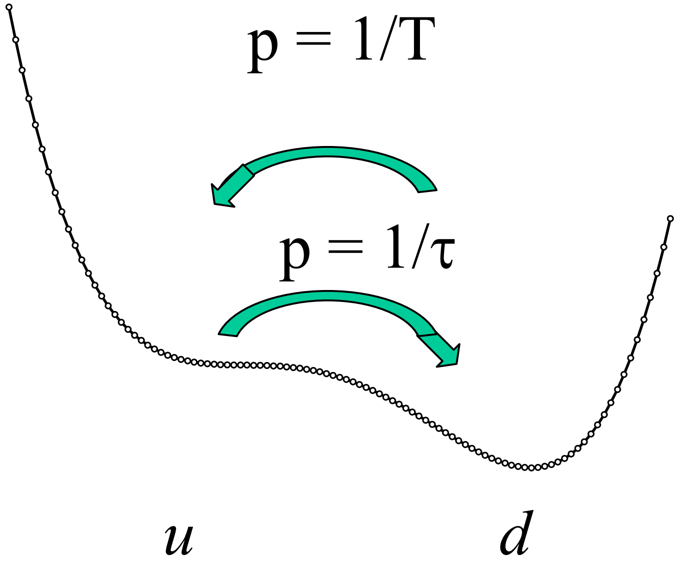

$$\tau = \tau_0 \exp[(E_m - E(u)) / kT]$$

$$T = \tau_0 \exp[(E_m - E(d)) / kT]$$

Calculation of τ_0

$$1/\tau_0 = \frac{\alpha}{1+\alpha^2} \underbrace{\frac{\gamma_0 \sqrt{cc'}}{\mu_0 M_s}}_{\omega_{\text{well}}} f(col)$$

formulas of Brown, Coffey…

$\tau_0 \approx$ qq. 10^{-10} s

with $\tau_0 = 0.1$ ns one has

$\tau =$	1s	1min	1h	1 jour	1 an	10 ans
$\Delta E/kT =$	23	27	31	34	40	43

Superparamagnetism : when $\tau < \tau_{\text{measurement}}$

Langevin field description of thermal fluctuations

$$\frac{d\vec{m}}{dt} = \gamma_0 \vec{H}_{eff} \times \vec{m} + \alpha \vec{m} \times \frac{d\vec{m}}{dt} \qquad \vec{H}_{eff} = -\frac{1}{\mu_0 M_s} \frac{\delta E}{\delta \vec{m}} + \vec{H}_{th}$$

$$\left\langle \vec{H}_{th} \right\rangle = \vec{0} \qquad \left\langle H_{th}^{i}(t) H_{th}^{j}(t') \right\rangle = \mu \, \delta_{ij} \, \delta(t - t')$$

$$\mu = \frac{2kT\alpha}{\gamma_0 M_s V} \qquad \sigma(H_{th}^{i}) = \sqrt{\frac{2kT\alpha}{\gamma_0 M_s V \, dt}}$$

From the fluctuation-dissipation theorem, or by matching the final probability distribution to Maxwell-Boltzmann

N.B. supposes a slow evolution

$$\hbar\omega < qq.kT \qquad \text{k/h} = 2\ 10^{10}\ \text{Hz/K}$$

Beyond Micromagnetics

Mn_{12}-acetate : a molecular magnet

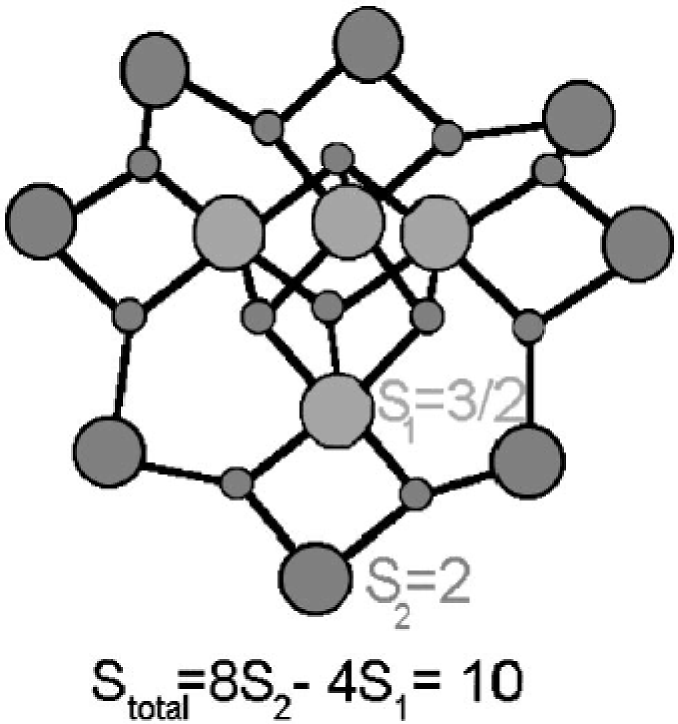

Fig. 1. Schematic representation of the molecule of Mn_{12}-ac.

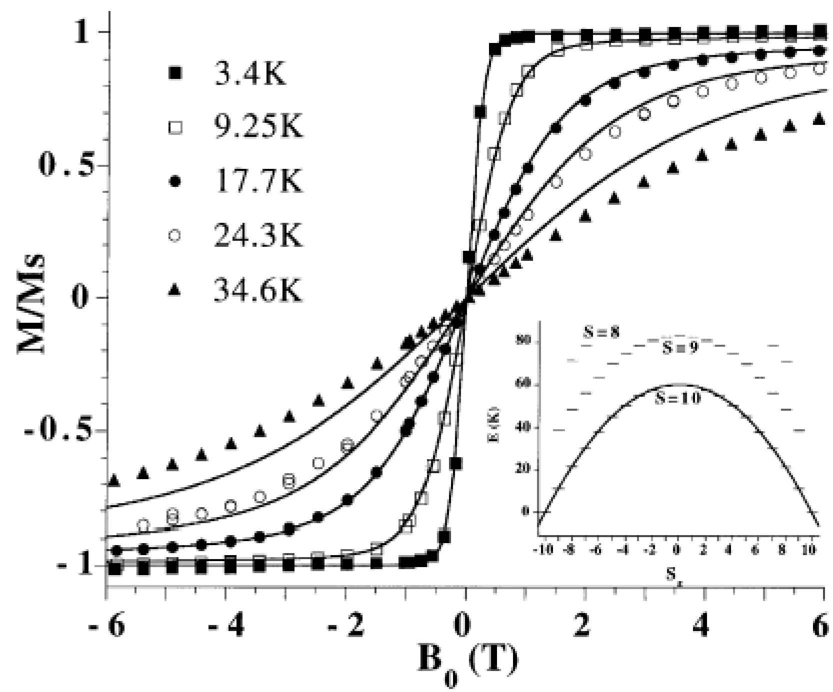

Fig. 2. Magnetization curves measured along the c-axis $M(H)$ in Mn_{12}-ac, above the blocking temperature. Fit to the $S = 10$ Hamiltonian. Inset: calculated energy levels $S = 10, 9, 8, \ldots$.

B. Barbara et al., JMMM **200**, 167 (1999)

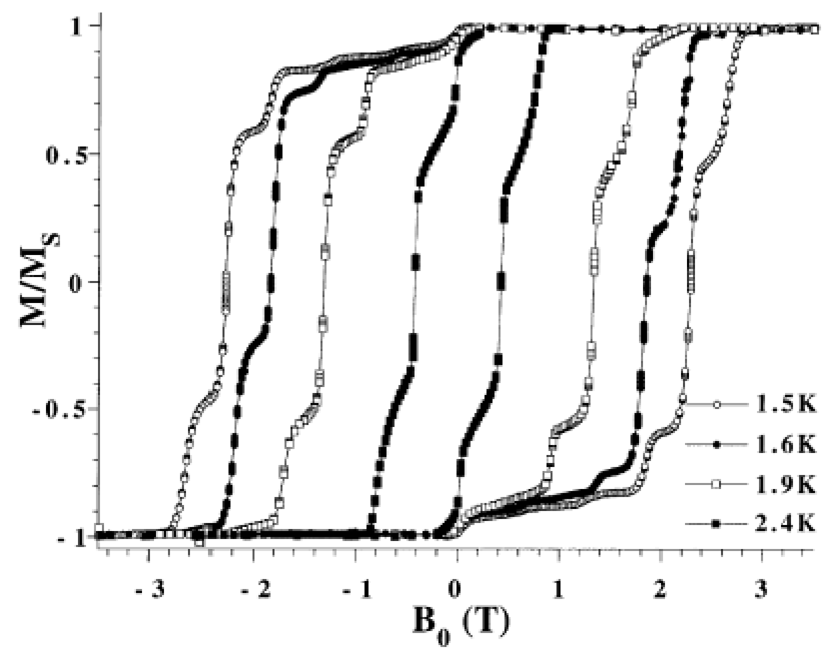

Fig. 3. Hysteresis loops of Mn_{12}-ac, with the field along the c-axis. Alternations of plateaux and steps suggest a 'macroscopic quantization' of the longitudinal magnetization component. This in fact simply riminiscent of the quantization of S_z of individual molecules + tunneling in the presence of a complex environment.

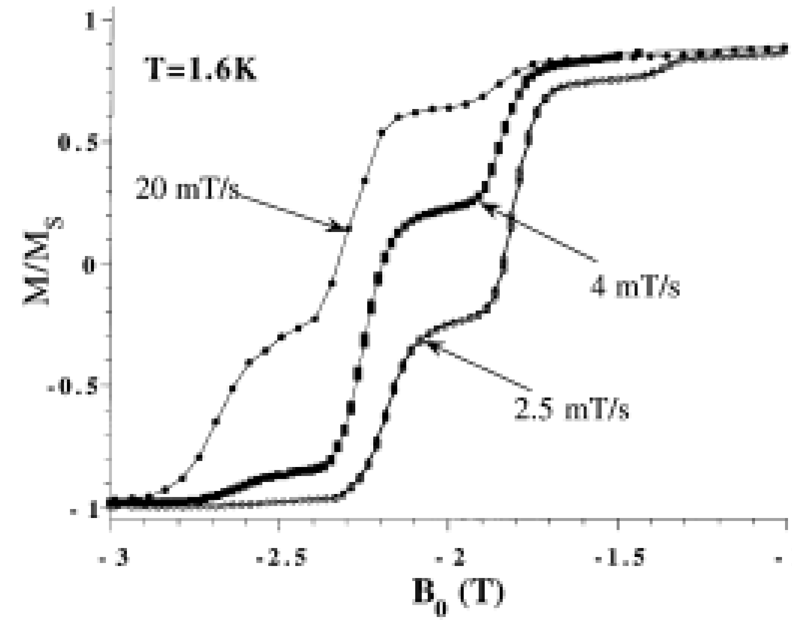

Fig. 4. Magnetization curves at different sweeping fields in Mn_{12}-ac.

B. Barbara et al., JMMM **200**, 167 (1999)

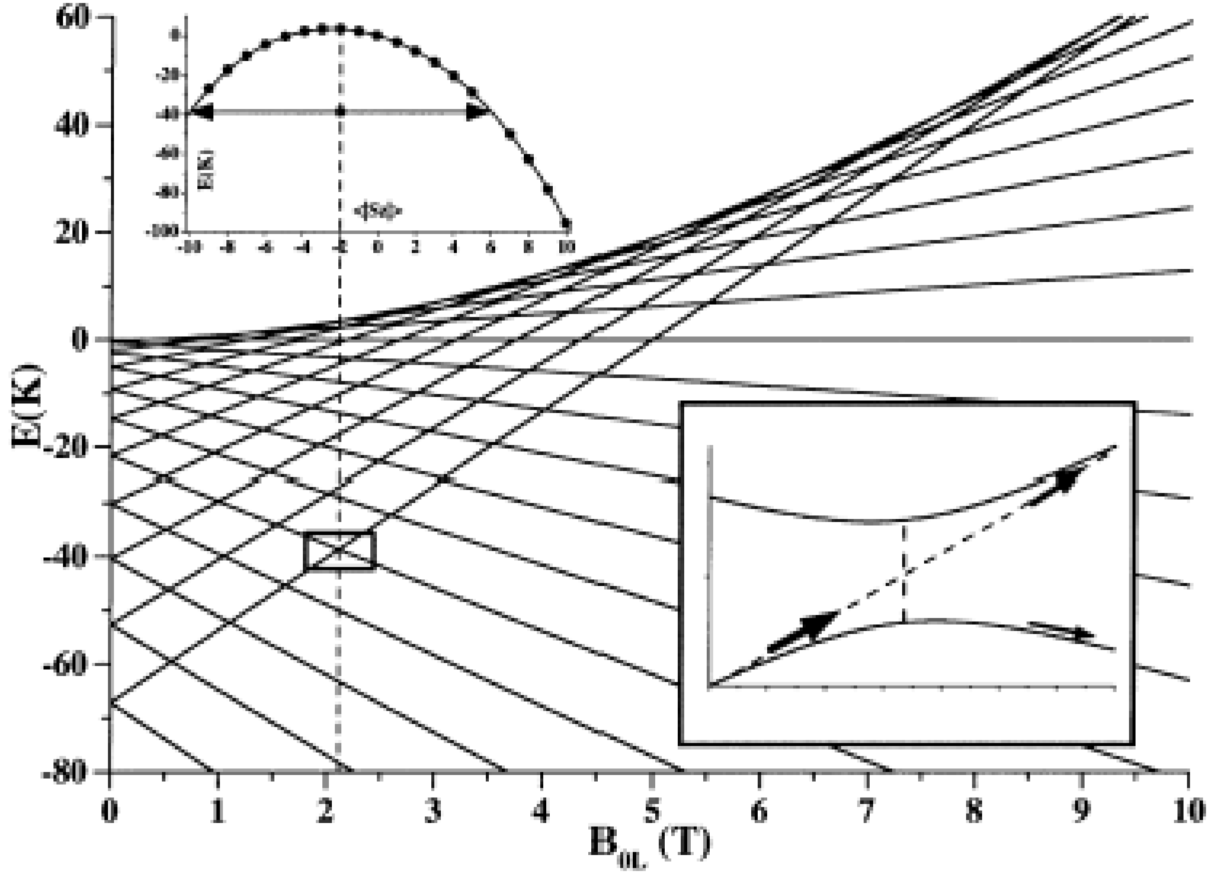

Fig. 6. Energy spectrum versus longitudinal field, calculated with the parameters given in the Appendix. Inset: enlargement of the $n = 4$ and $m = -10$ level anti-crossing with the tunneling gap and a representation of the adiabatic Landau–Zener mechanism. Top: energy barrier calculated for a field corresponding to $n = 4$.

Parity effect in tunneling

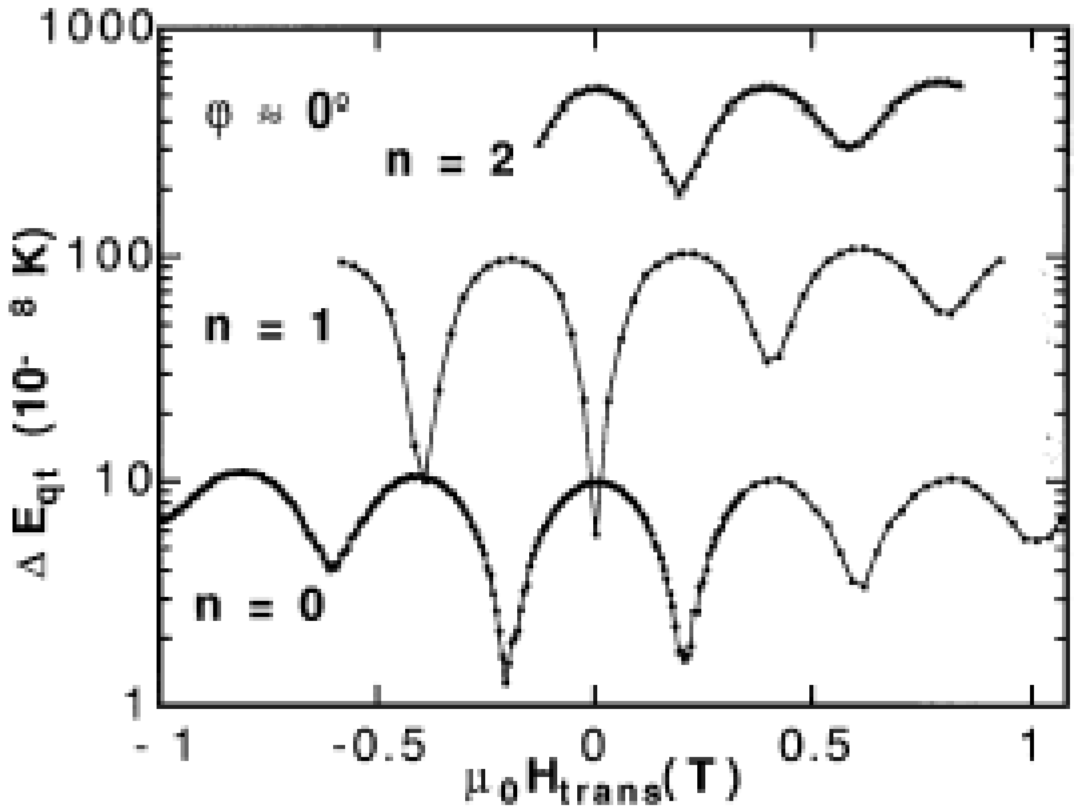

A. Caneschi et al. JMMM **200**, 182 (1999)

Fig. 12. Measured tunnel splitting ΔE_{qt}, at $T = 40$ mK, as a function of transverse field for $\varphi \approx 0^{\circ}$, and for quantum transition between $M = -10$ and $(S - n)$. Note the parity effect when n is odd which is analog to the suppression of tunneling predicted for half-integer spins.

Magnetism of Fe : free atom vs bulk

Free atom : Z= 28 $1s^2\ 2s^2 2p^6\ 3s^2 3p^6$ $\mathbf{3d^6\ 4s^2}$

Hund's rule : L=2 & S=2 : 6 μ_B (4 μ_B : spin + 2 μ_B : orbital)

Bulk metal : 3d & 4sp bands : 2.1 μ_B (2 μ_B : spin + 0.1 μ_B : orbital)

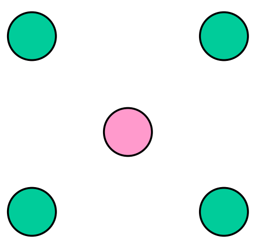

$< L_i > = 0$

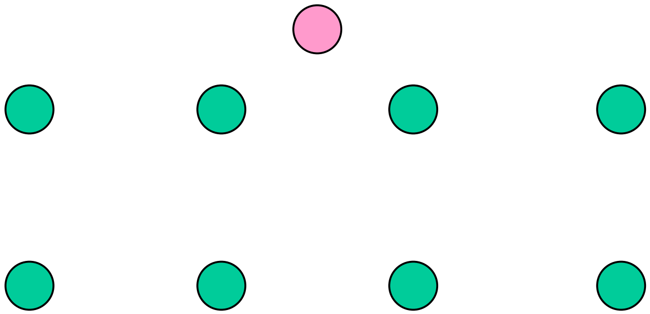

$< L_z > \neq 0$

The simple model of P. Bruno (simplified)

$$H_{spin-orbit} = \lambda \vec{L} \cdot \vec{S}$$ for an atom

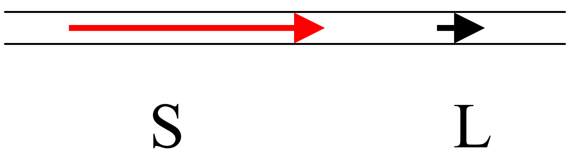

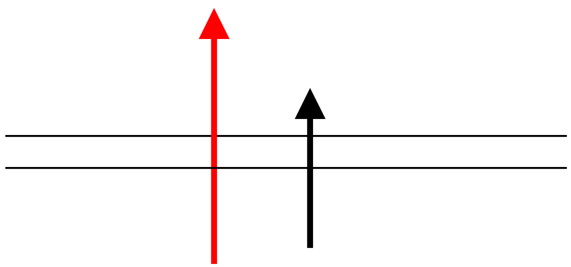

$$E_{\perp} - E_{//} = \lambda S \left(L_{\perp} - L_{//} \right)$$

$\lambda \approx 10$ meV : $\Delta L = 1$ → K= 10 meV/atom

(bulk Co : 5 10^5 J/m^3 = 25 μeV/atom)

Magnetic anisotropy and orbital moment in Co clusters of a few atoms

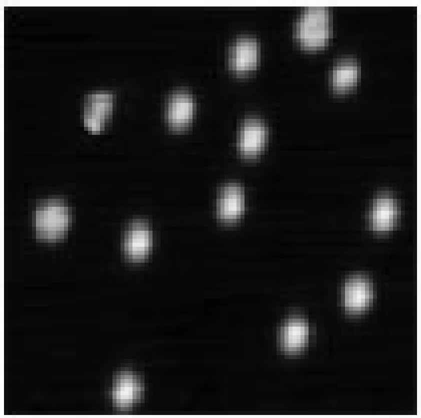

Co / Pt(111)
0.01 plan atomique
8.5 x 8.5 nm^2

P. Gambardella et al. Science <u>300</u>, 1130 (2003)

Fig. 3. (A) L as a function of $\bar{n}$ measured along the easy magnetization direction ($\theta_0 = 0°$). (B) K as a function of $\bar{n}$. For comparison, the dashed and dashed-dotted lines show the MAE per Co atom of the $L1_0$ CoPt alloy and hcp-Co, respectively. The values of $\bar{n}$ were determined in situ by fitting the superparamagnetic response of each particle assembly by means of Eq. 3. The average sizes so obtained are within ±10% of those determined by STM for the same growth conditions. For a given size, the particles consist of different isomers. Particles with $5 < \bar{n} \leq 40$ have a compact shape. The Co interatomic distance is that of the underlying Pt lattice. The error bars on the horizontal scale in (A) and (B) represent the standard deviation of the size distribution determined by STM. (Inset) K is plotted as a function of L (filled squares) and as a function of $\Delta r = r\,(0°) - r\,(70°)$ for $\bar{n} > 1$ (open diamonds). Δr = 0.1 corresponds to about ΔL = 0.2 μ_B; the errors on Δr (not shown) are on the order of ±0.04. The lines are guides to the eye.

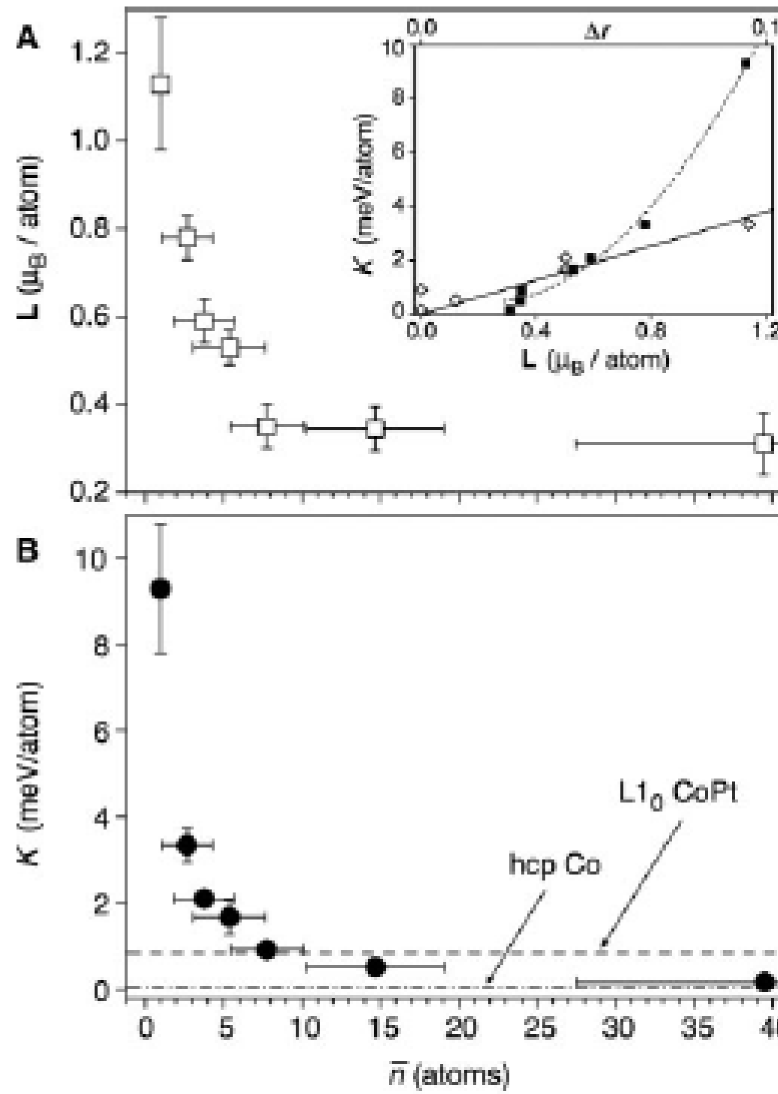

Magnetism and transport

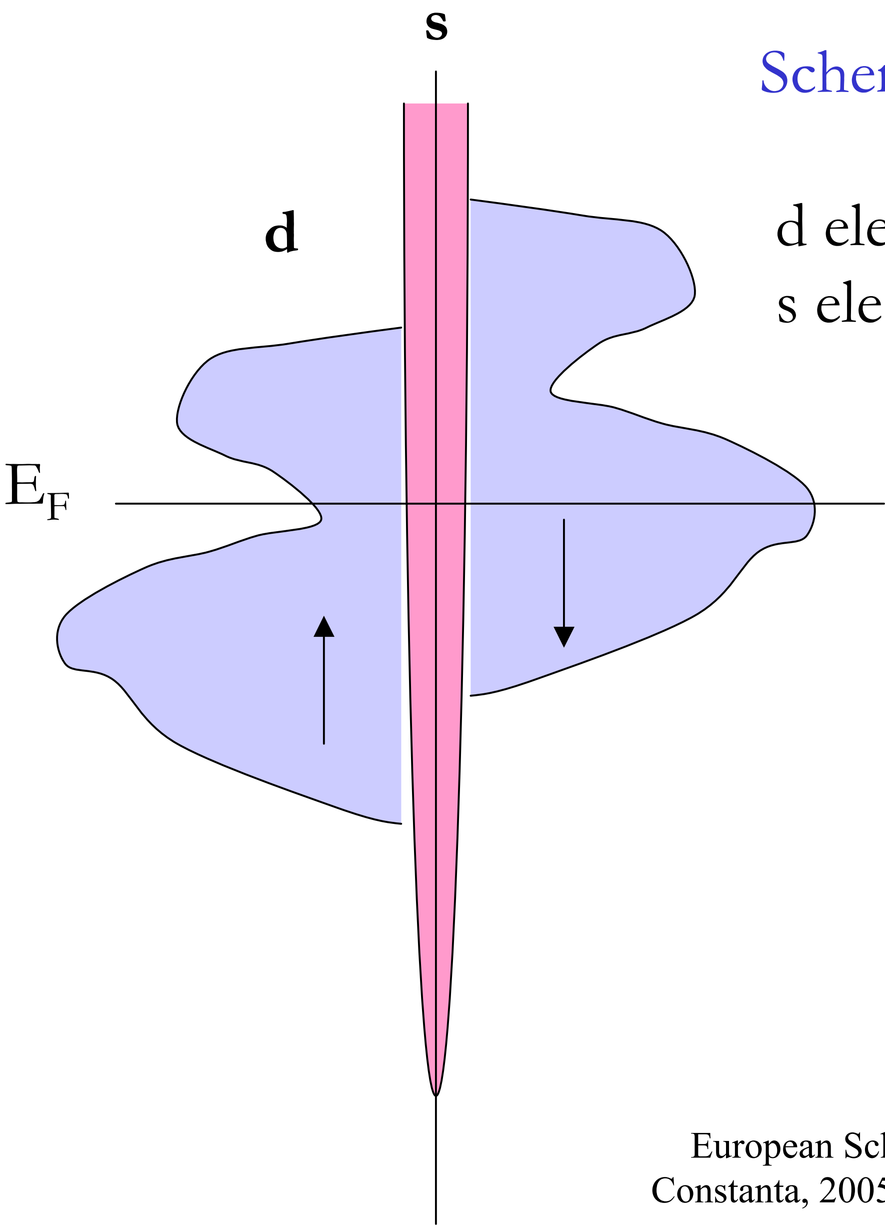

Schematic model of the 3D magnetic metals :

d electrons : localized, magnetism
s electrons : delocalized, transport

$$\sigma = \frac{ne^2\tau}{m}$$

$$\frac{1}{\tau} = \frac{2\pi}{\hbar}\left|V_{diff}\right|^2 k_B T\, N(E_F)$$

Interlayer exchange coupling (1986)

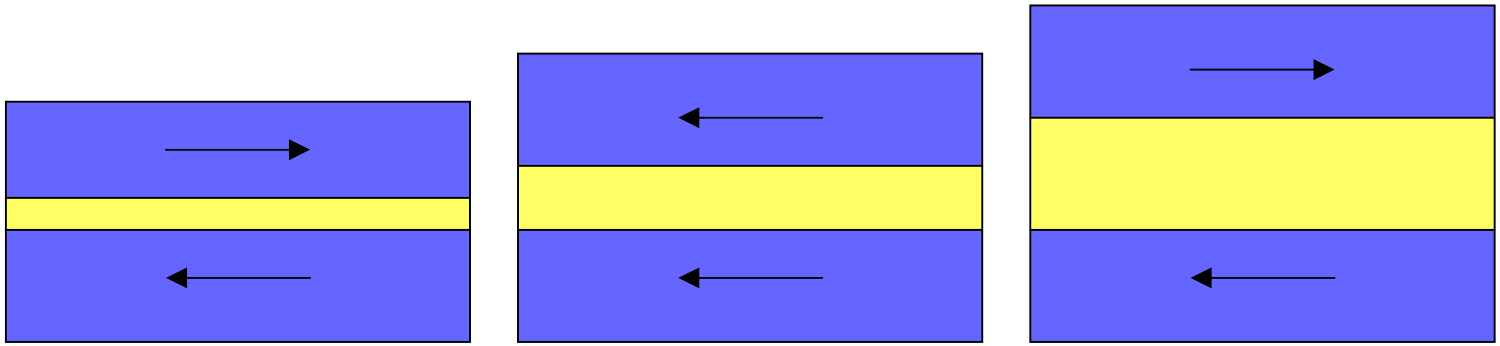

Oscillation periods depend on spacer material and crystalline orientation

Calculations based on the electronic structure

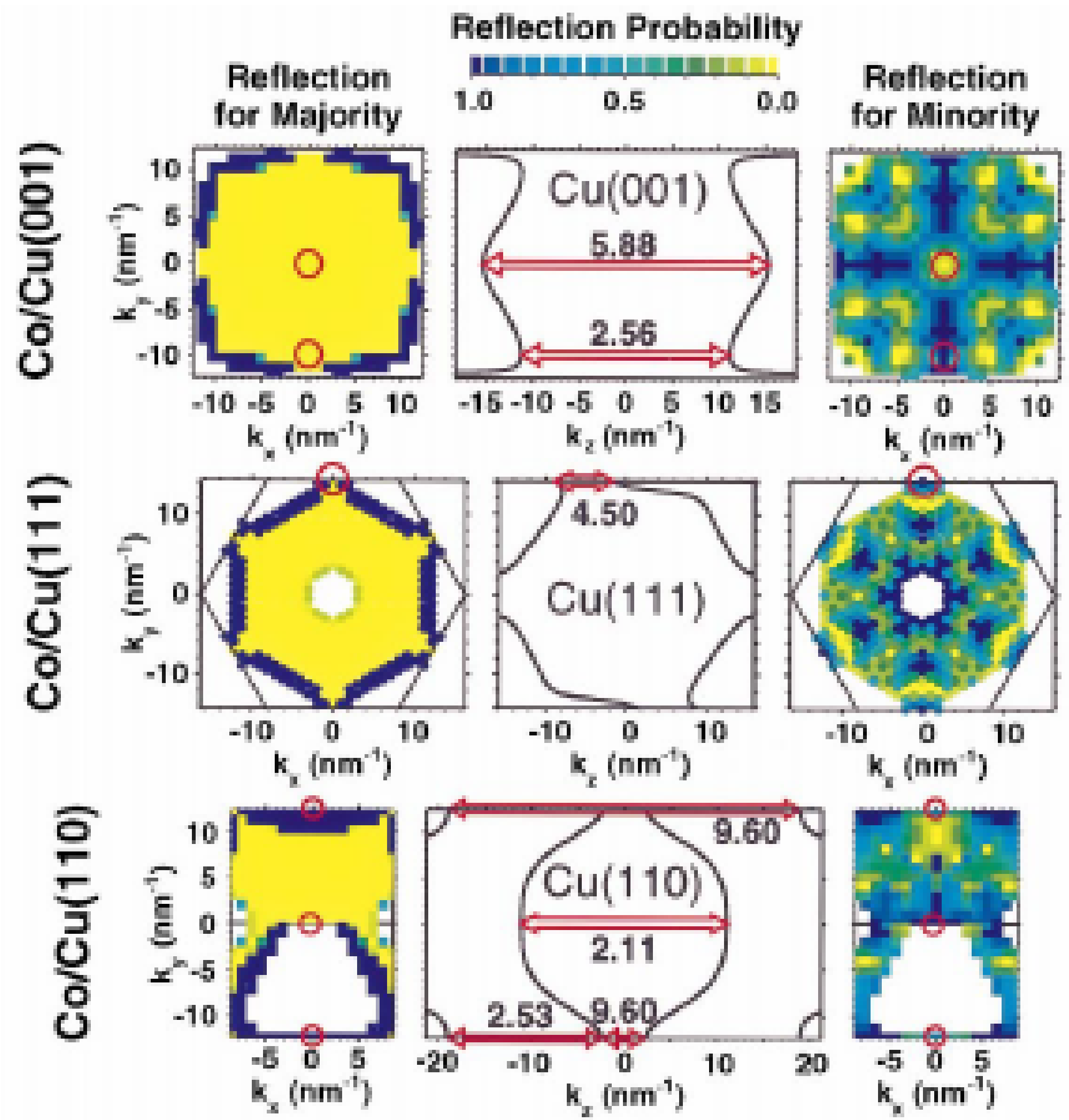

Fig. 1. Critical spanning vectors and interface reflectivities. For a series of spacer layers, magnetic materials, and interface orientations, organized in rows, the middle panels show slices though the Fermi surface of each spacer layer material for $k_x = 0$. The interface normal is the z direction in all cases. Superimposed in red on the Fermi surfaces are some of the critical spanning vectors. Each critical spanning vector is labeled by its associated coupling period in monolayers as determined from the experimental Fermi surfaces [22,114]. In the left and right panels, the Fermi surface is projected onto the $k_z = 0$ plane. It is color-coded based on the probability for an electron incident from the spacer layer material to reflect from the interface with the magnetic material. Probabilities for electrons with spins parallel to the majority and minority spin directions are shown in the left and right panels, respectively. The locations of the critical spanning vectors are labeled by red circles centered at the critical point. The Cu Fermi surface projected into a (1 1 0) interface and the Cr Fermi surface projected into a (0 0 1) interface have multiple sheets. To present these overlapping sheets, each is only shown in a faction of the interface Brillouin zone. The full Fermi surface can be reconstructed by rotating the various partial sheets into to the other symmetric parts of the zone.

M.D. Stiles,
JMMM **200**, 322 (1999)

Giant magneto-resistance (1988)

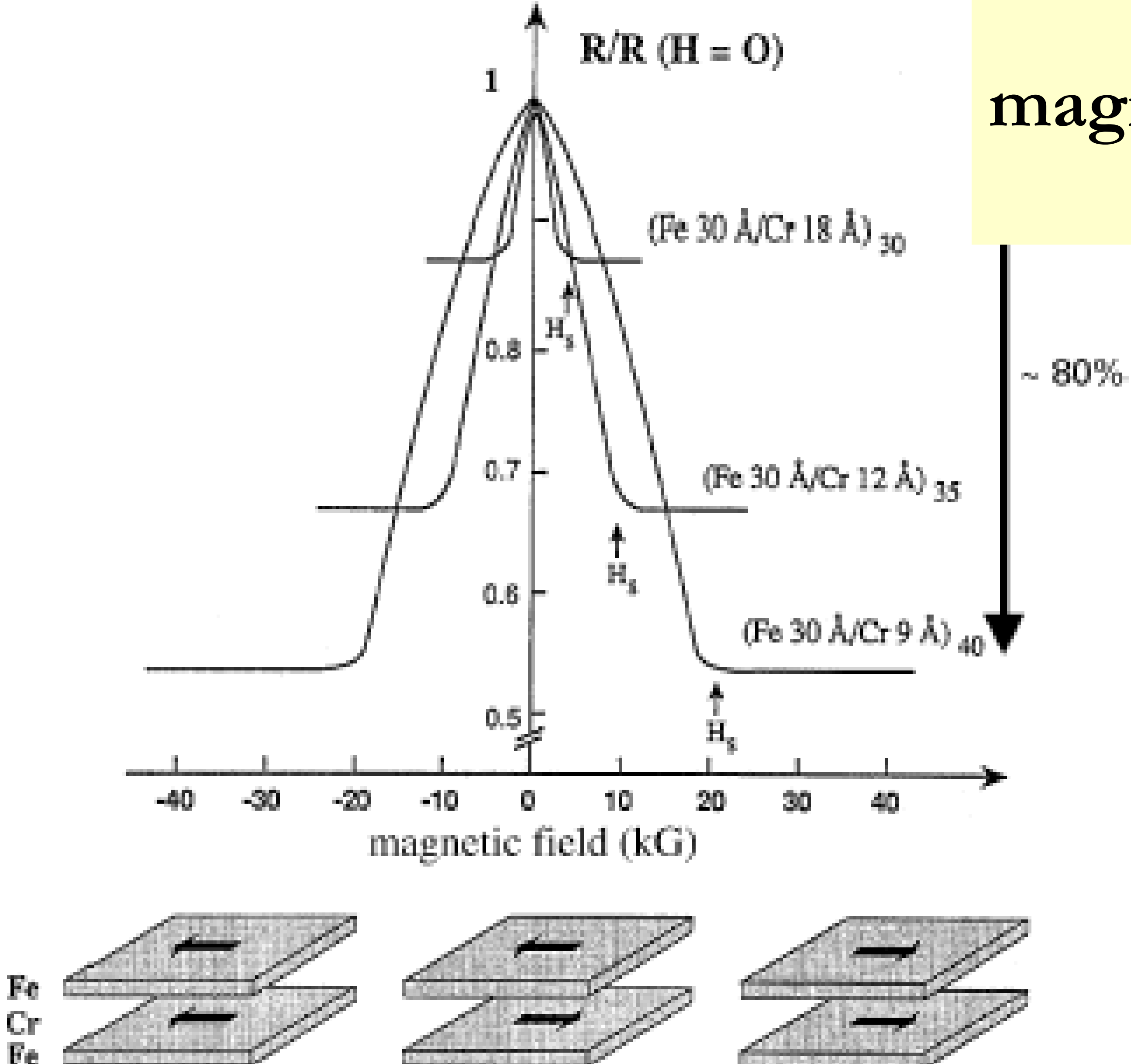

Fig. 1. Magnetoresistance curves at 4.2 K of (Fe/Cr) multi-layers [1].

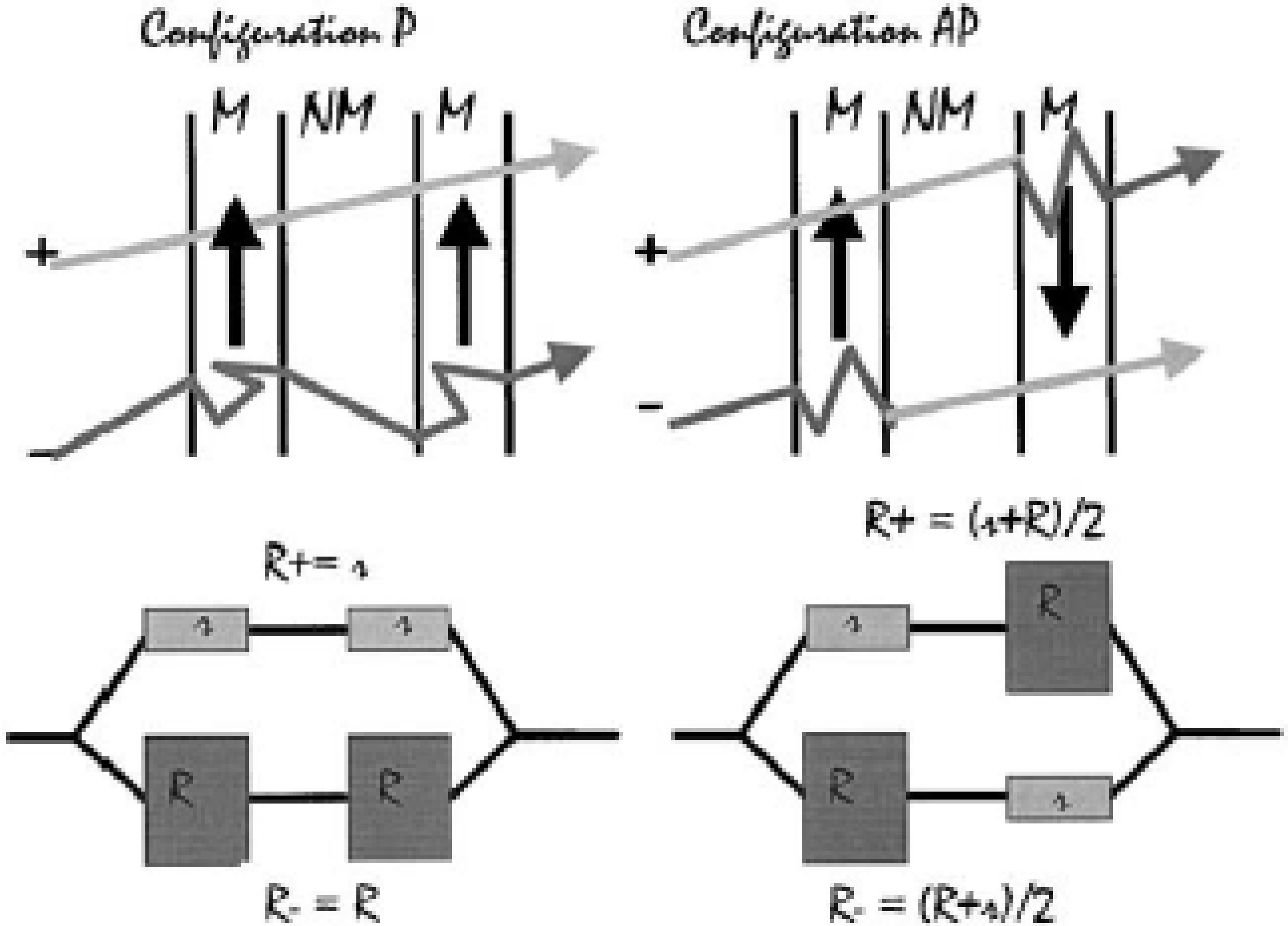

Fig. 3. Schematic picture of the GMR mechanism. The electron trajectory between two scatterings are represented by straight lines and the scattering by abrupt change in the direction. The signs + and − are for spins $S_z = \frac{1}{2}$ and $-\frac{1}{2}$, respectively. The arrows represent the majority spin direction in the magnetic layers.

Spin pumping

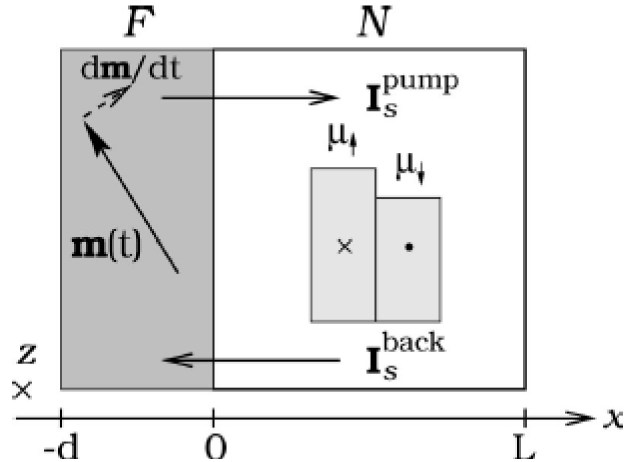

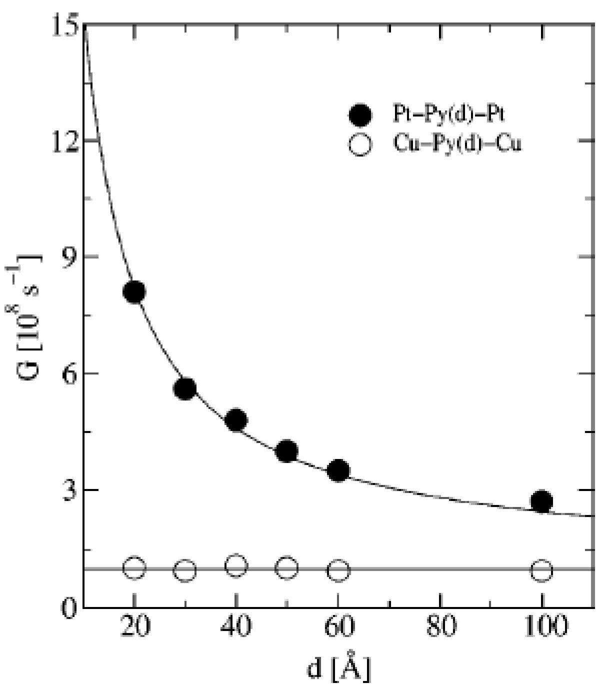

FIG. 3. Circles show measured (Ref. 6) Gilbert parameter G of a permalloy film with thickness d sandwiched between two normal-metal (Pt or Cu) layers. Solid lines are predictions of our theory with two fitting parameters, G_0, and $g^{\uparrow\downarrow}$-Py bulk damping and Py-Pt mixing conductance, respectively, see Eq. (22).

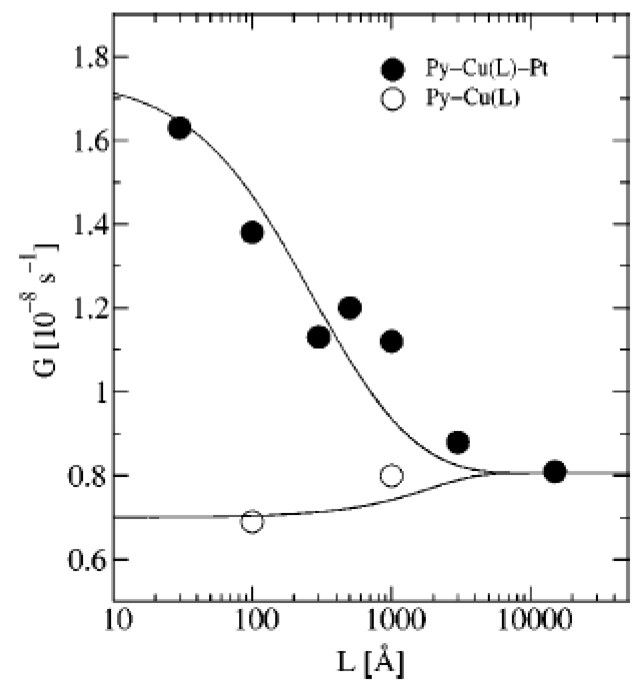

FIG. 5. Circles show the measurements by Mizukami *et al.* (Ref. 16) of the Gilbert damping in Py-Cu-Pt trilayer and Py-Cu bilayer as a function of the Cu buffer thickness L. Solid lines are our theoretical prediction according to Eqs. (26) and (27).

Spin transfer effects

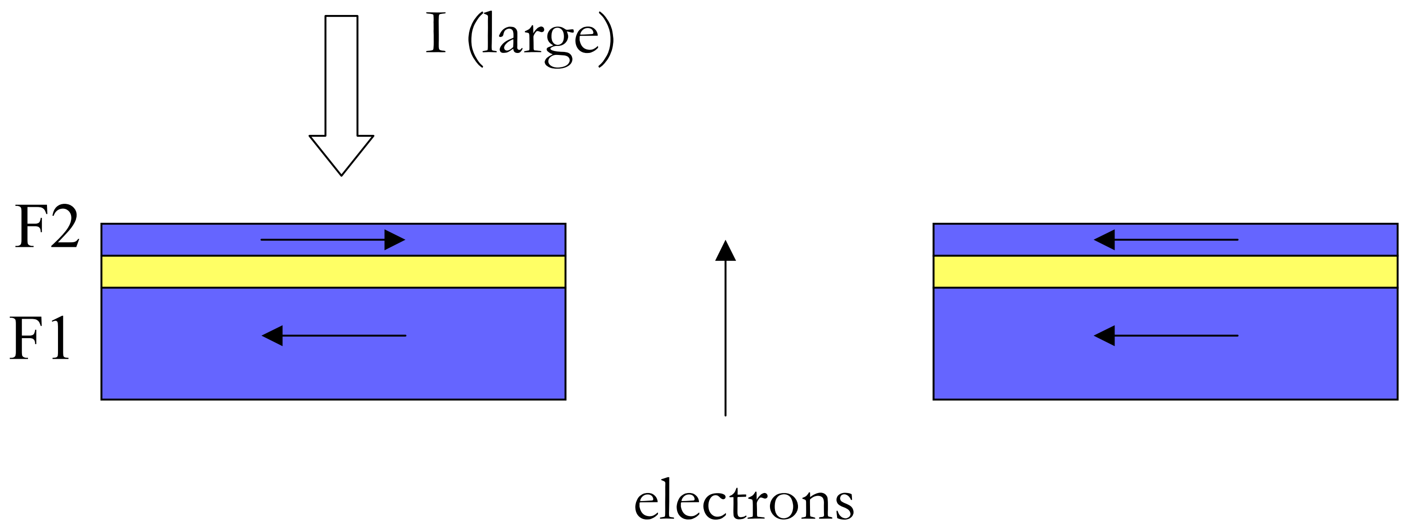

Angular momentum transfer due to the reorientation of the spins of the conduction electrons

Spin-polarized current switching of a Co thin film nanomagnet

F. J. Albert, J. A. Katine and R. A. Buhrman
School of Applied and Engineering Physics, Cornell University, Ithaca, New York 14853
D. C. Ralph
Laboratory of Atomic and Stolid State Physics, Cornell University, Ithaca, New York 14853

APPLIED PHYSICS LETTERS VOLUME 77, NUMBER 23 4 DECEMBER 2000

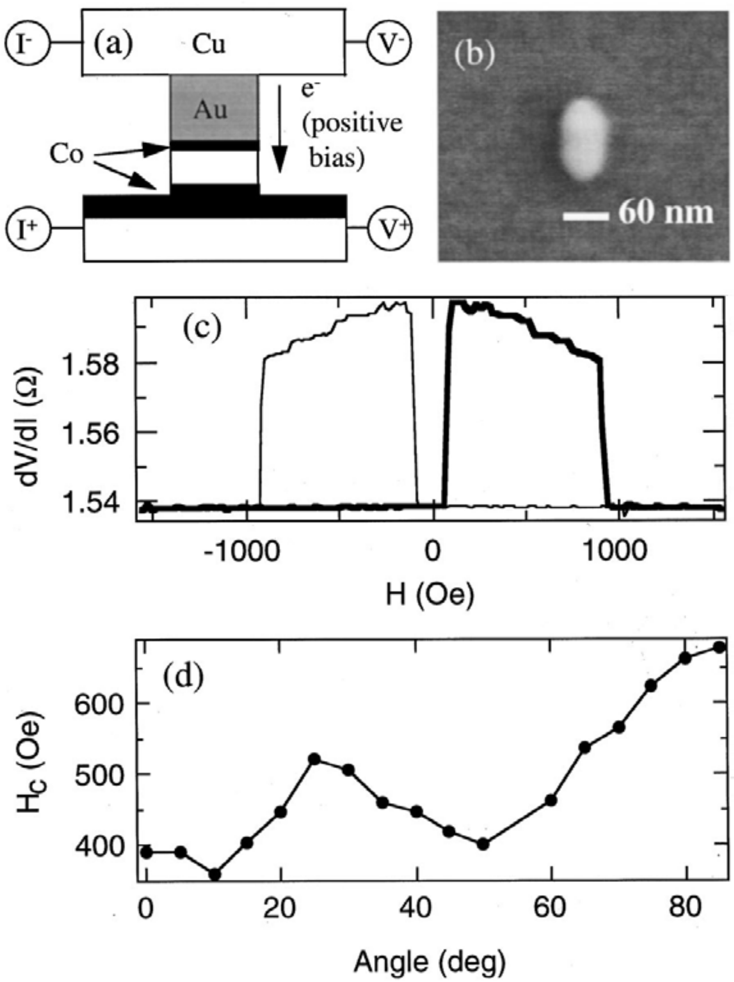

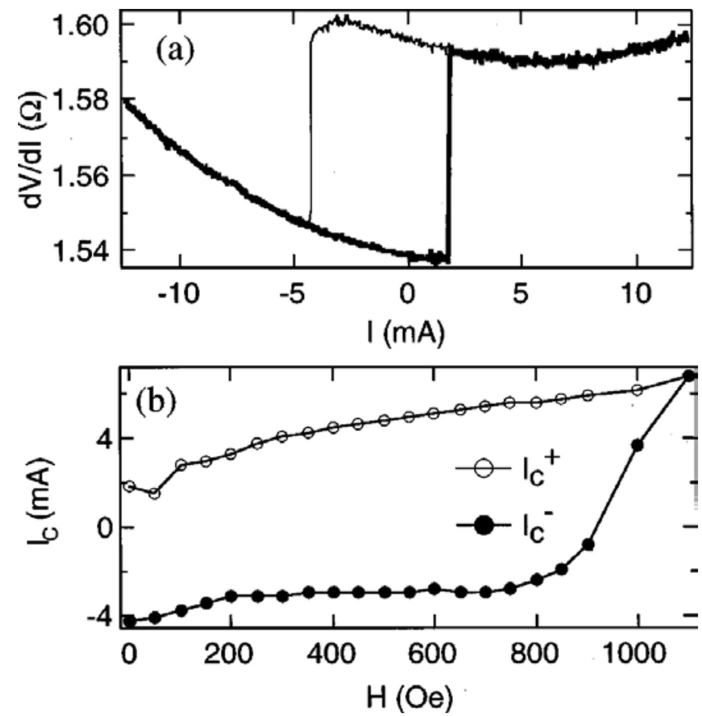

Conclusions :

Micromagnetics

- has witnessed many decades of increasing success

- becomes more and more challenged by experiments on nanoscale samples